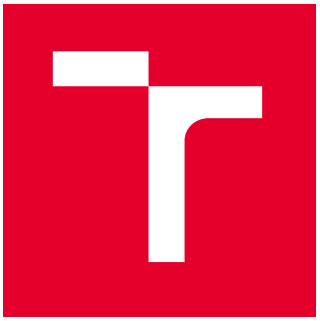

BRNO UNIVERSITY OF TECHNOLOGY

VYSOKÉ UČENÍ TECHNICKÉ V BRNĚ

FACULTY OF CIVIL ENGINEERING

FAKULTA STAVEBNÍ

INSTITUTE OF METAL AND TIMBER STRUCTURES

ÚSTAV KOVOVÝCH A DŘEVĚNÝCH KONSTRUKCÍ

DESIGN OF HOLLOW SECTION JOINTS: COMPARISON OF DESIGN METHODS

STYČNÍKY UZAVŘENÝCH PRŮŘEZŮ: SROVNÁNÍ NÁVRHOVÝCH METOD

BACHELOR'S THESIS

BAKALÁŘSKÁ PRÁCE

AUTHOR — Mykola Lastovetskyi

AUTOR PRÁCE

SUPERVISOR — Ing. Martin Vild, Ph.D.

VEDOUCÍ PRÁCE

BRNO 2025

BRNO UNIVERSITY OF TECHNOLOGY
FACULTY OF CIVIL ENGINEERING

Assignment Bachelor's Thesis

Department:	Institute of Metal and Timber Structures
Student:	**Mykola Lastovetskyi**
Supervisor:	**Ing. Martin Vild, Ph.D.**
Academic year:	2024/25
Study programme:	B0732A260005 Civil Engineering
Field of study:	Structural and Transport Engineering

The Dean of the Faculty, in accordance with Act No. 111/1998 on universities and the Study and Examination Regulations of the BUT in Brno, assigns you the following topic Bachelor's Thesis:

Desgin of hollow section joints: Comparison of design methods

Concise characteristic of the task:

The formulas for design of hollow steel joints are predominantly derived by curve-fitting method of experiments and numerical simulations. The current Eurocode is valid since 2005; the knowledge has been expanded and the second generation Eurocode contains précised formulae and expanded range of validity. In the USA, the Specification is published more frequently; the currently valid version is from 2022. Another design method is numerical design calculation according to FprEN 1993-1-14 using software, e.g. IDEA StatiCa.
The goal of this bachelor thesis is to compare these four design variants for selected geometries of hollow section joints within the validity range.
Another goal is to design a hollow-section steel truss with a 40 m span and welded joints.

Objectives and outputs Bachelor's Thesis:

The goals of bachelor thesis are:
- Comparison of design methods for a large varieties of geometry in the range of validity of design codes.
- Design of duopitch roof truss with a span of 40 m for typical dead load and climatic loading for Brno region including production drawings.

List of recommended literature and documents:

EN 1993-1-8:2005 Eurokód 3: Navrhování ocelových konstrukcí - Část 1-8: Navrhování styčníků

FprEN 1993-1-8:2023: Eurocode 3: Design of steel structures - Part 1-8: Design of joints

FprEN 1993-1-14:2024: Eurocode 3: Design of steel structures - Part 1-14: Design assisted by finite element analysis

ANSI/AISC 360-22 Specification for Structural Steel Buildings

ABSTRACT

This study conducts a comparative analysis of circular hollow section (CHS) connections using finite element analysis (FEA) and design codes (current EN 1993-1-8, AISC 360-22, and the upcoming EN 2026). Automated via Python API and IDEA StatiCa Connection, the methodology evaluates T/Y, X, and K connections under varying angles (30°–90°), steel grades (S235–S460), and chord pre-loading. Results reveal that the new EN code predicts 55% higher resistances for K-connections under compression chord loading but shows significant deviations from CBFEM results when chord stress is present. Nonlinear effects of steel grade on resistance were identified, contradicting code linear models. Publicly available scripts enable dataset replication, supporting future code refinement and machine learning applications. Limitations include CHS-only scope and chord loading inconsistencies from FEA resistance determination.

KEYWORDS

Steel truss; Hollow section joints; Second generation of Eurocodes; FEM; Circular hollow sections; EN 1993; AISC 360; CBFEM; Parametric analysis;

ABSTRAKT

Tato studie provádí srovnávací analýzu spojů kruhových dutých profilů (CHS) pomocí metody konečných prvků (FEA) a normativních postupů (aktuální EN 1993-1-8, AISC 360-22 a připravovaný EN 2026). Automatizovaná metodologie využívající Python API a software IDEA StatiCa vyhodnocuje spoje T/Y, X a K při různých úhlech (30°–90°), třídách oceli (S235–S460) a zatížení pásu. Výsledky ukazují, že nový EN kód předpovídá až o 55% vyšší únosnost u K-spojů při tlakovém zatížení, ale vykazuje významné odchylky od CBFEM při namáhaném pásu. Identifikován byl nelineární vliv třídy oceli na únosnost, který odporuje lineárním normovým modelům. Veřejně dostupné skripty umožňují replikaci dat pro budoucí zdokonalování norem a strojové učení. Omezení zahrnují zaměření pouze na CHS a zatížení pásu z důvodu použité metodologie získávaní únosnosti FEA.

KLÍČOVÁ SLOVA

Ocelová příhradová konstrukce; Styčníky uzavřených průřezů; Druhá generace Eurokódů; MKP; Kruhové duté profily; EN 1993; AISC 360; CBFEM; Parametrická analýza;

ROZŠÍŘENÝ ABSTRAKT

ÚVOD

Spoje dutých ocelových profilů mají v konstrukcích významnou úlohu a jejich spolehlivý návrh je nezbytný, zejména s ohledem na připravovanou revizi evropských norem pro návrh konstrukce [1]. Tato studie se zabývá porovnáním výpočtových metod pro posouzení takových spojů podle nové generace evropských norem EN (s předpokládaným vydáním do 30. března 2026), současného znění normy EN 1993-1-8 [2] a americké normy AISC 360-22 [3], a zahrnuje také postupy implementované v softwaru IDEA StatiCa Connection [4]. Cílem práce je systematické zhodnocení těchto návrhových metod s důrazem na sjednocení a aktualizaci návrhových postupů.

Pro numerickou analýzu byl využit programovací jazyk Python [5] s propojením na IDEA StatiCa Connection prostřednictvím API [6], což umožnilo automatizované provádění parametrických výpočtů. Výpočty byly realizovány pro různé typy zatížení, odlišná geometrická uspořádání a materiálové vlastnosti profilů, čímž vznikl rozsáhlý soubor dat pro porovnání výsledků mezi jednotlivými metodami. Studie se přitom vymezuje na posouzení únosnosti samotných nosných částí spojů bez zohlednění vlivu svarových a šroubových spojů, čímž je jasně definován rozsah a omezení analýzy.

Součástí studie je také optimalizace ocelového vazníku (krovu) s využitím genetických algoritmů v prostředí Grasshopper [7], přičemž statická analýza optimalizovaných konfigurací probíhá pomocí pluginu Kiwi!3D [8]. Tento případový příklad ilustruje aplikaci navrženého postupu pro vylepšení návrhu konstrukčních prvků a ověření efektivity procesu založeného na optimalizaci pomocí genetického algoritmu.

METODOLOGIE

Pro zajištění konzistentního srovnání metod výpočtu odolnosti spojů dutých profilů (CHS) byly ve studii použity identické průřezy a materiálové vlastnosti pro všechny analyzované normativní přístupy (nový Eurokód EN 2026, EN 1993-1-8, AISC 360-22 a IDEA StatiCa Connection). Výpočty charakteristické únosnosti byly provedeny bez aplikace součinitelů spolehlivosti, což umožňuje přímé srovnání s výsledky metody konečných prvků (FEA). Klíčovým nástrojem se stala Python API [6] integrace s komerčním softwarem IDEA StatiCa Connection, doplněná o konfigurační soubory ve formátu YAML [9] pro definici geometrických parametrů, mezí platnosti a výpočetních rovnic. Tento přístup výrazně zvýšil efektivitu generování tisíců kombinací spojů při zachování přehlednosti kódu.

Analýza se zaměřila na standardizované typy spojů T&Y, X a K. Pro spoje K byly uvažovány pouze konfigurace s mezerou $g \geq t_1 + t_2$. a symetrickými mezi-

pasovými pruty $\theta_1 = \theta_2$, $d_1 = d_2$, a $t_1 = t_2$. Pracovní postup začínal generováním kombinací průřezů z tabulky CHS profilů, následovaným algoritmickou kontrolou platnosti dle geometrických omezení norem (např. poměry d_1/t_0, d_1/d_0). Každá validní kombinace byla doplněna o třídu oceli (S235–S460) a kontrolu třídy průřezu podle EN 1993-1-8, přičemž nevyhovující kombinace byly vyloučeny. Finální výpočet únosnosti využíval YAML instrukce s explicitními rovnicemi pro jednotlivé normy, včetně pomocných parametrů $\gamma = \frac{d_0}{2 \cdot t_0}$ & $\beta = \frac{d_1}{d_0}$.

Pro FEA simulace v IDEA StatiCa Connection bylo klíčové nastavení zatížení: k dosažení rovnováhy spoje byly aplikovány normálové a smykové síly na pás. Odolnost FEA byla stanovena pomocí funkce *Stop at Limit Strain*, která přerušuje analýzu při dosažení 5% plastického přetvoření nebo 3% lokální deformace. Důsledně byly kontrolovány také parazitní účinky (např. koncové momenty u spojů T&Y, přičemž nekonzistentní výsledky byly vyloučeny).

Všechna výstupní data (analytické i FEA výsledky) byla ukládána do MySQL databáze, což umožnilo zpětnou validaci YAML rovnic, po každém generování grafu všechna data se přepočítávají. Postup umožnil při zjištění chyby upravit YAML rovnice a přegenerovat výstupy. Pro parametrické variace byly zvoleny klíčové vlivy: úhel θ přípoje (30°, 45°, 60°, 90°), zatížení pásu ($N_{0,Ed}$, $M_{0,Ed}$), třída oceli a geometrické poměry. Metodika výrazně těžila z automatizace – Python skript generoval spojové konfigurace, řídil FEA výpočty přes API a prováděl komparaci výsledků, čímž eliminoval manuální chyby a zajistil reprodukovatelnost pro budoucí rozšíření studie.

Pro vizualizaci rozdílů bylo provedeno srovnání mezi stávající a novou generací normy EN. Výpočet únosnosti dutých profilů dle AISC se shoduje s aktuálním EN. Analýza ukázala, že při nezatíženém pásu poskytuje nový EN vyšší únosnost pro spoje typu K a T&Y 4.3, 4.6, 4.9, zatímco u spojů typu X byla zachována vysoká shoda s původní normou.

Srovnání metody CBFEM s normativními výpočty nejlépe ilustruje spoj typu X, kde síly v přípojích jsou v rovnováze a experimentální ověření je technicky nejsnáze proveditelné. Pro konfiguraci X/45°/S355 vykazují výsledky konzistentní shodu, avšak při úhlu 30° s tlakem v nosníku se objevuje výrazný rozptyl výsledků. To naznačuje složitější vliv namáhání pásu na únosnost, než normy popisují.

Nelineární vliv třídy oceli na únosnost v CBFEM byl zjištěn. Rozdíly v mezní deformaci (5% plastické přetvoření vs. 3% lokální deformace) a geometrická nelinearita aplikovaná ve výpočtech významně ovlivňují bod porušení, zejména při vyšších třídách oceli. Tento jev vyžaduje další výzkum pro specifikaci přesných vlivů na únosnost.

V rámci studie byla provedena optimalizace návrhu ocelového vazníku pro rozpětí 40m. Statický výpočet byl proveden přímo v prostředí Grasshopper díky pluginu

Kiwi!3D. Přepočet vnitřních sil byl proveden po každé iteraci. Celkem byly dva druhy parametrů: geometrické a průřezové. Geometrické: výška uprostřed, výška na konci a počet polí, celkem 3. Průřezové: různé průřezy pro horní a dolní pás, svislice, diagonály a koncové diagonály, celkem 5. Vyhodnocení po každé iteraci splnění podmínek únosnosti, stability, deformace a proveditelnosti následovalo. Pokud některý z parametrů nevyhověl, hmotnost vazníku se penalizovala a se měnila na velké číslo, což mělo za následek nepoužitelnost konkrétní konfigurace a tím pádem vyřazení z procesu. Pro optimalizaci byl použit Galapagos řešič [10], který je součástí prostředí Grasshopper.

ZÁVĚR

Srovnání norem potvrzuje, že nová generace EN je obecně méně konzervativní, zejména u spojů typu K s mezerou (při 30° a 80% tlaku v pásu rozdíl až 55%, 4.10). Zatímco normy redukují únosnost pouze pomocí zjednodušených funkcí, tato aproximace nemusí přesně zachycovat reálné chování. U tahových konfigurací je patrný výrazný rozdíl oproti EN/AISC, neboť nový EN zohledňuje redukci pro tah v pásu.

Srovnání s CBFEM ukazuje shodu při nezatíženém pásu, avšak při přítomnosti namáhání pásu vznikají významné rozdíly, naznačující potřebu zkoumat redukční funkce. Metoda CBFEM také vykazuje nelineární vliv třídy oceli na únosnost (oproti lineárnímu popisu v normách), což vyžaduje další výzkum.

Omezení studie: Analýza se omezuje na spoje CHS v rovině. Výsledky pro RHS jsou nedostatečné pro hodnocení chování. Konzistence zatížení pásu je limitována funkcí "Stop at limit strain" – skutečné zatížení kolísá (viz obr. 5.1).

Datová sada může být využitelná pro vývoj norem či strojové učení. Skript je veřejně dostupný na platformě GitHub[11].

Finální optimalizační konfigurace vazníku měla hmotnost 20kg/m^2, ale z důvodu návrhu přípojů některé průřezy musely být zvětšeny, aby vyhověly Hmotnost tím pádem se zvětšila na 35kg/m^2. Avšak návrh pomocí optimalizačních nástrojů například v prostředí Grasshopper má potenciál využití i při reálném návrhu, ale příprava celého cyklu výpočtu vyžaduje zkušenosti z důvodu odhadu některých okolností.

LASTOVETSKYI, Mykola. *STYČNÍKY UZAVŘENÝCH PRŮŘEZŮ: SROVNÁNÍ NÁVRHOVÝCH METOD*. Brno: Brno University of Technology, Fakulta stavební, ÚSTAV KOVOVÝCH A DŘEVĚNÝCH KONSTRUKCÍ, 2025, 137 p. Bachelor's Thesis. Advised by Ing. Martin Vild, Ph.D.

Author's Declaration

Brno . . . .

author's signature

Acknowledgement

I would like to express my gratitude to the supervisor of the bachelor's thesis, Mr. Ing. Martin Vild, Ph.D., for his professional guidance, consultation, patience and constructive suggestions for the thesis. In addition, I would like to express my gratitude to all those who provided me with their support. :)

Contents

List of Figures

List of Tables

Listings

Introduction

Motivation

The following text will present the results of a comparative analysis of design hollow cross sections steel connections, various methods, and the results of finite element analysis (FEA). This analysis promises to be of particular interest, as the analytical solution provided in the code standard for hollow section cross sections is based on the integration of FEA and experimental results. As computational power becomes increasingly accessible, the potential for conducting a greater number of simulations for diverse types of topology, cross-sections, loading, and other boundary conditions increases. The primary objective is to compare the results of the new generation

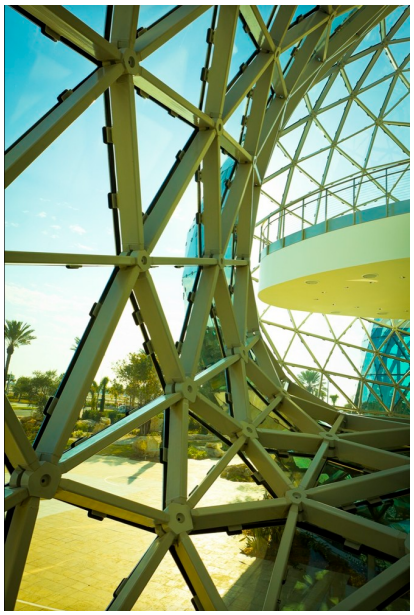

Fig. 1: Museum Spotlight: Dalí Museum in St. Petersburg FL, USA. Source: [12].

of the EN, scheduled for release no later than March 30, 2026 (Date of Availability - DAV)[1], with the existing standard EN 1993-1-8 [2] and the American standard AISC 360-22 [3], as well as the commercial software for analyzing connections IDEA StatiCa Connection [4].

Research Objectives

Hollow sections have found widespread application in all structural domains, ranging from residential housing to offshore and onshore structures. The primary factor contributing to their employment is their superior uniformity in terms of stability,

a quality that surpasses that of open sections. Additionally, they are more easily protected against corrosion than traditional sections and are more aerodynamic.

A comparison was facilitated through the utilization of Python programming language[5] for the calculation of analytical outcomes and the access of IDEA StatiCa Connection through the API[6]. A limited selection of connection types was chosen, and calculations were performed for various load conditions of the chord member and additional parameters, including the angle of the connected member and chord, and the steel grade of the connections. The employment of rapid time computation facilitated the assessment of the range of validity in accordance with the prevailing code standard. This capability enables a precise comparison of the standards, highlighting both the discrepancies and the commonalities across the entire study.

Scope and Limitations

The present study will focus exclusively on connection resistance, while the effects of welds and bolts on connection behavior are out of the scope of this study. For instance, a more exhaustive examination of the impact of welds and bolts on connection resistance can be found in the following reference: Willibald [13].

The present work focuses primarily on the pure resistance assessment code standards. The cases selected for comparison in this study are straightforward, as they are defined directly by the code. However, in engineering practice, more complex designs are often encountered. In response to these more intricate scenarios, codes may employ combinations of complex geometries as loads are applied. While this topic is noteworthy, it falls outside the scope of this particular study.

The employment of hollow cross-sections in concrete steel composite cross-sections is a salient advantage due to its widespread utilization in engineering practice, which simplifies concrete pouring and enables on-site execution without additional formwork. While this topic is undoubtedly intriguing, it falls outside the purview of this particular study.

Hollow section connections have gained significant popularity in the field of offshore and onshore structures. However, when employed in the context of fluid waves, their use necessitates a comprehensive consideration of fatigue design. The complexity of the geometry may present a significant challenge, necessitating the calculation and consideration of whole lifetime to ensure the structure's resistance to all anticipated loads. These considerations, however, extend beyond the primary scope of this study.

This analysis does not take into account the extant research on the behavior of connections under varying tolerance conditions. For instance, each code design

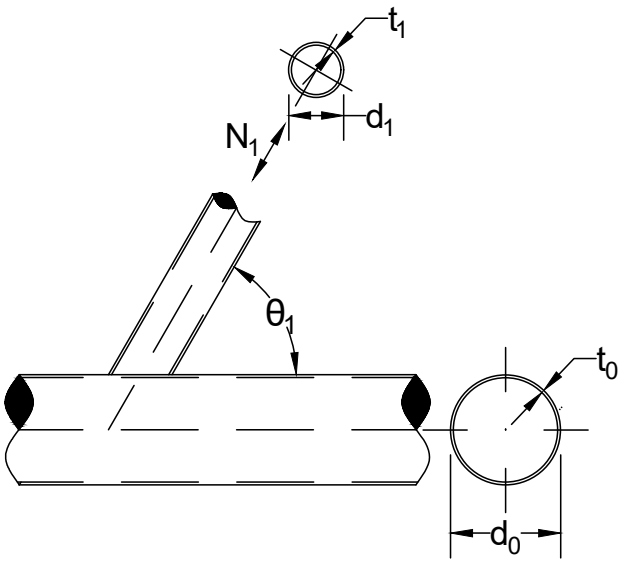

Fig. 2: CHS T connection

incorporates a certain degree of tolerance, both real and nominal. Therefore, it is imperative that the code design be sufficiently robust to accommodate such circumstances. For a more thorough examination of this topic, please refer to the following source: CIDECT DG1 [14].

Optimization of the roof truss

This work also presents the calculation of the duo-pitch roof truss for a span of 40m and 5m distance between roof trusses. Total length of the structure was considered as 60m located in the Brno city region.

The primary objective of the calculation is to employ an optimization method to achieve optimal roof weighting. This objective was accomplished through the utilization of parametric modeling and the implementation of genetic algorithms.

The calculation was performed using the Grasshopper programming language [7], which is based on the Rhinoceros commercial software [15]. This approach enables rapid parametric geometry modeling. The calculation of the internal forces was also

conducted in Grasshopper using the Kiwi!3D plugin for structural analysis [8]. The final result calculation's corresponding drawings are also provided.

Optimization assumptions

In each iteration of the roof truss optimization, a recalculation of internal forces was conducted, and a structural examination was performed to ascertain the alignment of the design with resistance, stability, and feasibility criteria. The roof truss's topology was pre-designed, and its use of cross-sections and geometric parameters was facilitated. The geometrical parameters that are susceptible to modification include the end height, the middle height, and the number of fields in the truss. A range of cross-sectional parameters were identified as candidates for modification, including alterations to the cross-sections of the top and bottom chord, diagonals (with the exception of end diagonals), end diagonals and struts.

1 Literature Review

1.1 Existing Design Methods

The present design process employs limit state design (also known as Load Resistance Factor Design, LRFD in AISC notation), wherein loads are factorized, and certain coefficients and resistances are divided by material properties uncertainties coefficients. This ensures that the probability of failure is equivalent to 10^{-5}, as required by the current EN code [16]. This methodology is expected to account for the uncertainty of the load mode and resistance prediction. Consequently, resistance is partitioned from material partial safety factors (γ_m) and resistance partial safety factor γ_{m5} for hollow cross section connection design.

As stated in the CIDECT DG 1 [14] in general EN $1/(\gamma_m)$ is almost equal to AISC ϕ. This finding underscores the common ground shared by these methodologies.

As for all the methods, they have the requirements for the ductility of the connection as stated in EN 1993-1-8 [2], the nominal yield strength f_y should not be greater than 80% of the nominal tensile strength f_u.

Hollow cross section joints are susceptible to multiple failure mechanisms, which depend on the geometry of the joint (e.g., diameter, wall thickness, brace-to-chord ratios) and the type of loading (e.g., axial compression, axial tension, bending). Understanding these failure modes is critical for designing safe and efficient structures, particularly in offshore, bridge, and space-frame applications where CHS joints are widely used. Design codes provide equations to predict failure loads for specific modes (e.g., chord plastification). However, these codes primarily address compression-dominated failures at member intersections. They may overlook interactions between failure modes (e.g., buckling triggering plastification). Simplifying joints as rigid in the global model and ignoring lateral joint flexibility (LJF), possible deformation in joint affected by loading, may lead to unsafe design without reserve capacity in structure design. While LJF is not a failure mode itself, it redistributes stresses and can accelerate failure (see Asgarian et al. [17] for quantification methods).

The CIDECT Design Guide underscores the fact that joint resistance formulae are constrained by particular validity ranges, which mirror the empirical boundaries of their underlying experimental or numerical validation CIDECT DG 1 [14]. These ranges ensure that the intended failure mechanism governs the design and streamline the design process by eliminating unclear failure mode interactions. While joints exceeding these prescribed limits are allowed, they often exhibit reduced joint efficiency and require strict engineering verification due to unpredictable failure mechanisms CIDECT DG 1 [14].

The design codes explicitly presents geometric constraints and validity limits for each joint type to assist designers in maintaining code-compliant solutions. For example basic requirements of the EN 1993-1-8 for CHS to CHS member connections:

$$\begin{aligned} &0.2 \leq d_i/d_0 \leq 1.0 \\ &10 \leq d_0/t_0 \leq 50 \\ &d_i/t_i \leq 50 \end{aligned} \tag{1.1}$$

Important geometrical aspect is brace connection angle, for possible connection assembly at least $\theta > 30°$ required. For the lower-angle construction assembly, the connection may be problematic, and the welding of the modified tube end could also pose challenges, stated in CIDECT DG 1 (2008) [14].

In K-type joints, where tubes are connected in the same plane, it is imperative that a gap is left between the tubes to facilitate the welding process. The term *gap* is defined as follows:

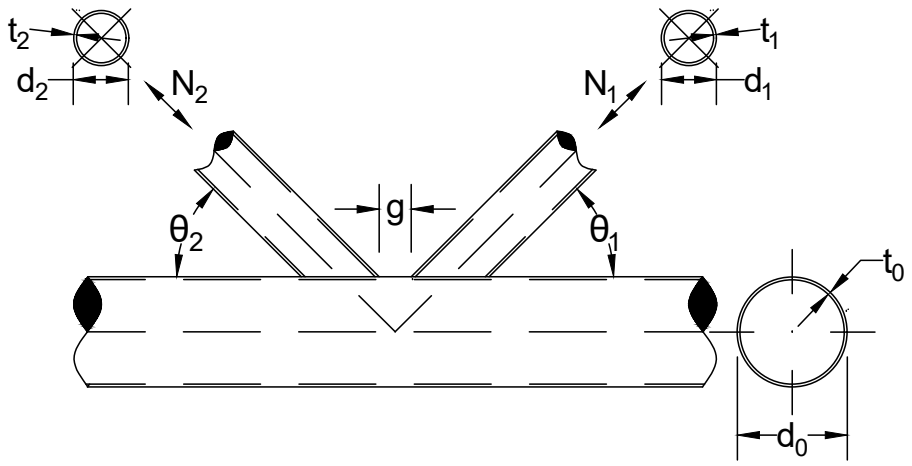

Fig. 1.1: CHS K connection, *gap* can be observed

$$g \geq t_1 + t_2 \tag{1.2}$$

For the K joints, where CHS are overlapping, overlap needs to be at least 25%, overlap is calculated as:

$$\lambda_{ov} = \frac{q}{p} \tag{1.3}$$

In the context of assessing the resistance of hollow cross-sections, the relevant code specifies six distinct failure modes. The predominant engineering practice is characterized by two fundamental mechanisms: chord plastification and shear of the wall. This enhancement is attributed to its adaptability in handling high-strength steels, a category for which conventional classification methods prove ineffective due to the unique properties of the materials.

The failure of the hollow cross-section can occur under different conditions, depending on the cross-section parameters and the configuration of the connection. To address this, the code must define specific failure modes that may occur and the range of validity for the connected member and the configuration of the connection. The development of a model for each failure mode is predicated on assumptions about that failure mode, with the objective of providing resistance to the connected members. The developed failure models were verified by experiments and numerical simulations to get simple and, more importantly, safe resistance that can be used in structural civil engineering daily practice.

Code design also facilitates the consideration of loading on the chord member, a common practice in civil engineering. These members are subjected to loading and undergo stress, which influences overall connection resistance and, consequently, reduces resistance. In this study, a comparison of these scenarios is also provided, although experimental validation is challenging due to the complexity of certain loading conditions, for example, the combination of bending moment and axial force. Therefore, it can be posited that outcomes exhibiting minimal stress on the chord member, resulting from pre-loading, are the most realistic. However, a comparison of the manner in which codes address this issue is one of the objectives of this work.

1.2 Codes limitations

In this section, we examine the limitations inherent in the current codes. The key difference among these codes is the maximum allowable steel grade used in calculations. The new generation of EN codes, for instance, can utilize steel grades with a yield strength of up to 700 MPa. This is a significant improvement when compared to the 360 MPa limit of AISC 360-22 and the 460 MPa limit of EN 1993-1-8.

AISC 360-22 and EN 1993-1-8 use similar methodologies to compute stress at the chord. They consider compression stress, the axial force stress at the connection

point, and the bending moment at the connection point, using elastic resistance only. However, both codes do not account for tension stress at the brace connection point.1.4

$$n_p = \frac{N_{0,Ed}}{A_0} + \frac{M_{0,Ed}}{W_{el,0}} \tag{1.4}$$

In contrast, the new generation of EN 1993-1-8 incorporates a different approach. It calculates the compression stress at the connection point as the sum of the axial force compression and the bending moment, using the plastic bending resistance.1.5 Moreover, it acknowledges that tension stress plays a role in determining the overall resistance.

$$n_p = \frac{N_{0,Ed}}{A_0} + \frac{M_{0,Ed}}{W_{pl,0}} \tag{1.5}$$

EN Code

The primary assumptions of the EN code will be considered first. The material properties are set at a maximum of fy 460 MPa, and the geometrical properties are specified in Table 7.1 of EN 1993-1-8 [2]. While the CIDECT DG 1 [14] asserts the feasibility of designing joints within this range of validity, it does not guarantee that the failure mode will remain consistent with the expected outcomes. The code imposes a clear limitation on the angle connection, $\theta > 30°$, and it also stipulates limitations for cross-section classes 1 and 2 to ensure that local buckling does not affect the resistance. The minimum thickness requirement for the tube is 2.5mm, and the maximum is 25mm, unless special measurements are indicated to ensure that the through thickness properties of the material are not significantly different EN 1993-1-8 7.1.1 - (2) [2].

Resistance reduction based on the chord stress:

$$\begin{aligned} &n_p = \tfrac{N_{0,Ed}}{A_0} + \tfrac{M_{0,Ed}}{W_{el,0}} \\ &\text{For } n_p > 0 \text{ (compression)}: \quad k_p = 1 - 0,3n_p\,(1 + n_p) \text{ but } k_p \leq 1,0 \\ &\text{For } n_\mathrm{p} \leq 0 \text{ (tension)}: \quad k_\mathrm{p} = 1,0 \end{aligned} \tag{1.6}$$

AISC

In this text, AISC 360-22 code standard will be compared; although the edition of the code is more actual compared to the EN code standard [2], it shows concordance with it. It can be noticed that design is complying with CIDECT design guide. But one of the main differences is that the maximum steel grade to account with is F_y = 52ksi(360MPa). It is evident that geometrical parameters for limitations in connection design are closely aligned with the EN code standard. In addition, AISC 360-22 establishes that connections which do not adhere to the stipulated limits of

applicability are not inherently prohibited; rather, they must be designed through rational analysis.

Resistance reduction based on the chord stress:

$$\begin{gathered}\text{For HSS chord member connecting surface in tension, } Q_f = 1 \\ U = \left|\frac{P_{ro}}{F_c A_g} + \frac{M_{ro}}{F_c S}\right| \leq 1.0 \\ Q_f = 1 - 0.3U(1+U) \leq 1.0\end{gathered} \tag{1.7}$$

Fpr EN

The EN as new generation provides a greater number of possibilities in terms of connection design. Primarily, it explicitly allows for the use of high-strength steel up to S700, which constitutes a significant enhancement to the design. The new generation of the EN will allow the use of tube thicknesses from 1.5 mm, thus enabling the utilization of a larger range of cold-formed sections. The new generation of EN code also defines the minimal throat thickness of the weld as $a \geq 3$mm. However, lower thickness can also be used in cases where weld resistance is higher than cross-section design resistance per unit length of the perimeter. The new code employs a different approach for defining reducing resistance due to chord stresses; it is now based on the following table:

Tab. 1.1: Chord Stress Function Parameters for Joint Configurations

Brace and Plates	Chord	$Q_{\mathrm{f,min}}$	C_1[e] T-, Y- & X- Compression ($n_0 < 0$)	C_1[e] T-, Y-& X- Tension ($n_0 \geq 0$)	C_1[e] K -& N - gap[d] Compression ($n_0 < 0$)	C_1[e] K -& N - gap[d] Tension ($n_0 \geq 0$)
CHS	CHS	0,4	0,45-0,25 β	0,2	0,25 [a]	$0,2^{a}$
Plates [b]	CHS	0,3	0,25	0,2	-	-
CHS or RHS	RHS	0,4	0,6-0,5 β	0,1	$0,5 - 0,5\beta \geq 0,1$	0,1
Longitudinal plates	RHS	0,3	0,2	0,1	-	-
Transverse plates [c]	RHS	0,3	0,03 γ	0,1	-	-

a If brace moments have to be considered C_1 and the minimum chord stress function $Q_{\mathrm{f,min}}$ for T$-$, Y - and X-joint configurations should be adopted.

b Longitudinal, transverse plates, I or H sections and RHS.

c Also applies to I or H sections and RHS.

d Joint configuration with gap acc. to Equation 1.2

e Exponent C_1 for joint configurations with chords loaded in compression and in tension acc. to Equation 1.8

$$Q_{\mathrm{f}} = (1 - |n_0|)^{C_1} \geq Q_{\mathrm{f,min}} \tag{1.8}$$

As illustrated in the table, the connection type exerts an influence on the reducing function, $Q_f(n_0)$. Moreover, a clearer definition has been established for the point at which stress should be checked for the reducing function. Additionally, tension normal stress is now a factor in reducing connection resistance.

In contrast to the prevailing EN code standard, one modification is the explicit allowance of cross-section class 3 for chord members only experiencing tension stresses. This necessitates a modification of the Equation 1.5 to account for the elastic limit of bending:

$$n_p = \frac{N_{0,Ed}}{A_0} + \frac{M_{0,Ed}}{W_{el,0}} \tag{1.9}$$

The implementation of these novel enhancements has enabled the conceptualization of high-strength steels, albeit necessitating intricate manual calculation procedures.

1.3 Previous Comparative Studies

As previously stated, analytical solutions introduced in design codes and recommendations are based on the curve-fitting functions of experimental and numerical results. One of the most significant contributions is attributed to Kurobane et al. [18], in which the researchers utilized experimental results of X, T connection and performed linear regression of the results in combination with ring model theory which consequently resulted in equations.

Wardeniere's [19] study constitutes a noteworthy contribution to the field, as it integrated the influence of chord stress on resistance. The experimental database, linear regression of the results, and the ring model theories developed by Togo [20] and Washio et al. [21] were utilized in his research. This combination resulted in the definition of analytical solutions. This solution is analogous to that of Kurobane et al. [18], yet it incorporates a reduction of the resistance in the form of a stress function, $f(n)$. This reduction is subsequently incorporated into the final equations.

Consequently, Lu et al. [22] made another significant contribution to the development of hollow section joint resistance. In his work, he described the importance of the pure resistance factor and the impact of local deformations on resistance. It is imperative to acknowledge the significance of incorporating these factors into the analysis and constraining the chord local deformation to a maximum of 3%. Subsequent numerical simulations of rectangular hollow sections (RHS) by Kosteski et al. [23] demonstrated that connections loaded in tension with values of $\beta < 0.6$ exhibited lower resistance than analytically predicted for local deformation failure. Conversely, connections with values of $\beta > 0.6$ demonstrated behavior aligned with the analytical solution. Where $\beta = \frac{b_1}{b_0}$.

The development of the hollow section resistance was significantly impacted by the CIDECT organization [24], which was established by steel hollow section fabricators. This initiative has successfully convened a diverse group of researchers, facilitating a comprehensive examination of behavioral phenomena. The initiative has produced design guides that are widely acclaimed for their practical recommendations. These guides are particularly pertinent to engineers specializing in areas such as resistance determination, fatigue analysis, and structural feasibility assessment.

It is also important to acknowledge a study that recommended simplifying the CHS-CHS connection and examined its impact on resistance, CIDECT report 5AH - 85 / 1E [25]. In the modern era, however, this subject is not very relevant due to technological advancements in CHS cross-section cutting, which have significantly decreased costs and made proper cutting relatively straightforward.

Modern trends in the development of hollow cross-section resistance are focused on the utilization of high-strength steels, which, being non-ductile, exhibit different behavior. Consequently, a thorough investigation into this phenomenon is imperative. For instance, the process of brittle fracture, localized buckling, and welding of these steels is a formidable task, which is not without significant difficulty. The utilization of high-strength steel in construction results in a number of advantages, including a reduction in material consumption when compared with the use of mild steel.

1.4 Ring model theory

The ring model serves as the theoretical foundation for plate-to-CHS and CHS-to-CHS connection design methodologies. While connection plastification behavior resists full analytical characterization through classical yield line models due to complex three-dimensional curvature, the ring model addresses this through strategic simplifications:

- **Geometric Simplification**: The curved connection surface is reduced to a two-dimensional ring structure with plastic hinges distributed over an effective length B_e, Togo [20].
- **Loading Idealization**: Concentrated branch forces are replaced by distributed line loads acting over B_e, as shown in Figure 1.2.
- **Compensation Factor**: B_e simultaneously accounts for both geometric simplification and load distribution approximations, calibrated through regression analysis of experimental/numerical data.

Notably, normal forces in the chord longitudinal direction remain excluded from the ring model formulation, being addressed separately in design equations. Two

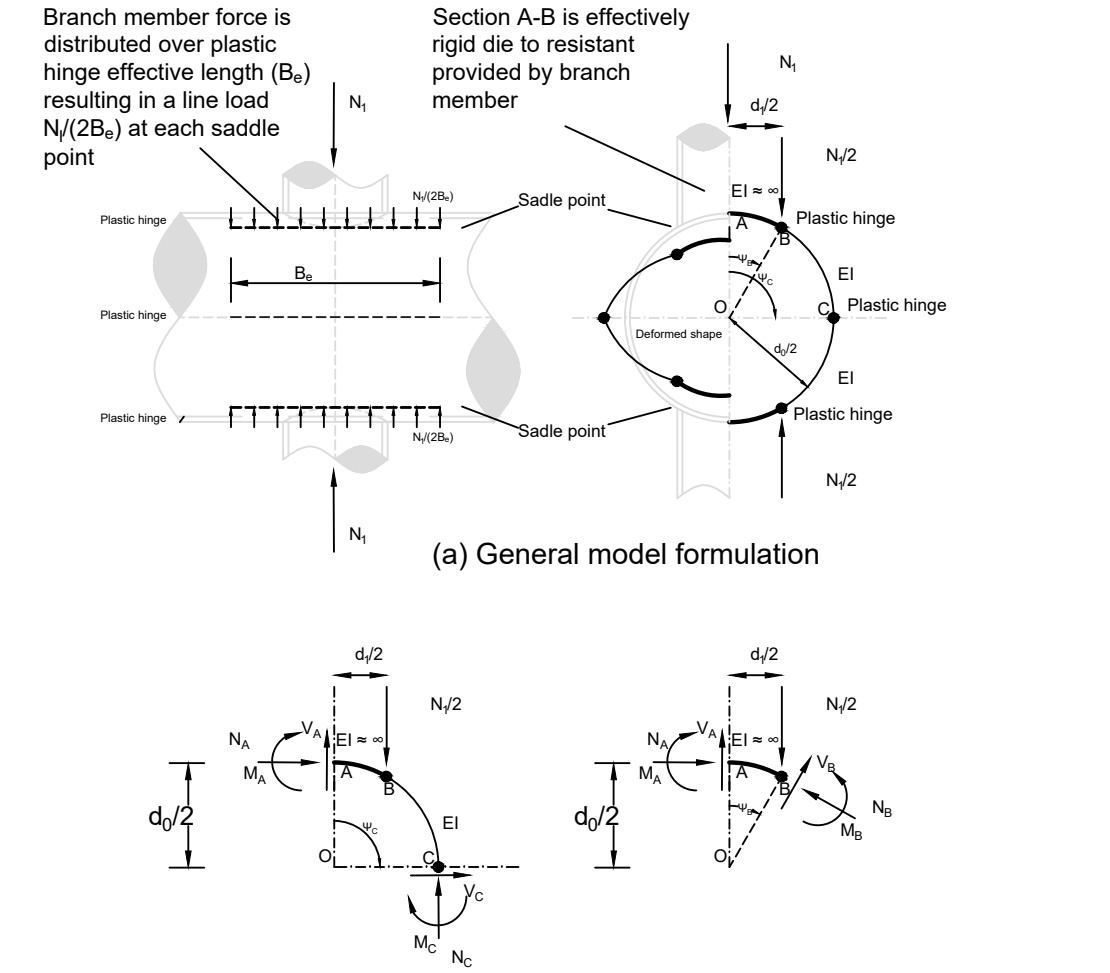

Fig. 1.2: Analytical model for axially loaded X-type connections (adapted from van der Vegte; Wardenier) [26] [19]

primary ring model variants have emerged [26]:

$$\begin{cases} \text{Exact Model: } f(M,V,N) & \text{(Considers moment-shear-axial interaction)} \\ \text{Simple Model: } f(M) & \text{(Moment-only formulation)} \end{cases} \tag{1.10}$$

The simplified model's computational efficiency made it prevalent in early design codes Kurobane et al.[18, 27], Wardenier et al. [19]. However, its instability at width ratios $\beta \to 1.0$ necessitates the exact formulation's enhanced accuracy. Subsequent sections detail both models' derivations for X- and T-type CHS connections.

$$\text{Simple Model: } M_{\text{ult}} = f(B_e, \sigma_y, ...) \tag{1.11}$$

$$\text{Exact Model: } F_{\text{cap}} = g(M, V, N, \beta) \tag{1.12}$$

1.5 Ring model equilibrium equations

To derive expressions for axial forces (N: tangential to the ring surface), shear forces (V: normal to the ring surface), and bending moments (M) at plastic hinge locations i, the equilibrium of ring segments is analyzed. Free body diagrams of sections A-B and A-C (Figures 1.3 and 1.4), with a positive sign convention aligned with the assumed force directions at hinge points, yield two sets of equilibrium equations. The plastic moment direction alternates between adjacent hinges (hogging or sagging) in the assumed yield model, resulting in opposing moments at hinges B and C, which are incorporated into the equations. General equilibrium expressions are formulated below, with plastic hinges assumed at point B (saddle connection: $\psi_{\text{B}} = \sin^{-1}\beta$) and point C ($\psi_{\text{C}} = \pi/2$). For plastic hinge B (section A-B), the equilibrium equations

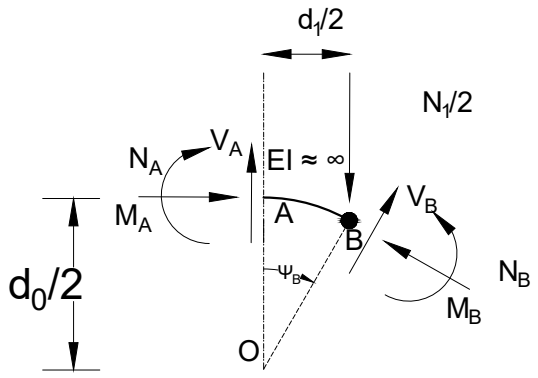

Fig. 1.3: A-B section (adapted from van der Vegte; Wardenier) [26] [19]

are:

$$\begin{aligned} &\Sigma \text{N}_\text{B} = 0: \\ &\text{N}_\text{B} + \text{V}_\text{A} \sin\psi_\text{B} - \text{N}_\text{A} \cos\psi_\text{B} - \tfrac{\text{N}_1}{2} \sin\psi_\text{B} = 0 \end{aligned} \tag{1.13}$$

$$\begin{aligned} &\Sigma \text{V}_\text{B} = 0: \\ &\text{V}_\text{B} + \text{V}_\text{A} \cos\psi_\text{B} + \text{N}_\text{A} \sin\psi_\text{B} - \tfrac{\text{N}_1}{2} \cos\psi_\text{B} = 0 \end{aligned} \tag{1.14}$$

$$\begin{aligned} &\Sigma \text{M}_\text{B} = 0: \\ &\text{M}_\text{B} - \text{M}_\text{A} - \text{V}_\text{A} \tfrac{\text{d}_1}{2} - \text{N}_\text{A} \tfrac{\text{d}_0}{2} (1 - \cos\psi_\text{B}) = 0 \end{aligned} \tag{1.15}$$

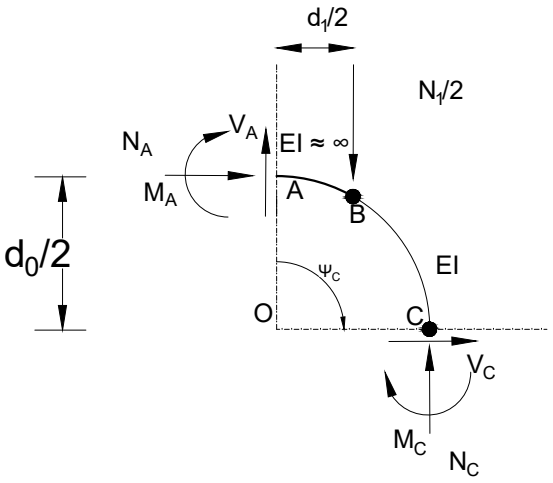

Fig. 1.4: A-C section (adapted from van der Vegte; Wardenier) [26] [19]

For plastic hinge C (section A-C), the equilibrium equations are:

$$\begin{aligned} &\Sigma \mathrm{N_C} = 0 : \\ &\mathrm{N_C} + \mathrm{V_A} \sin\psi_\mathrm{C} - \mathrm{N_A} \cos\psi_\mathrm{C} - \tfrac{\mathrm{N_1}}{2} \sin\psi_\mathrm{C} = 0 \end{aligned} \tag{1.16}$$

$$\begin{aligned} &\Sigma \mathrm{V_C} = 0 : \\ &\mathrm{V_C} + \mathrm{V_A} \cos\psi_\mathrm{C} + \mathrm{N_A} \sin\psi_\mathrm{C} - \tfrac{\mathrm{N_1}}{2} \cos\psi_\mathrm{C} = 0 \end{aligned} \tag{1.17}$$

$$\begin{aligned} &\Sigma \mathrm{M_C} = 0 : \\ &\mathrm{M_C} + \mathrm{M_A} + \mathrm{V_A} \tfrac{\mathrm{d_0}}{2} \sin\psi_\mathrm{C} + \mathrm{N_A} \tfrac{\mathrm{d_0}}{2} (1 - \cos\psi_\mathrm{C}) - \tfrac{\mathrm{N_1 d_0}}{4} (\sin\psi_\mathrm{C} - \sin\psi_\mathrm{B}) = 0 \end{aligned} \tag{1.18}$$

Substituting known parameters ($\mathrm{N_A} = 0$, $\mathrm{V_A} = 0$, $\sin\psi_\mathrm{B} = \beta$, $\cos\psi_\mathrm{B} = \sqrt{1-\beta^2}$, $\sin\psi_\mathrm{C} = 1$, $\cos\psi_\mathrm{C} = 0$) simplifies Equations 1.13–1.15).

For hinge B:

$$\begin{aligned} \mathrm{N_B} &= \tfrac{\mathrm{N_1}}{2} \sin\psi_\mathrm{B} = \tfrac{\mathrm{N_1}}{2} \beta \\ \mathrm{V_B} &= \tfrac{\mathrm{N_1}}{2} \cos\psi_\mathrm{B} = \tfrac{\mathrm{N_1}}{2} \sqrt{1-\beta^2} \\ \mathrm{M_B} &= \mathrm{M_A} \end{aligned} \tag{1.19}$$

For hinge C:

$$\begin{aligned} \mathrm{N_C} &= \tfrac{\mathrm{N_1}}{2} \sin\psi_\mathrm{C} = \tfrac{\mathrm{N_1}}{2} \\ \mathrm{V_C} &= \tfrac{\mathrm{N_1}}{2} \cos\psi_\mathrm{C} = 0 \\ \mathrm{M_C} &= -\mathrm{M_A} + \tfrac{\mathrm{N_1 d_0}}{4} (1 - \beta) \end{aligned} \tag{1.20}$$

The plastic capacities (axial, shear, moment) for rectangular cross-sections (thickness t_0, effective hinge width B_e) under the von Mises criterion are:

$$\mathrm{N_p} = \mathrm{f_{y0}} t_0 B_e \tag{1.21}$$

$$\mathrm{V_p} = \frac{1}{\sqrt{3}} \mathrm{f_{y0}} t_0 B_e \tag{1.22}$$

$$\mathrm{M_p} = \frac{1}{4} \mathrm{f_{y0}} t_0^2 B_e \tag{1.23}$$

1.6 Simple ring model

The development of the simple ring model disregards the impact of shear and axial forces at each plastic hinge location, focusing exclusively on expressions for plastic hinge moment behavior (see Equations 1.15 and 1.18). It can be demonstrated that Equations 1.15 and 1.18 become Equations 1.24 and 1.25 establishing the equivalence $M_i = M_p$ for all values of i from B to C. This is achieved by a rearrangement of the equations for $\mathrm{M_A}$.

$$M_A = \frac{1}{4} f_{y0} t_0^2 B_e \tag{1.24}$$

$$M_A = \frac{N_1 d_0}{4}(1-\beta) - \frac{1}{4} f_{y0} t_0^2 B_e \tag{1.25}$$

By setting Equations 1.24 and 1.25 equal to each other and solving, a simplified analytical expression for the strength of an axially loaded X-type connection ($\mathrm{N_1}$) is given by:

$$\frac{\mathrm{N_1\ d_0}}{4}(1-\beta) - \frac{1}{4}\mathrm{f_{y0}} \mathrm{t_0^2\ B_e} = \frac{1}{4}\mathrm{f_{y0}} \mathrm{t_0^2\ B_e} \tag{1.26}$$

$$\frac{\mathrm{N_1\ d_0}}{4}(1-\beta) = \frac{1}{2}\mathrm{f_{y0}} \mathrm{t_0^2\ B_e} \tag{1.27}$$

$$\mathrm{N_1} = \frac{2\mathrm{f_{y0}} \mathrm{t_0^2} (\ \mathrm{B_e/d_0})}{1-\beta} \tag{1.28}$$

1.7 Numerical Modeling in Structural Engineering

Since the 1970s, numerical simulation utilizing the finite element method (FEA) has become a staple in structural engineering due to its ability to calculate the load and geometry of complex structures through mathematical approximations of structural behavior.

In the domain of hollow section connections, this method is employed extensively due to the necessity of assessing the connection resistance for topologies, a task that is not straightforward and cannot be adequately addressed through design recommendations defined in code standards. In such circumstances, the question arises of how to accurately define the resistance of the connection. In contemporary practice, recommendations are being made with the understanding that the connection is to

be reinforced with a certain degree of plasticity. This is defined as a maximum of 5% plastic strain in the connection, and with local deformation limited to 3%. This limitation has the effect of simplifying the practice of engineers and leading to the safe design of systems and equipment. A compendium of recommendations has been established to delineate the types of finite element analysis (FEA) elements that can be utilized and the corresponding material models that should be employed.

Although finite element analysis (FEA) can result in safe and proper designs, it is often too complicated or time-consuming for daily engineering practice. In the context of finite element analysis (FEA) simulations, there is a need to ensure that parameters such as mesh size and sensitivity are appropriately configured. The simulation of weld resistance constitutes an additional challenging aspect of the process. The structural civil engineering community's current practice is to utilize this method exclusively in instances where code recommendations are not provided for a particular topology or other boundary conditions that impact the design.

It is imperative to acknowledge that the utilization of sophisticated tools for effective analysis is often not financially accessible to structural civil engineers in practice.

1.8 CBFEM method

IDEA StatiCa Connection employs a component-based finite element method (CBFEM) [28], a synthesis of the component method and finite element method. Plates and cross sections are 2D shell elements, while bolts and welds are 1D spring elements. This approach facilitates the calculation of stress for nonstandard geometries and loadings. It also enables the definition of resistance through the component method. Consequently, the results can be interpreted in accordance with code standards. CBFEM employs the CM2 mesher [30]. A benefit of CBFEM is its utilization of condensed elements, which possess exclusively elastic material properties. This methodology minimizes the length of shell elements necessary for finite element analysis (FEA) computations, thereby expediting the calculation process. This development is particularly advantageous for hollow sections, which exhibit sensitivity to member length. In accordance with the recommendations of certain authors, the length of the model should be designated as $4 \cdot d_0$ for 3D elements, see Kožich [31].

The default CBFEM length of the shell member is equivalent to $1.25 \cdot d_0$; meanwhile, the length of condensed elements is equivalent to $4 \cdot d_0$ [29].

Also CBFEM is utilizing reduction of the shell bending resistance for hollow sections, as stated [32] to capture initial imperfections and residual stresses. Reduction is based on $\gamma = \frac{d_0}{2 \cdot t_0}$.

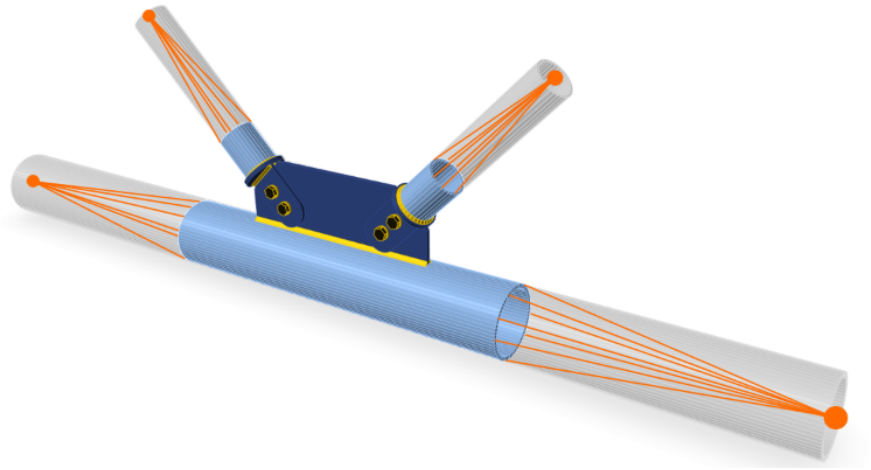

Fig. 1.5: Condensed elements implemented in CBFEM [29]

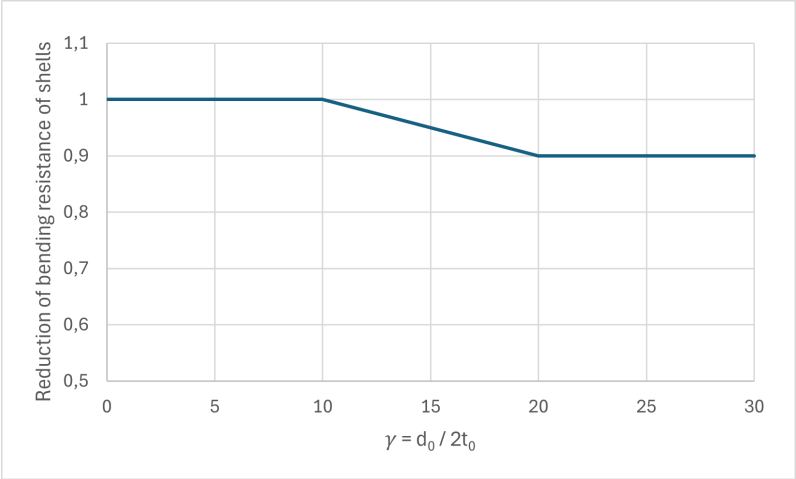

Fig. 1.6: CBFEM shell bending resistance reduction [32]

The CBFEM method for the calculation of hollow sections involves the reduction of f_y in accordance with the recommendation of EN 1993-1-8 [2]. For $f_y > 355$MPa, the reduction factor is set at 0.9. The CBFEM method aligns with the recommendation outlined in EN 1993-1-14, which stipulates that the limit on plastic strain, for a value of $f_y > 460$MPa, is set at 1%.

2 Methodology

2.1 Code Selection and Scope

In order to facilitate a valid comparison in this study, all codes were selected to employ identical cross-sections and material properties. The calculated resistance used for comparison is characteristic; no design resistance factors were applied. Consequently, the resistances can be evaluated in relation to one another and in conjunction with the results of the finite element analysis (FEA).

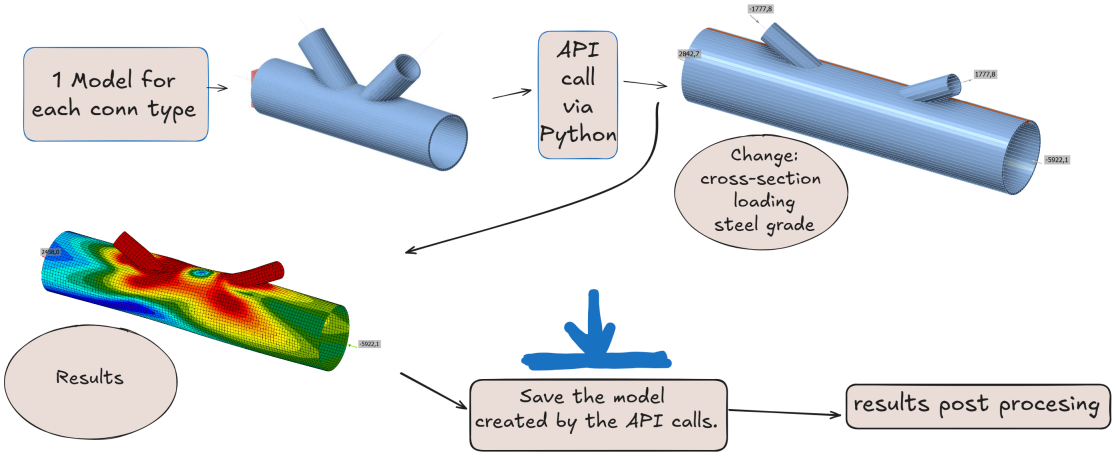

Fig. 2.1: Calculation workflow via Python API

To ensure the creation of clear, efficient code and to minimize redundancy, each design code and geometry type was represented as a configuration tailored to its specific requirements, implemented using .yaml files [9]. YAML is a human-friendly data serialization language for all programming languages, significantly reduced complexity and enhanced the overall clarity of the code.

A comparison will be provided exclusively for the standardized connection type of X, T, and Y, as well as for K, the resistance by normal force. The range of validity for each code applied to the generation of connection pairs is a comprehensive spectrum. However, for the X and K connections, for purpose of the simplification, the brace members had equivalent cross-sections and angles of intersection $\theta_1 = \theta_2$, $d_1 = d_2$, and $t_1 = t_2$. It is noteworthy that for the K connection type, there are only scenarios in which the brace members do not intersect, means only gapped K connections were considered. In these scenarios, the gap distance satisfies the conditions for $g \geq t_1 + t_2$.

The initial phase of the procedure was the generation of connection pairs. These connection pairs are derived from the table of cross-sections. The following example illustrates a table of connection pairs that were retrieved from IDEA StatiCa Connection, see Listings 2.1.

Listing 2.1: Example CSV table with cross-section data

```
"MPRL table v3.0"
"TableName";;"CHS(cf)"
"TableType";"CrossSection"
"Group";"#LNG003"
"TableParam1";"CircularHollow"
;;
"Header";"ElementID";"D";"t";"Fabrication"
"Unit";;"mm";"mm";
"UnitCoeff";;0,001;0,001;
"Data"
"CHS(cf)21.3/2.0";"{d7a1bac2-0dcc-4d9d-a5f4-0c948dbad64f}
   ";21,3;2;3
```

Subsequently, each combination was examined to ascertain its conformance with the established range of validity for each design code, see Listings 2.2. Subsequent to the generation of pairs that satisfied all conditions, steel grade was incorporated, and cross-section classes were calculated. This is imperative for the detection of local buckling failure modes, as stipulated by EN 1993-1-8, which dictates that the connection class of the brace member must not exceed 2. Consequently, resistance values were determined by calculating the YAML instructions for each individual design code. It is imperative that the examination of the connection's resistance is limited to the axial resistance of the brace member. In instances where the condition was not met, the resistance of the connection was higher than resistance of the brace member by axial force, the connection pair was excluded from the process. It should be noted that the ability to exclude connection pairs based on different criteria is also present. For example, EN 1993-1-8 explicitly defines the range of CHS thickness that is allowed to be calculated. Therefore, these conditions can be checked if they are included in the YAML instruction.

Listing 2.2: Example YAML instruction for validity condition check

```
validity_conditions:
  - (d_1 / d_0) >= 0.2
  - (d_1 / d_0) <= 1.0
  - (d_0 / t_0) >= 10
  - (d_0 / t_0) <= 50
  - (d_1 / t_1) <= 50
```

Consequently, analytical resistance by code was calculated. The development of a script was necessary for the purpose of obtaining information about the cross-sections of the members of the application programming interface (API) [33] calling

IDEA StatiCa Connection software. The most important task was to set the loading. The necessity of establishing a pre-loading requirement on the chord was determined in order to achieve the desired stress and study the influence of those factors on the connection resistance behaviour. Therefore, the loads were established, and equilibrium was achieved within the joint for every connection generated.

In order to achieve the desired resistance in the finite element analysis (FEA) calculation, the *Stop at Limit Strain* functionality was employed. During the analysis, loads are applied incrementally. The functionality permits the interruption of the analysis upon the occurrence of either the limit plastic strain of 5% or the limit local deformation of 3%. In such cases, the analysis returns *the percentage of the applied load*.

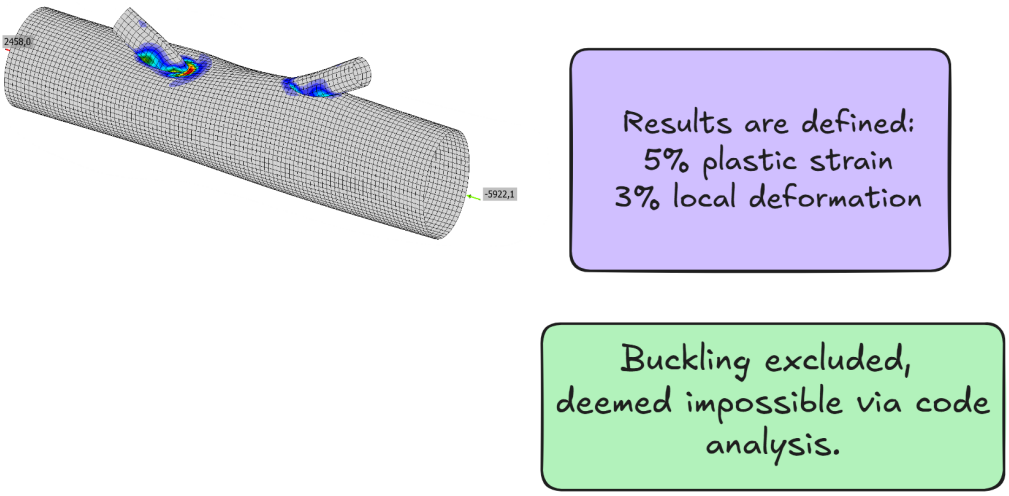

Fig. 2.2: CBFEM resistance definition

In the initial phase of the calculation, the validity of the connection was examined. The end moment, which was derived from loads necessary for equilibrium, was initially assessed to ascertain whether it would result in failure at the end of the chord member. In order to execute the procedure, the length from the theoretical point of intersection was first calculated. Thereafter, the check was performed with the actual applied bending moment and shear force. It is imperative to note that this test was applied before the calculation. The validity of this check is restricted to the T&Y connections. In the case of the X connection, the application of vertical force is not necessary to achieve a state of equilibrium, and the end moment remains uninfluenced.

Consequently, maximum strain checks were conducted to ascertain the maximum strain on the chord member. In the event that this condition was not met, exact connections were excluded from the evaluation. It was assumed that in case of the

more significant plastification of the brace member connection resistance is limited to the brace member resistance.

Listing 2.3: Example YAML instruction for CHS T resistance calculation

```
equations:
  betta: d_1/d_0
  gamma: d_0 / (2 * t_0)
  np: (N_chord/A_0 + M_chord/W_0)/ fy_0

  kp: >
    1 if np > 0 else
    (1 - 0.3 * np * (1 + np))
  Nrd_chord_plastificaction: ((( (gamma ** 0.2) * kp * fy_0 *
      (t_0 ** 2) ) / math.sin((thetta_1 * math.pi / 180.0)))
     * (2.8 + 14.2 * (betta ** 2) ))

  Nrd_shear: ((1 / math.sqrt(3)) * fy_0 * t_0 * d_1 * math.pi
      * ((1 +  math.sin(thetta_1 * math.pi / 180.0) ) / (2 *
     ( math.cos(thetta_1 * math.pi / 180.0)**2 ))))

  Nrd_shear_cond: >
    Nrd_shear if d_1 < (d_0 - (2 * t_0)) else
       Nrd_chord_plastificaction

  Nrd: min(Nrd_shear_cond, Nrd_chord_plastificaction)
```

The subsequent step in the CHS-to-CHS connection process involved the verification of the weld FEA element. It should be noted that this information is not directly accessible from the graphical user interface (GUI) of IDEA StatiCa Connection. Instead, it is only available via a direct API call of the raw results. Consequently, in instances where the quantity of parts was found to be less than expected, the connection was excluded from the evaluation process. This suggests the possibility that the weld segments are not always properly generated in IDEA StatiCa Connection for CHS members as they exhibited more complex meshing rather opened cross-sections.

Storing fundamental connection parameters and CBFEM calculated resistance rather than precomputed resistances by design code in the MySQL database [34] proved methodologically advantageous. This approach enabled dynamic resistance recalculation during each comparative analysis, automatically incorporating equation refinements. Consequently, discovered inaccuracies in the original YAML resistance equations were systematically resolved through iterative code updates without

requiring manual database revisions.

Listing 2.4: Example Python function for generation connection pairs

```
1  def sample_generation(config_path:str, nrd_sign:str,
       m_el_perc:float, n_perc:float, steel_g:int, angle_conn:
       float) -> list[MainCalculationInfo]:
2      time_start = time.time()
3      samples:list[ConnSetup] = generate_samples(config_path,
           nrd_sign, m_el_perc, n_perc, steel_g)
4      prepared_samples:list[ConnSetup] = get_stl_and_angle_conn
           (samples, steel_g, angle_conn)
5      loaded_samples:list[MainCalculationInfo] = get_loading(
           prepared_samples, m_el_perc, n_perc)
6      assign_my_sql_key(loaded_samples)
7      code_calculated:list[MainCalculationInfo] = code_calc(
           loaded_samples)
8      nrd_valid_samples:list[MainCalculationInfo] =
           additional_excluding(code_calculated)
9      time_finish = time.time()
10     script_speed = time_finish - time_start
11     print(f'Script generate_sample speed is {script_speed}' +
           '\n')
12     print(f'Number of excluded connections due cross section
           class and N_max brace resistancce   {len(
           nrd_valid_samples)- len(code_calculated)}'+ '\n')
13     print(f'Length of valid connections {len(
           nrd_valid_samples)}'+ '\n')
14     return nrd_valid_samples
```

The YAML instructions for the resistance calculation were selected because they permitted the calculation to be performed independently of the calculation process. This approach enabled the determination of the necessary number of helper values to achieve the desired results. The final resistance was the sole parameter that needed to be returned; all other helper values were recorded but not used directly for the subsequent comparison.

Listing 2.5: Example Inicialization variables required for calculation

```
for p_sample in prepared_samples:
    equations = p_sample.conn_setup.config_.equations
    variables_for_calc = {
        'b_0': p_sample.conn_setup.chord.get_base("b", 0),
        'h_0': p_sample.conn_setup.chord.get_base("h", 0),
        't_0': p_sample.conn_setup.chord.t,
        'd_0': p_sample.conn_setup.chord.d,
        'csc_chord':p_sample.conn_setup.chord.css_class,
        'b_1': p_sample.conn_setup.conn_member.get_base("b",
           0),
        'h_1': p_sample.conn_setup.conn_member.get_base("h",
           0),
        't_1': p_sample.conn_setup.conn_member.t,
        'd_1': p_sample.conn_setup.conn_member.d,
        'csc_conn_memb': p_sample.conn_setup.conn_member.
           css_class,
        'thetta_1': p_sample.conn_setup.c_angle,
        'fy_0': p_sample.conn_setup.steel_grade,
        'A_0': p_sample.conn_setup.chord.A,
        'W_0': p_sample.conn_setup.chord.W_el,
        'W_0_pl':p_sample.conn_setup.chord.W_pl,
        'I_0': p_sample.conn_setup.chord.I,
        'A_1': p_sample.conn_setup.conn_member.A,
        'W_1': p_sample.conn_setup.conn_member.W_el,
        'W_1_pl': p_sample.conn_setup.conn_member.W_pl,
        'I_1': p_sample.conn_setup.conn_member.I,
        'N_chord': p_sample.N_chord,
        'M_chord': p_sample.M_chord,
        'math': math,
    }
    hand_calc_results = yaml_calculator(equations,
       variables_for_calc)
```

2.2 Parametric Framework

In order to facilitate a meaningful comparison of the various resistance design methods, the following parameters were selected for analysis:

- Angle of the intersection θ (30°, 45°, 60°, 90°)
- Chord pre-loading, by normal force $N_{0,Ed}$ and/or bending moment $M_{0,Ed}$. Or

absence of the pre-loading

- Steel grade of the member (S235, S355, S420, S460)
- Geometrical parameters, $\gamma = \frac{d_0}{2 \cdot t_0}$ and $\beta = \frac{d_1}{d_0}$
- Geometrical parameters, connection types CHS-to-CHS: T&Y, X, K

2.3 FEA Modeling Workflow

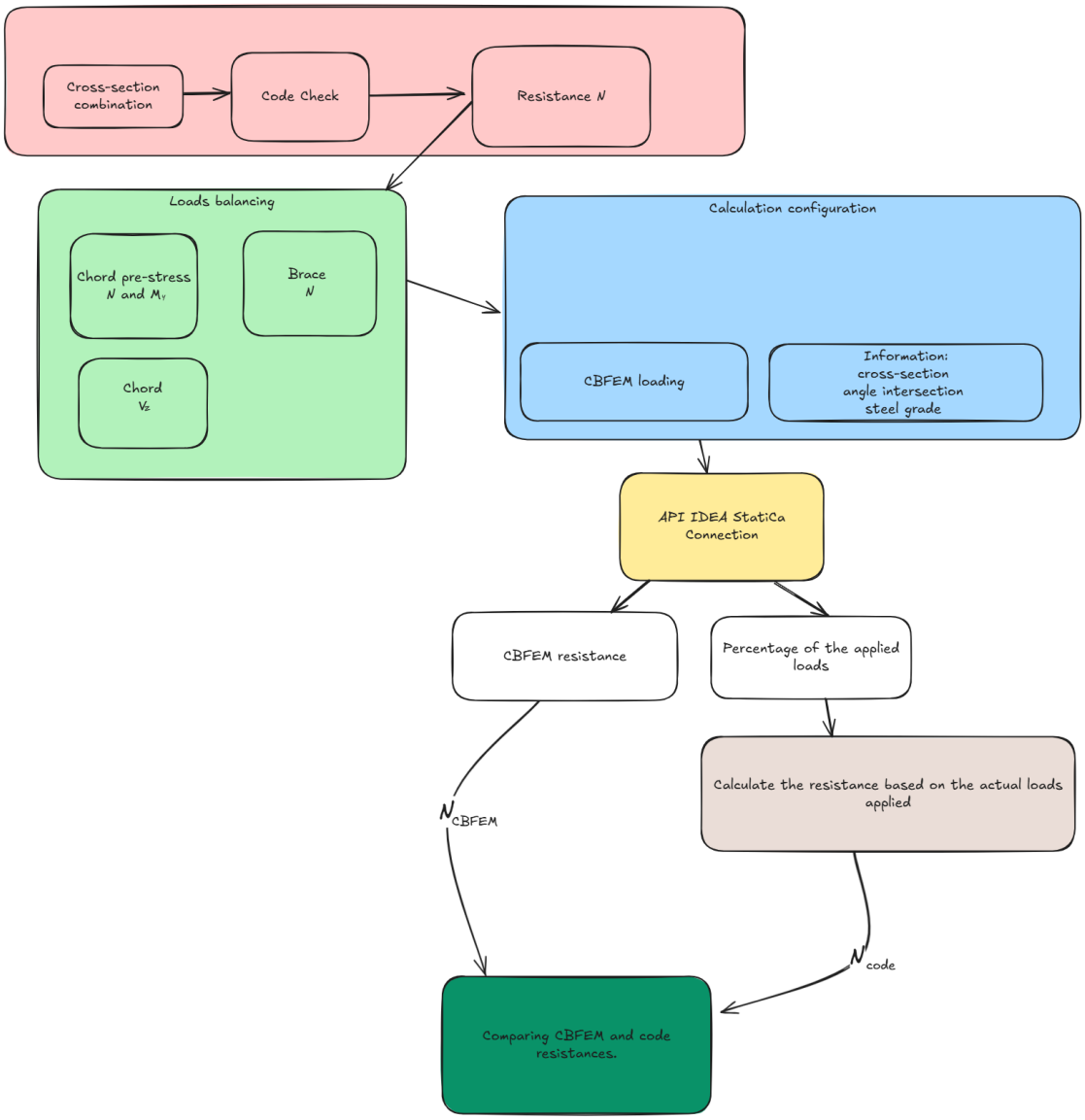

Fig. 2.3: Detailed workflow diagram

In order to execute this analysis, three models of the connection type T&Y, K, and X were configured within the GUI of the IDEA StatiCa Connection, see Figure 2.1. This was done to achieve parametric calculation of the plenty of cross-section

combinations. Implementation of the API calls was executed through the Python programming language.

In the models under consideration, a single cut of the brace member is utilized, and butt welding is employed. As previously stated, this study does not provide an analysis of the connection behavior influenced by welds.

Mesh and all analyze parameters were used by default setting provided by IDEA StatiCa Connection:

Tab. 2.1: Default parameters of IDEA StatiCa Connection

Description	**Value**	**Unit**
Division of the largest CHS member	64	-
Default length of member with a hollow section [c]	1.25	-
Division of arc of RHS member	3	-
Number of elements on biggest web of RHS member	16	-
Minimal size of elements	8	mm
Maximal size of elements	50	mm
Limit plastic strain	5.0	%
Limit plastic strain for high strength steel [a]	1.0	%
Limit deformation limit [b]	3.0	%
a) High strength steel $f_y > 460$MPa b) For CHS $3\%d_0$, RHS $3\%b_0$ c) For CHS chord member length is equal $1.25 \cdot d_0$		

The objective of this procedure is to establish a connection to the desired connection type, modification of the cross section, and steel grade of the component, as well as the establishment of the desired loading to achieve equilibrium within the joint. The intersection angle was not directly modified via the API; rather, it was manually adjusted to achieve the desired angle. This approach was adopted to enhance the script's efficiency, as the connection calculations are performed in sets and the pre-loading and steel grade remain constant, obviating the need for frequent recalibration.

Subsequent to each calculation through the API in the IDEA StatiCa Connection model, the results were stored as native files of the application in the .ideaConn extension. This facilitated the verification of the API calls and the debugging process. Given the absence of implementation of this functionality by the author, the interpretation of the numerical results alone proved challenging in terms of gaining a comprehensive understanding of the actual occurrences within the specific connection.

2.3.1 CBFEM method implementation

For the purpose of conducting a finite element analysis (FEA) comparison, the IDEA StatiCa Connection was selected due to its utilization of the CBFEM (component based finite element method) approach, which was developed by IDEA StatiCa. The CBFEM method is a comprehensive approach that integrates the use of finite element method (FEM) calculation with a detailed analytical examination of connection elements, such as bolts and welds. The results are promising, as the process has been validated and verified, see Wald et al. [35]. However, further validation is required through additional experimentation to ensure the reliability of the results.

IDEA StatiCa Connection employs shell elements to facilitate the calculation of connections with nonlinear materials and geometric calculations. The material is described by a bilinear material diagram, which includes the yield strength and the limit plastic strain.

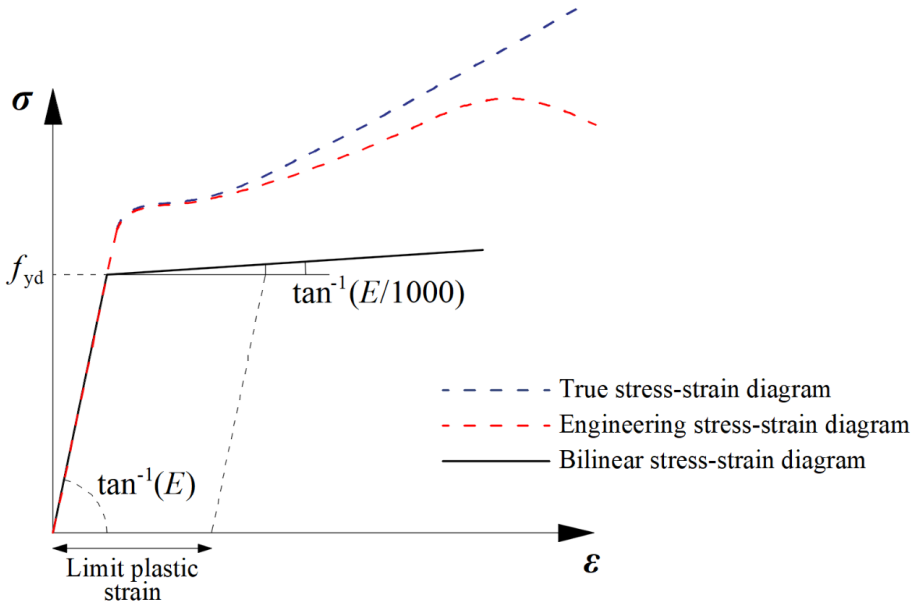

Fig. 2.4: CBFEM bilinear material diagram [32].

The determination of resistance from IDEA StatiCa Connection functionality of the software was achieved through the implementation of a stop at limit strain analysis, as load is applied incrementally; this functionality allows stopping the analysis at the point reaching failure criteria. This analysis was interrupted once the limit plastic strain 5% or limit local deformation $3\%d_0$ ($3\%b_0$) had been reached.

The comparison default analysis setting was implemented, incorporating the maximum and minimum mesh size, the division of the largest CHS, the restriction of plastic strain, and the limitation of local deformation, see Table 2.1.

The entire comparison was executed with the analytical calculation of the connection. The subsequent stage in the procedure entails the preparation of the loading for the finite element analysis (FEA) calculation, with the objective of achieving a close match between the resistance and the desired stresses of the chord. To this end, the analytical resistance was scaled. In order to achieve the desired behavior, it was necessary to establish equilibrium among all forces. Consequently, analyses were performed to obtain the applied load. Therefore, the resistance of the analytical solution was recalculated based on the information regarding the exact load that was applied to facilitate a comparison of analogous situations. Subsequently, the results of the calculation were stored.

It is imperative to acknowledge that the calculation via the CBFEM method has been correctly configured for utilization in routine structural engineering practice. Notably, this approach does not demand the configuration of FEA settings, and convergence to the results is very promising. This was a critical factor in the study's context.

3 Validation of FEA Models

3.1 Benchmarking Against Experimental Data

A comparison of the CBFEM and experiment was conducted on the report CIDECT Project final report 5CC-6/13 by Ummenhofer et al. [36]. In the aforementioned study, sets of CHS-to-CHS X connections were pre-loaded at varying levels of chord axial tension, while braces were loaded by the compression force. A measurement of the geometrical and material properties was conducted during the test program, as illustrated in Table 3.1. Researchers confirmed the joint resistance at the point of local deformation $3\%d_0$, see Figure 3.3. Refer to Figure 3.3, which illustrates the relationship between x-resistance and local resistance.

The corresponding model in the IDEA StatiCa Connection was produced, with measured geometrical and material properties provided from the final report 5CC-6/13 by Ummenhofer et al. [36]. CBFEM resistance was identified through iterations, with each iteration exhibiting a consistent level of pre-loading comparable to the experimental condition. In the context of exact simulations, safety factors were not utilized, a key aspect that enables direct comparison of resistances.

As illustrated in Table 3.2, the CBFEM simulation prediction exhibited a discrepancy with the experimental results, with a margin of difference of at least -13%. As illustrated in Figure 3.1, the linear regression model demonstrated differences between test program and the CBFEM method results.

Tab. 3.1: Test specimens with measured dimensions, weld sizes, and material properties

Specimens	Dimensions (mm)				Weld sizes (mm)			Material properties (N/mm²)	
	d_0	t_0	d_1	t_1	a_c	a_b	a	$f_{y,0}$	$f_{u,0}$
CHS_X_1	101,7	4,1	51,0	4,2	10	10	7	458	603
CHS_X_2	–	–	51,0	4,2	10	9	7	458	603
CHS_X_3	101,7	4,1	51,1	4,1	11	10	7	458	603
CHS_X_4	–	–	51,1	4,1	10	9	7	458	603
CHS_X_5	–	–	51,0	4,1	11	8	7	458	603
CHS_X_6	–	–	51,0	4,1	10	8	6	458	603
CHS_X_7	–	–	51,0	4,0	10	8	6	458	603
CHS_X_8	–	–	51,1	4,2	10	8	6	458	603

As demonstrated in Table 3.2, the CBFEM predictions exhibited a systematic underestimation of resistance. Although these discrepancies may indicate conservative modeling tendencies, it is imperative to employ comprehensive statistical

validation to determine their statistical significance:

- A two-sample t-test ($\alpha = 0.05$) should be applied to evaluate whether the mean resistance difference between CBFEM and experimental results exceeds random variability.
- The limited sample size ($n = 8$ specimens) necessitates expanded datasets to improve statistical power and generalizability. Future studies should incorporate more specimens per connection type to satisfy central limit theorem requirements.

Tab. 3.2: Experimental comparison of the resistances with CBFEM

Specimens	Tension pre-loading [-]	EXP. [kN]	CBFEM [kN]
CHS_X_5	n = 1	43.9	0.0
CHS_X_6	n = 1	43.9	0.0
CHS_X_3	n = 0.9	38.9	17.2
CHS_X_4	n = 0.9	39.5	17.2
CHS_X_7	n = 0.75	62.3	48.1
CHS_X_8	n = 0.6	77.9	64.5
CHS_X_2	n = 0	89.2	77.7
CHS_X_1	n = 0	93.1	77.7

* n: Axial tension pre-loading parameter calculated from chord CHS measured geometry and measured yield strength.

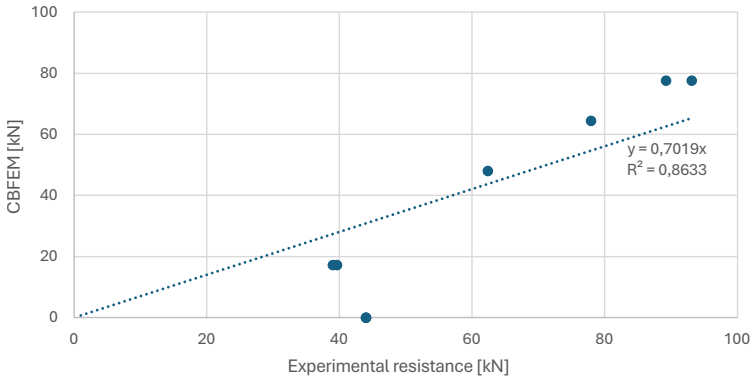

Fig. 3.1: Comparison experimental resistances and CBFEM

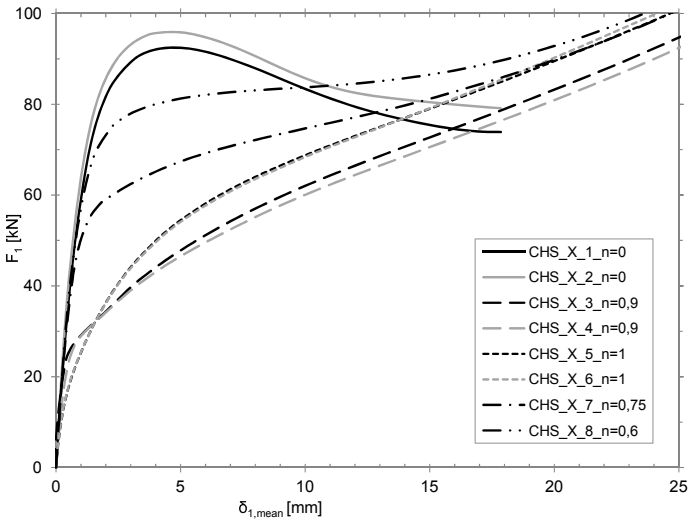

Fig. 3.2: Experimental load-displacement curves of the CHS-X-joints, Source: [36]

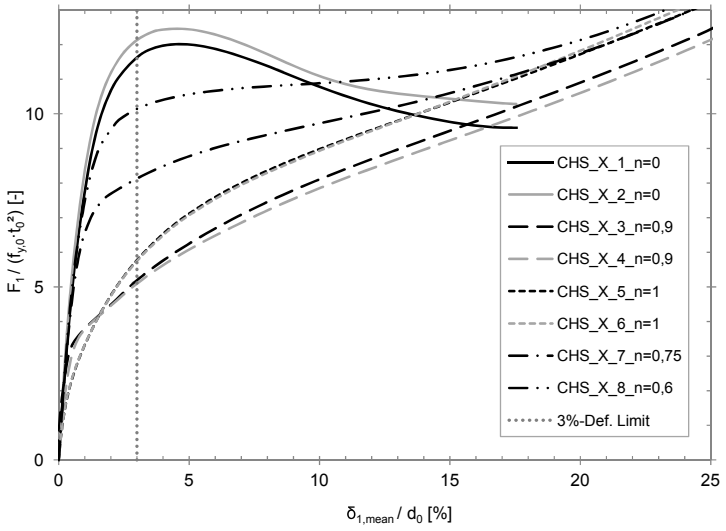

Fig. 3.3: Experimental load-displacement curves of the CHS-X-joints, Source: [36]

4 Comparative Analysis of Code Predictions

4.1 Code to CBFEM comparison

In order to visualize the areas requiring inspection, a code-to-code comparison was performed. This method was utilized due to its reduced computational time requirements when compared to finite element analysis (FEA) calculations. The comparison was made between the current and new generation of the EN code. It was established that the AISC code is identical to the current EN code in terms of hollow section resistance calculation. The findings demonstrate that, in the absence of stress at the chord member, the new generation of the EN code exhibits global behaviour that provides higher resistances for CHS K and CHS T&Y connections, see Figure 4.3, 4.6, 4.9. As illustrated, see Figure 4.3, 4.6, 4.9, the CHS X connection exhibits a high degree of alignment with the prevailing EN code.

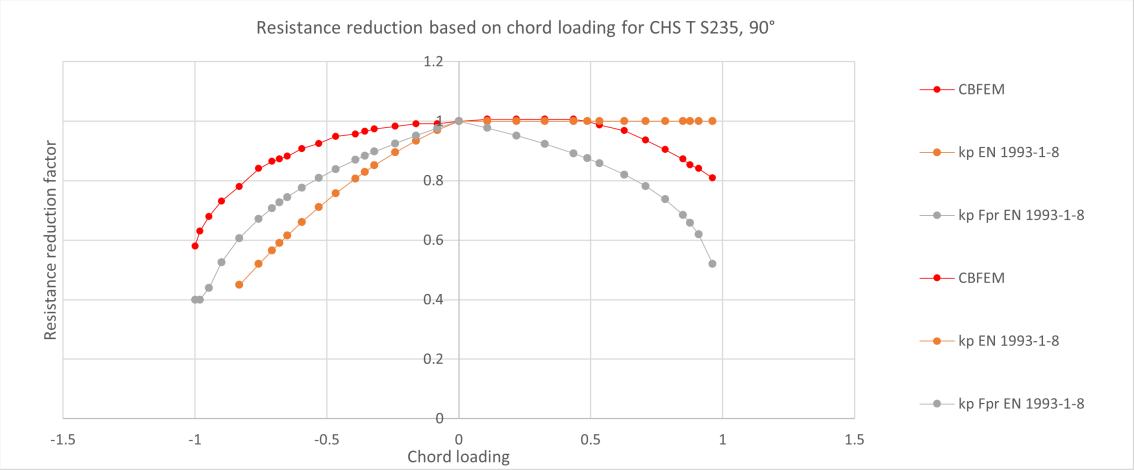

Fig. 4.1: Resistance reduction based on the chord loading

The comparison between CBFEM to code results will be the most clear for CHS X connection, because forces from brace members are in equilibrium; in other words, to provide experimental comparison from which code equations were derived is the easiest to technically carry out. It is assumed that CHS X is of a connection type that is most accurately described by the design code.

As illustrated in Figure 4.2, the results demonstrate a high degree of concordance in the slope of the global behaviour and the scatter of the results, particularly when considering CHS X in configuration 45° and steel grade S355 (52ksi). However, in the case of different configurations, the scatter of the results is no longer so consistent, see Figure 4.15 for CHS X 30° where chord compression stress is present. This observation suggests the possibility of a more complex influence of the chord

stress than that which is being described by the code. Further investigation is recommended into the influence of chord stress on the resistance of CHS to CHS connection.

As demonstrated in Figure 4.15, the findings illustrate that the influence of steel grade on resistance does not align with the linearity described in the code. The discrepancy in yield strength can be attributed to several factors. Firstly, it is important to note that the CBFEM method utilizes a bilinear diagram, see Figure 2.4. The variation in yield strength and 5% plastic strain across distinct steel grades has a notable impact on the convergence point of the results. As demonstrated in Equation 4.1 4.2, the reduction in resistance based on the steel grade is 1.5%.

$$\begin{aligned}
5\%\text{ pl. strain for S235 } &= 235\text{MPa} + \tfrac{210000\text{MPa}}{1000} \cdot 0.05 = 235\text{MPa} + 10.5\text{MPa} = 245.5\text{MPa} \\
5\%\text{ pl. strain for S355 } &= 355\text{MPa} + \tfrac{210000\text{MPa}}{1000} \cdot 0.05 = 355\text{MPa} + 10.5\text{MPa} = 365.5\text{MPa} \\
5\%\text{ pl. strain for S420 } &= 420\text{MPa} + \tfrac{210000\text{MPa}}{1000} \cdot 0.05 = 420\text{MPa} + 10.5\text{MPa} = 435.5\text{MPa}
\end{aligned} \tag{4.1}$$

$$\begin{aligned}
\tfrac{245.5\text{MPa}}{235\text{MPa}} &= 1.045 \\
\tfrac{365.5\text{MPa}}{355\text{MPa}} &= 1.03 \\
\tfrac{435.5\text{MPa}}{420\text{MPa}} &= 1.025
\end{aligned} \tag{4.2}$$

However, the outcomes demonstrate a considerably greater reduction in yield strength, as illustrated in Figure 4.15. This phenomenon can be explained by the fact that, for these outcomes, the deformation of the material can be more significant, thereby resulting in the criteria of the 3% local deformation becoming more significant. Important to note that further investigation is required in order to prove what is influencing resistance non-linearly based on the yield strength. It is also noteworthy that CBFEM enables the calculation of geometrically non-linear hollow sections, with loads applied incrementally. The present study employed geometrical nonlinearity in its calculation. Consequently, these factors can influence the connection's failure, characterized by a rapid increase in plastic strain and deformation due to the influence of eccentricities, which are created by geometrically non-linear behaviour.

Following the CBFEM computations, the results were analyzed by generating plots to facilitate comparison. A critical aspect of this process involved selecting appropriate plotting parameters and determining how to segment the dataset. The parameters chosen for plotting were $\gamma = \frac{d_0}{2t_0}$ and $\beta = \frac{d_1}{d_0}$, which are key geometric indicators representing the slenderness of the connection. Additionally, the plots incorporated color scaling to visually distinguish the compared resistance values, thereby simplifying the interpretation of the data, see Figure 4.13. The dataset was divided based on the diameter of the chord member, with each data point in the

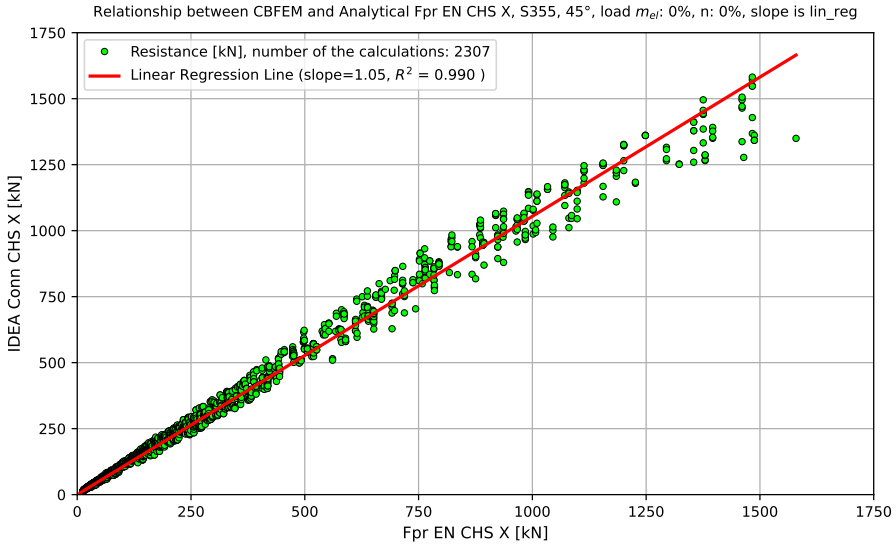

Fig. 4.2: Comparison Analytical Fpr EN and CBFEM resistances.

plot representing a pair of connections. These connections can be distinguished by their slenderness and diameter ratio parameters. However, since parameters γ and β do not account for the thickness of the connected members, there were cases where points had the same abscissa and ordinate but different resistance comparison values (i.e., the ratio of the resistances). To address this issue, results were presented with third parameters for providing illustration of the influence thickness of the brace member, but there wasn't any significant difference in presented results so in practical aspects of the connection design, see Figure 4.14. A linear regression is also displayed for the selected data set. The global behaviour exhibited by these parameters can be observed.

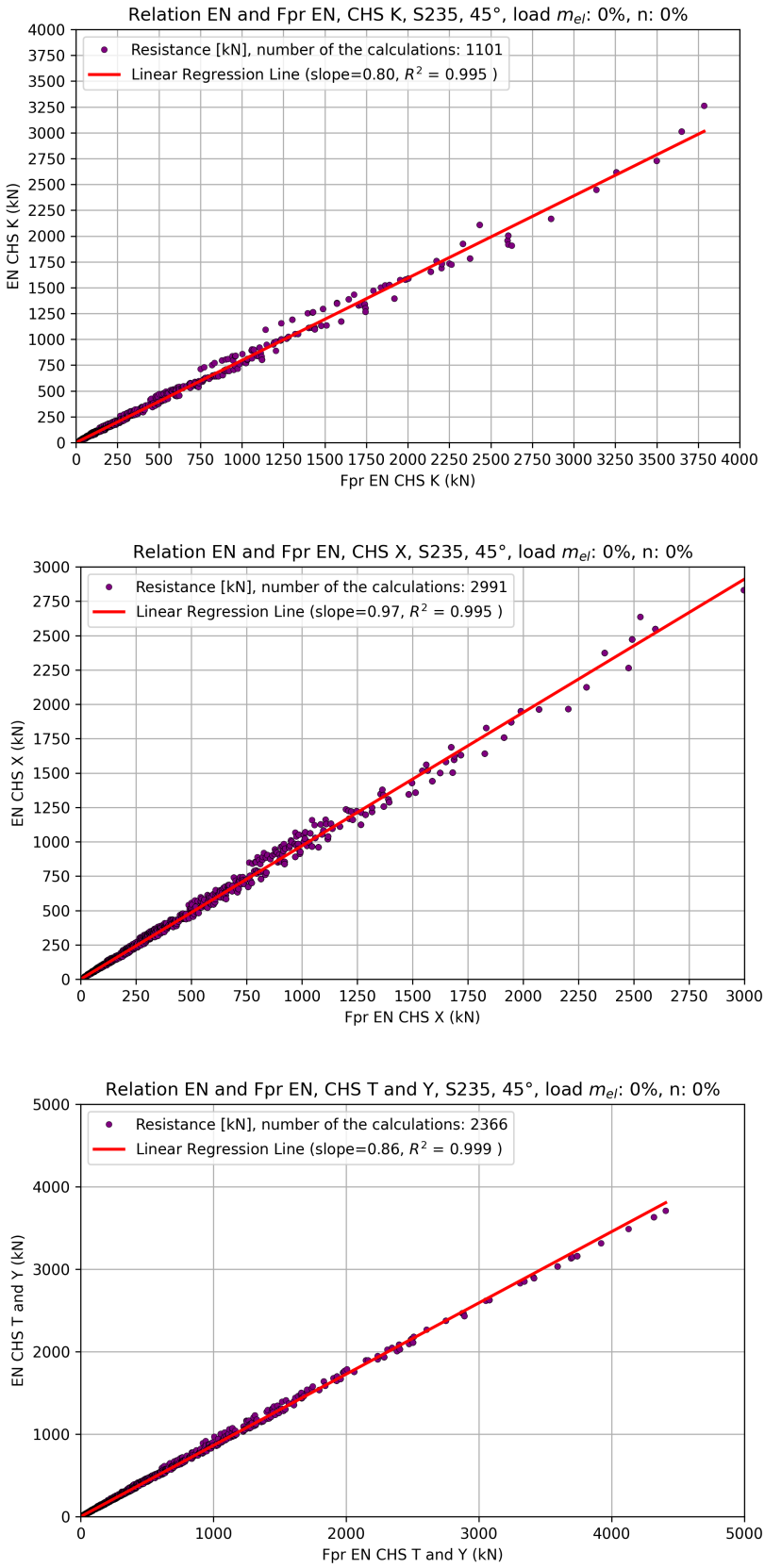

Fig. 4.3: EN to Fpr EN S235, 45°, chord stress absence

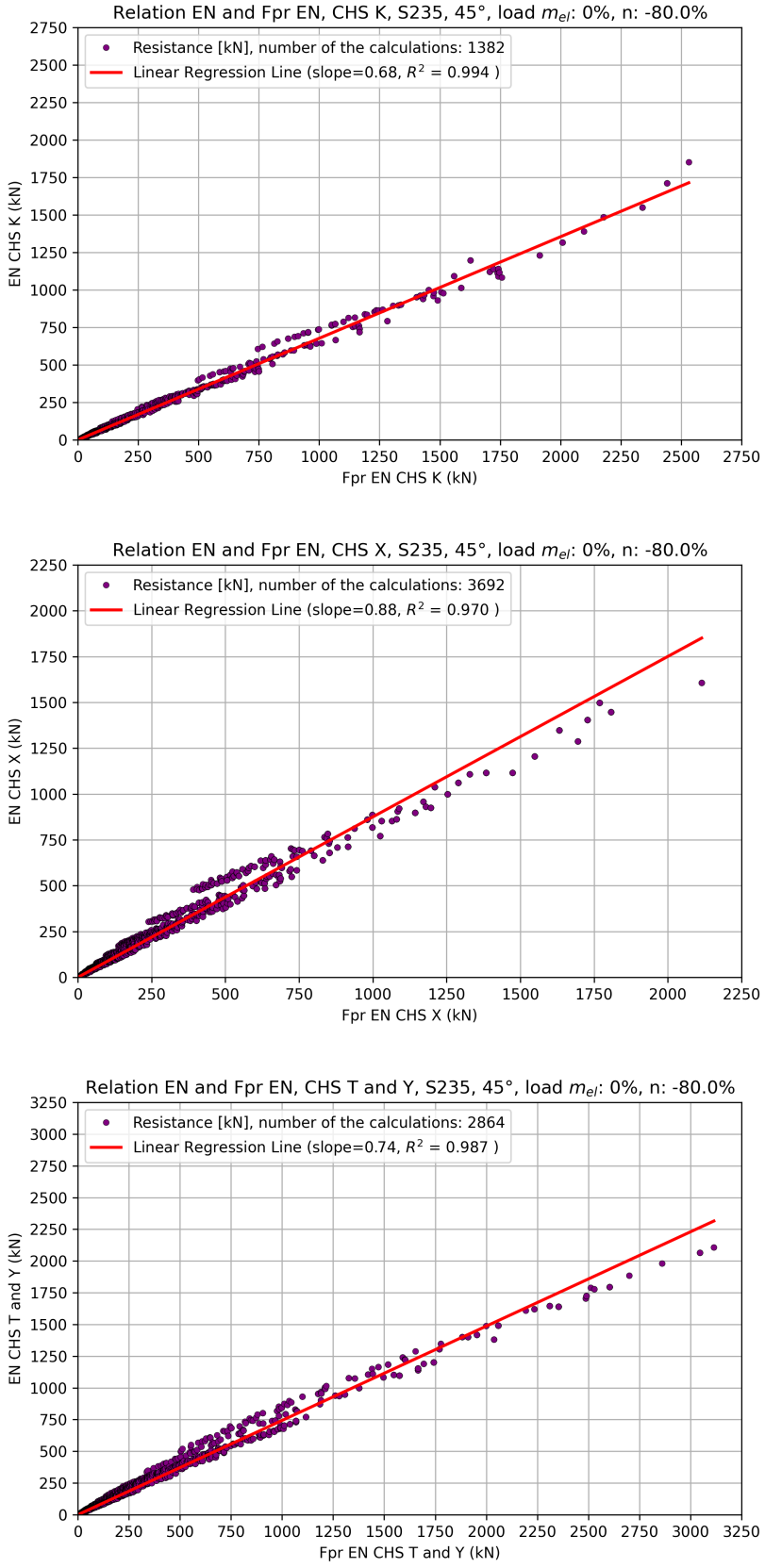

Fig. 4.4: EN to Fpr EN S235, 45°, chord axial compression 80%$N_{d_0,rd}$

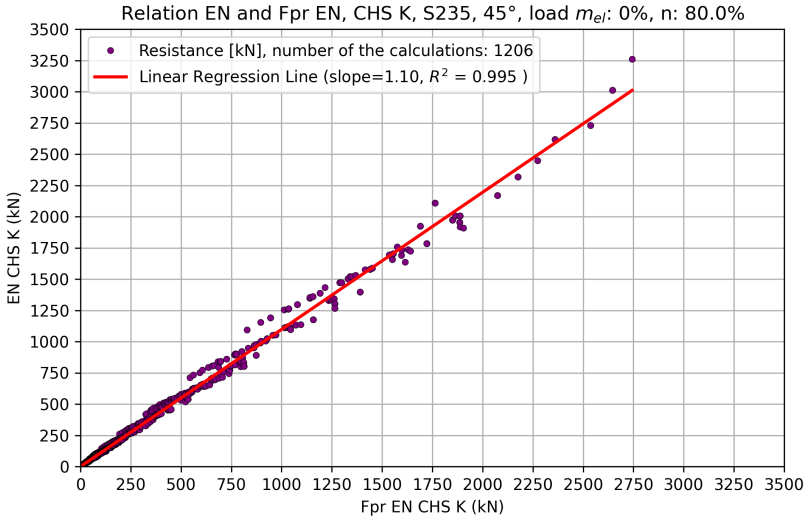

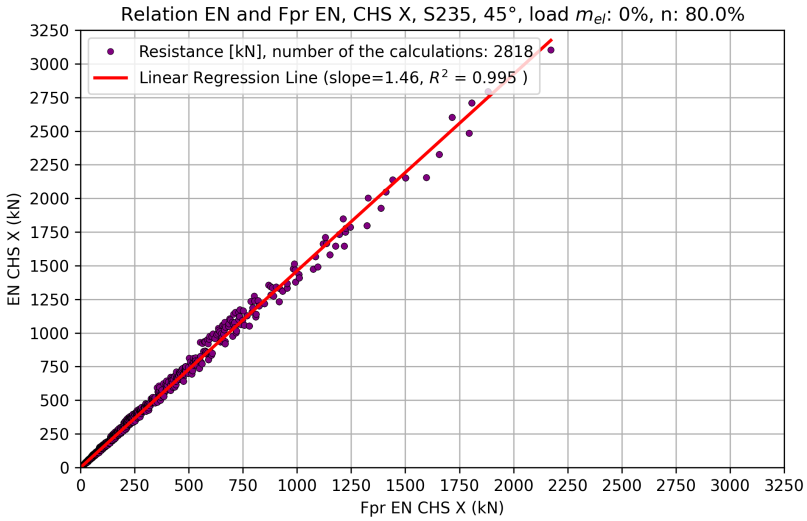

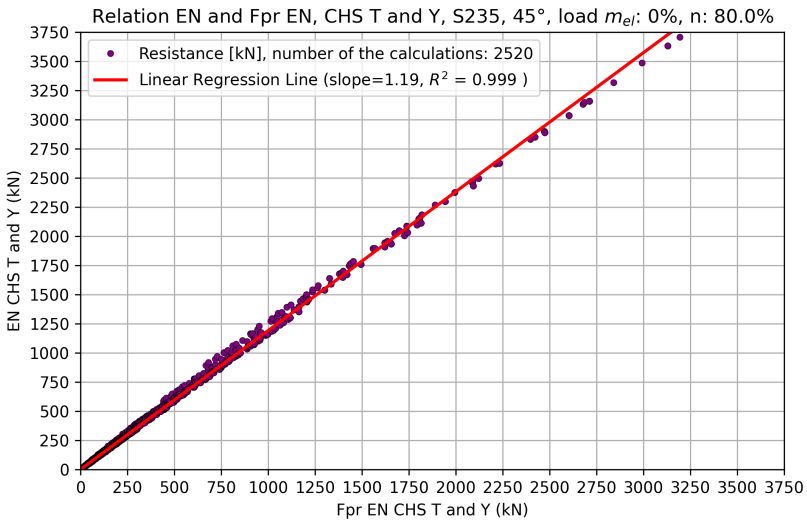

Fig. 4.5: EN to Fpr EN S235, 45°, chord axial tension 80%$N_{d_0,rd}$

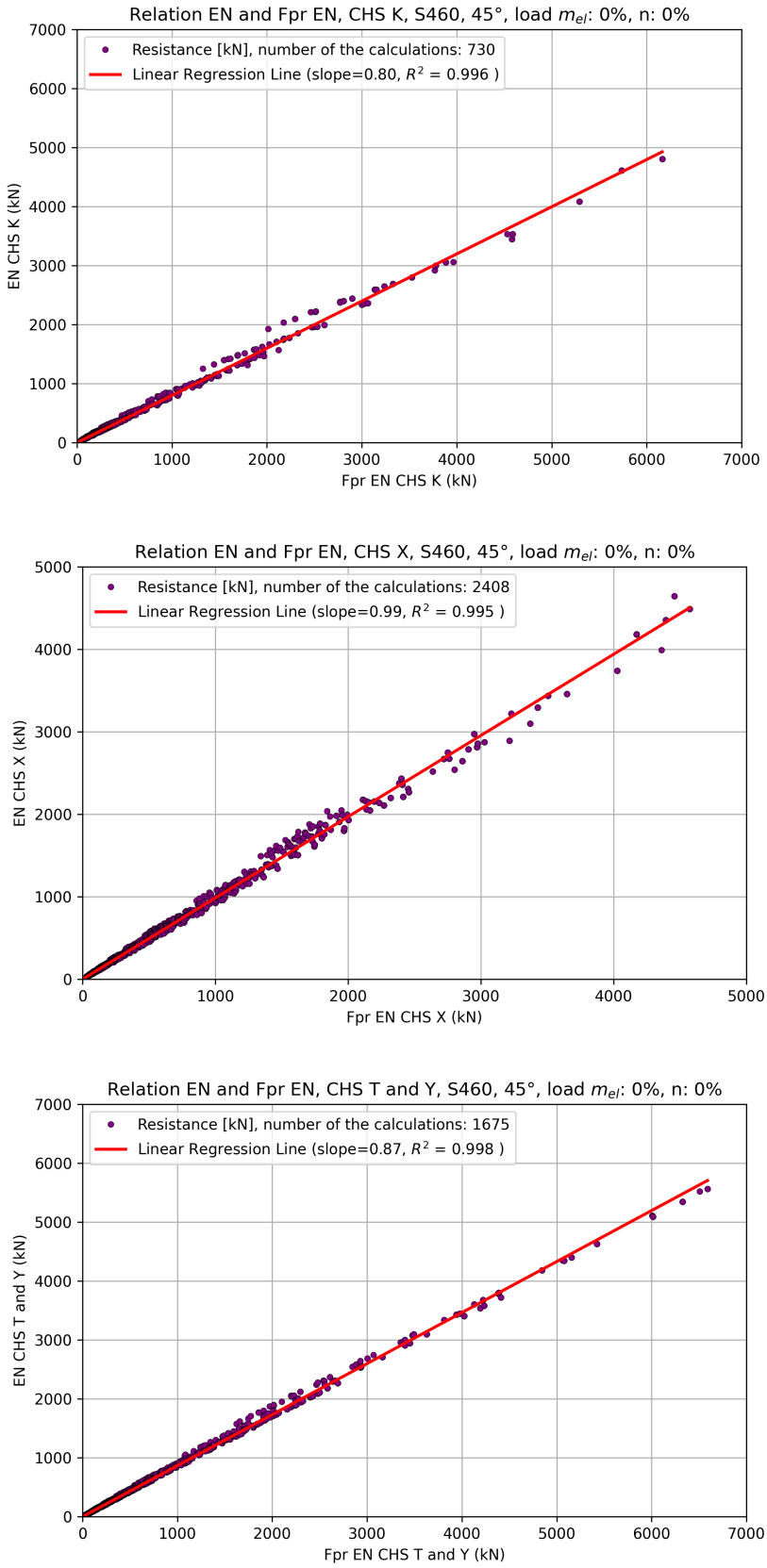

Fig. 4.6: EN to Fpr EN S460, 45°, chord stress absence

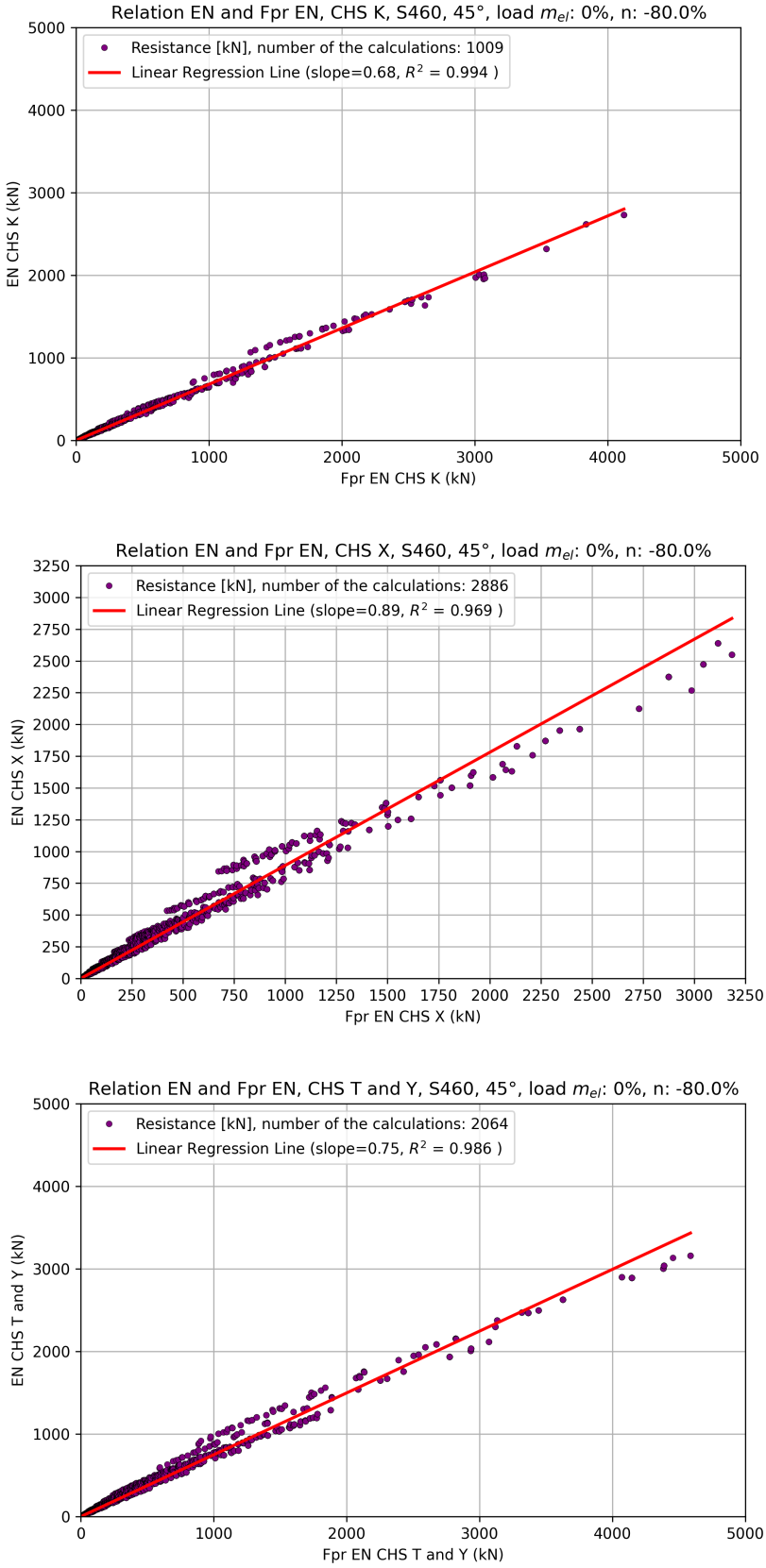

Fig. 4.7: EN to Fpr EN S460, 45°, chord axial compresion 80%$N_{d_0,rd}$

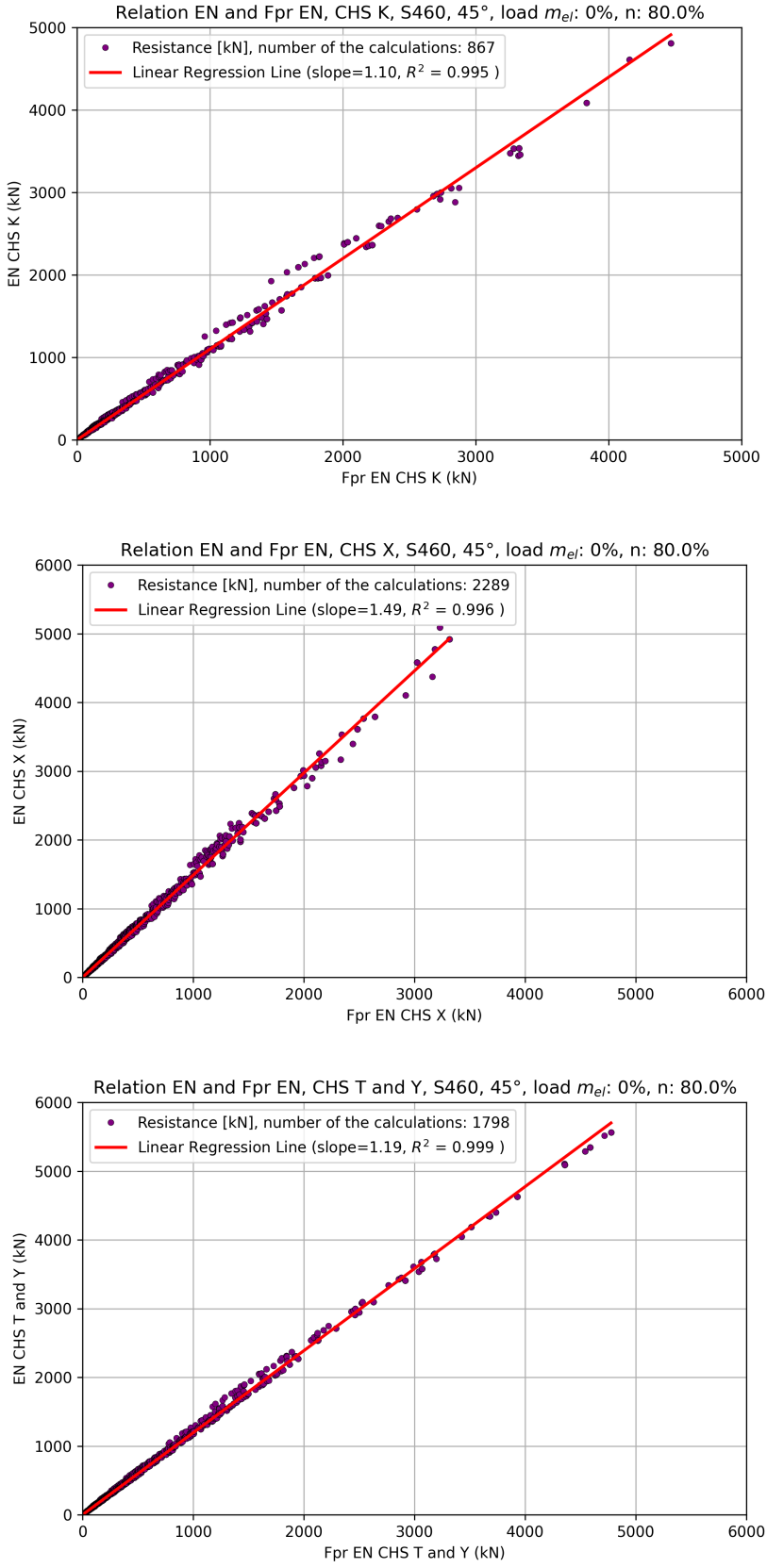

Fig. 4.8: EN to Fpr EN S460, 45°, chord axial tension 80%$N_{d_0,rd}$

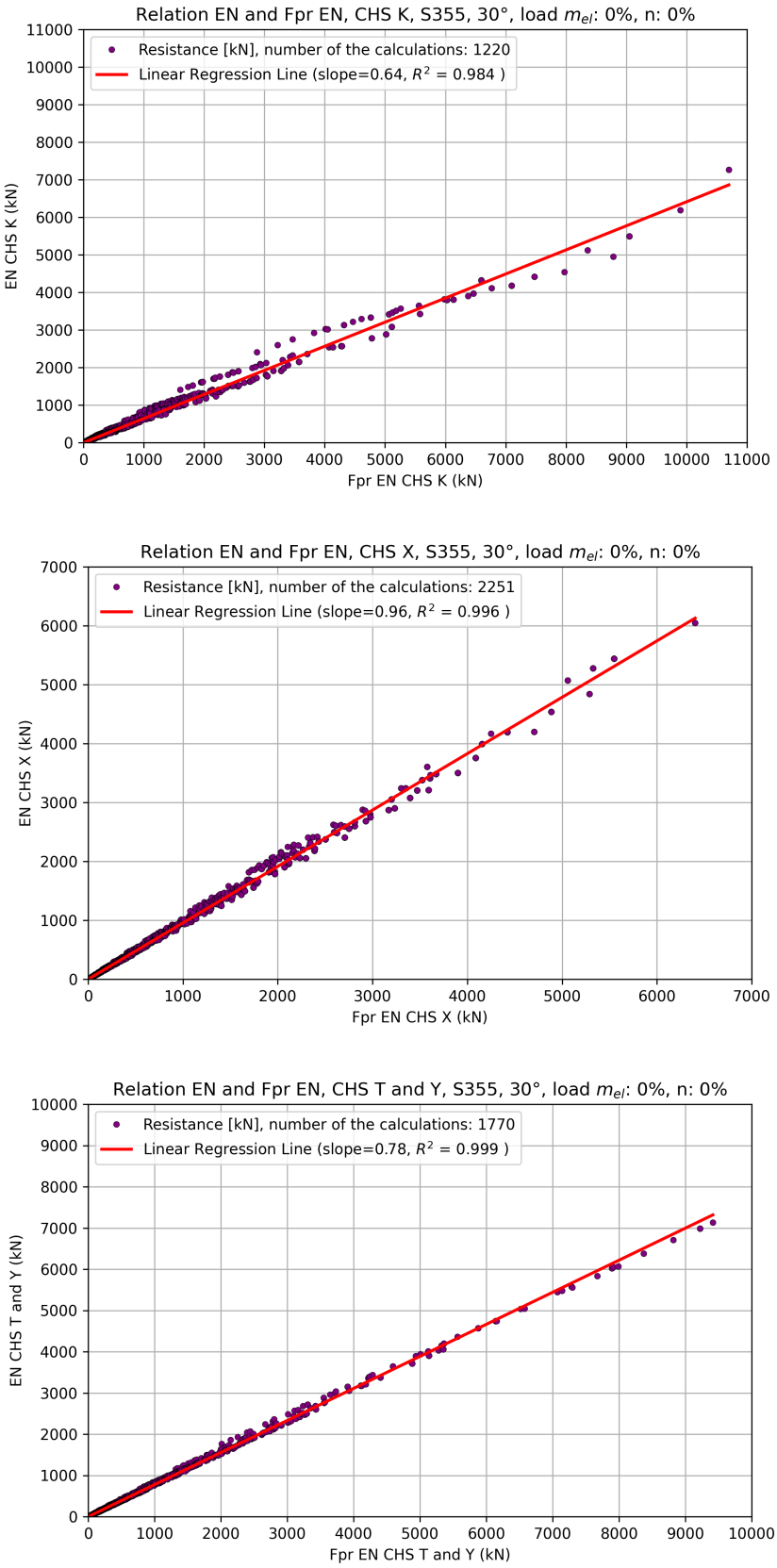

Fig. 4.9: EN to Fpr EN S355, 30°, chord stress absence

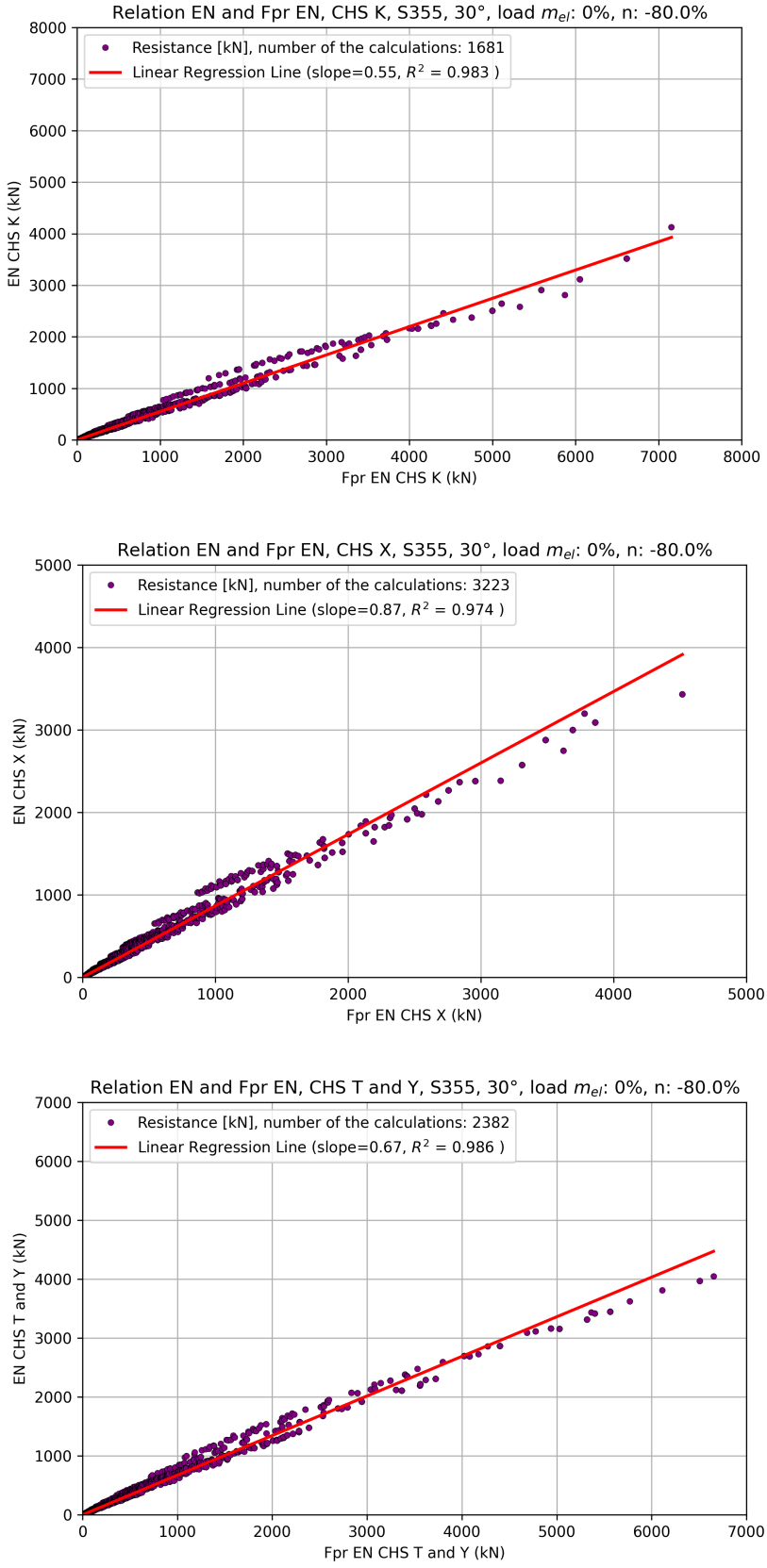

Fig. 4.10: EN to Fpr EN S355, 30°, chord axial compresion $80\%N_{d_0,rd}$

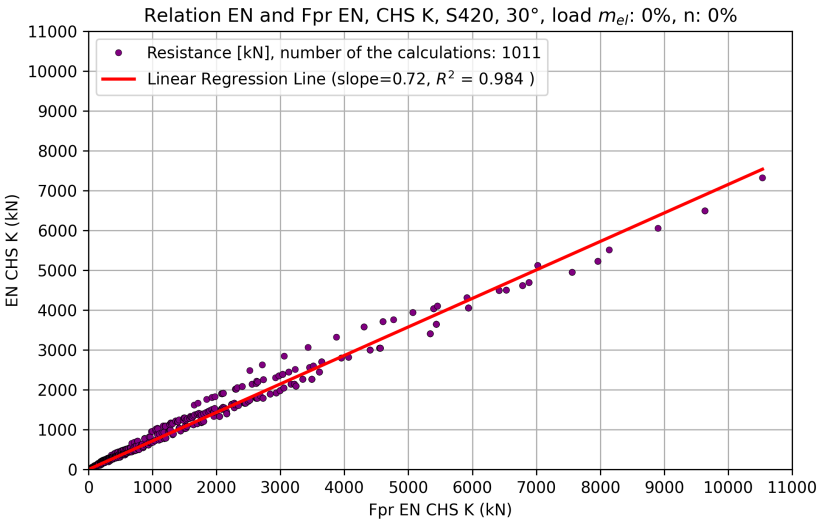

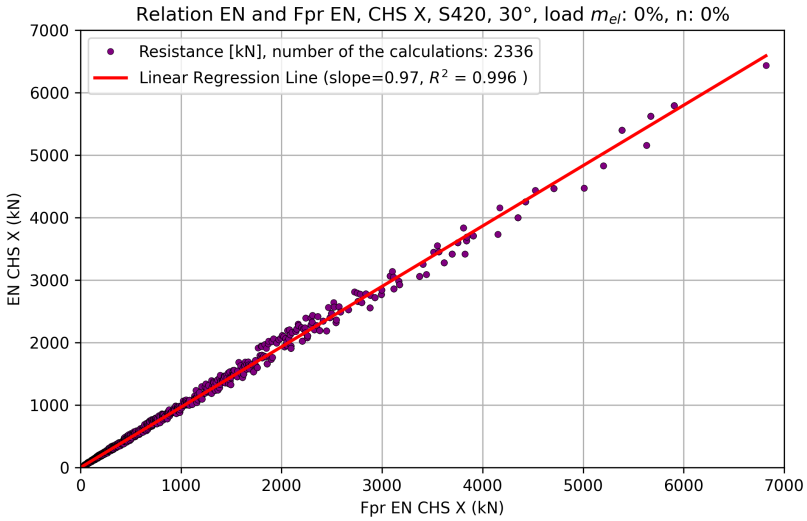

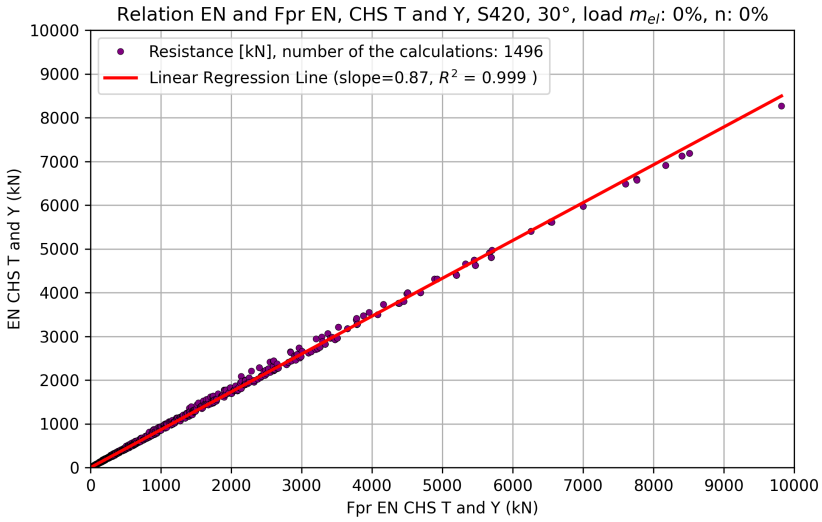

Fig. 4.11: EN to Fpr EN S420, 30°, chord stress absence

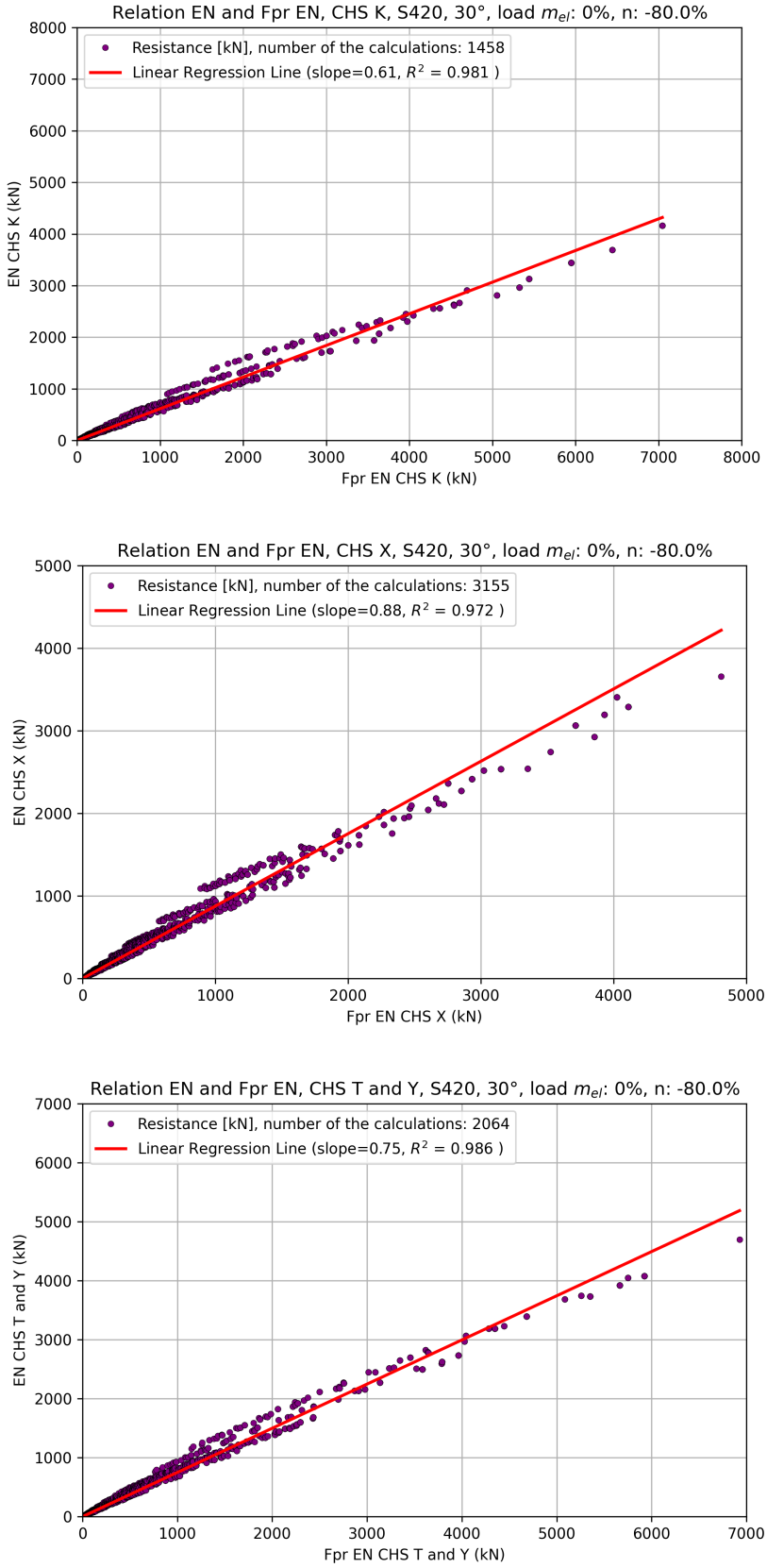

Fig. 4.12: EN to Fpr EN S420, 30°, chord axial compresion $80\%N_{d_0,rd}$

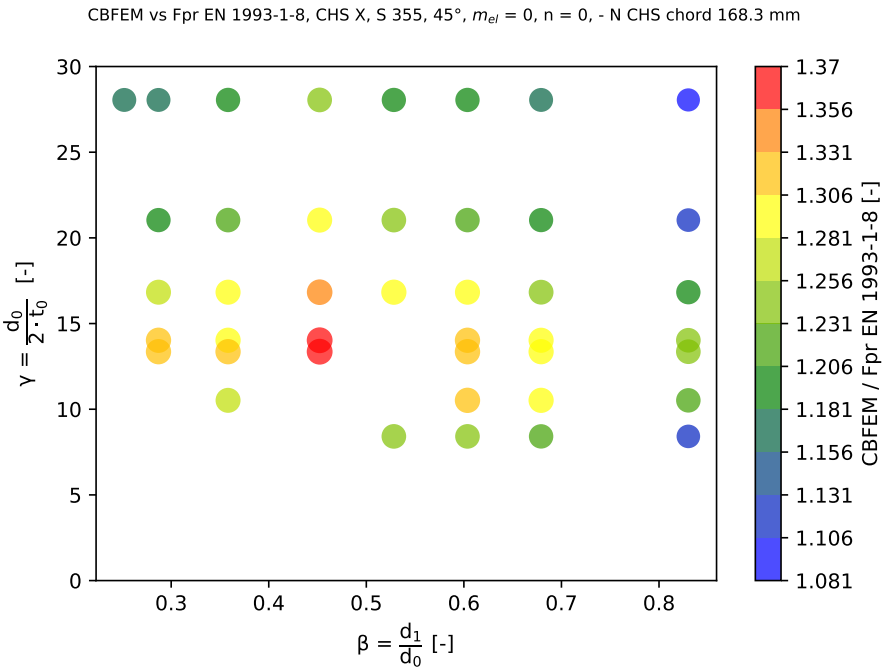

Fig. 4.13: Detailed results for CHS X with chord $d_0 = 168.3$mm

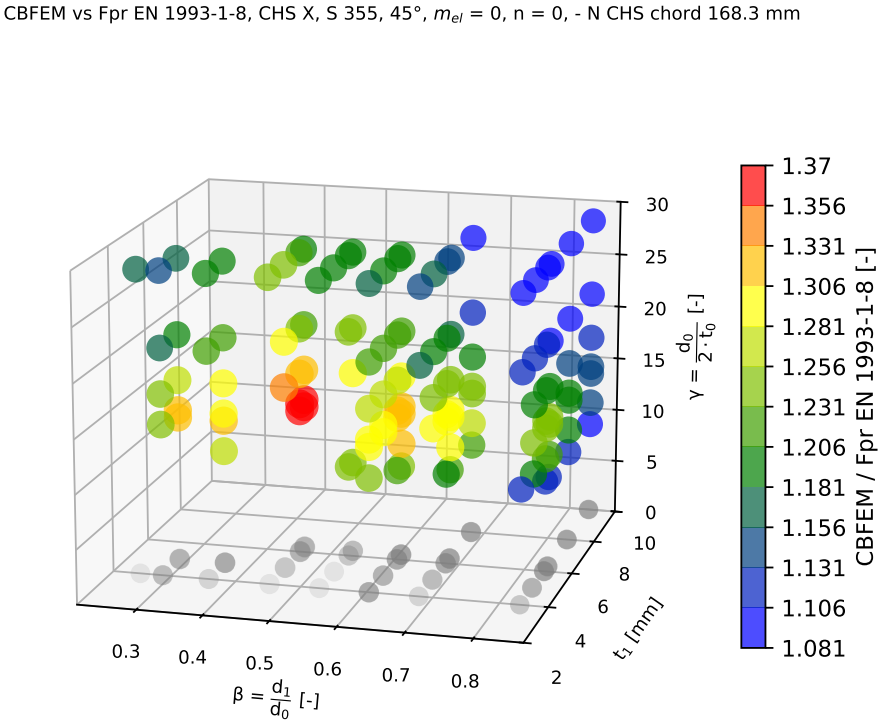

Fig. 4.14: Detailed results for CHS X with chord $d_0 = 168.3$mm, with influence of t_1

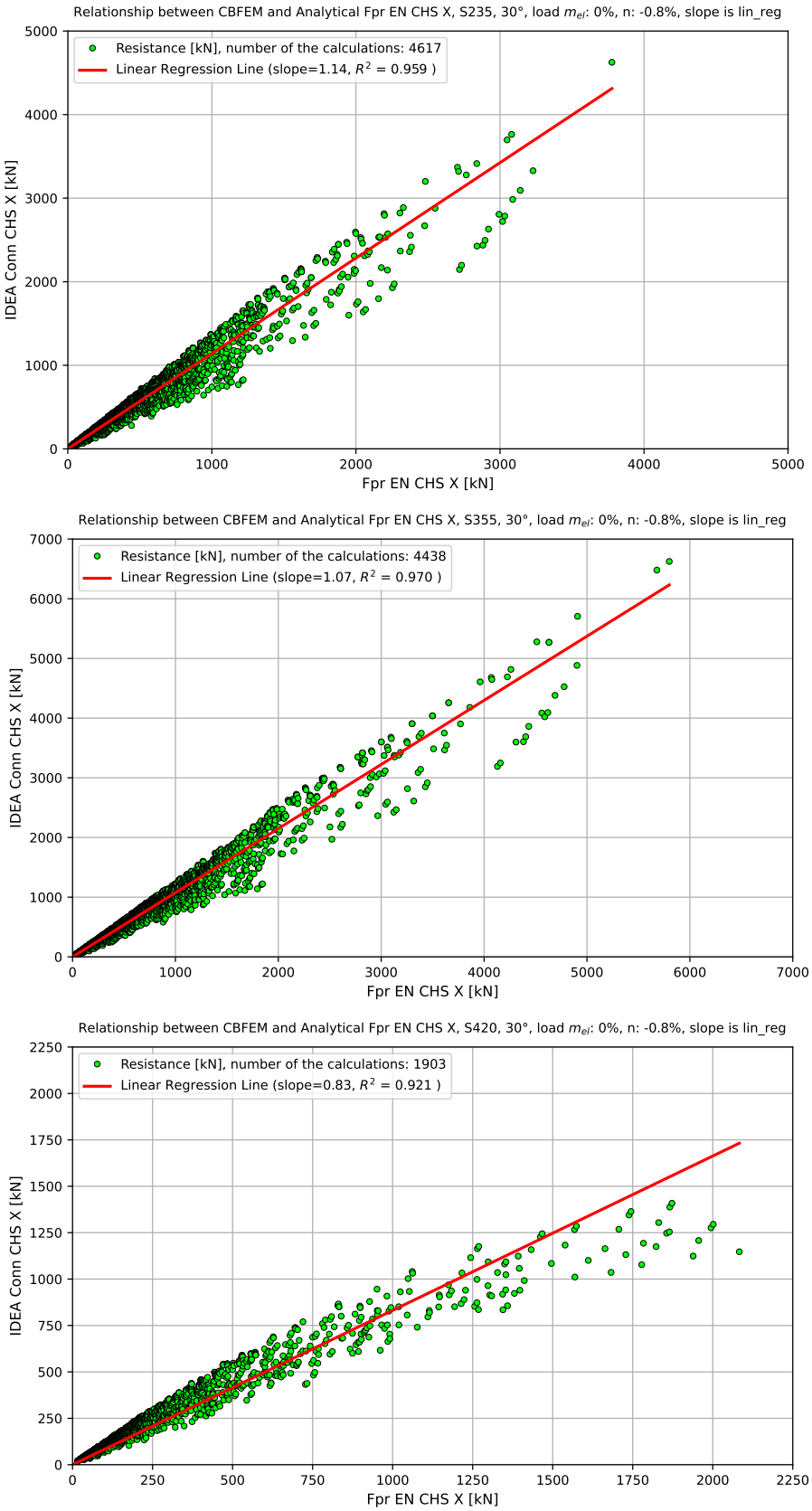

Fig. 4.15: CBFEM to Fpr EN, 30°, chord axial compresion $80\% N_{d_0,rd}$

5 Discussion

5.1 Interpretation of Results

A comparison of the codes indicates that the new generation of EN codes is less conservative in its resistance prediction, as evidenced by the results obtained for cases where there is an absence of chord stress pre-loading. The most notable of the CHS-to-CHS K gapped connections is that which is shown in configuration with 30° and chord pre-loading of $80\%N_{0,Rd}$. The maximum observed percentage difference is 55%, see Figure 4.10. It is imperative to acknowledge the fact that, since the code has been meticulously engineered to gauge stress exclusively through the utilisation of functions, there exists a possibility that the outcomes may not always correspond precisely with the actual behaviour exhibited.

It is evident that a discernible discrepancy exists in the new EN generation and both EN and AISC when tension configuration is applied. This phenomenon can be attributed to the fact that resistance is not reduced for tension stress, see Equation 1.6 1.7. According to CIDECT DG 1 [14], the equations underlying the new generation of the EN code predict up to 40% lower resistances for connections with tension chord stress. Figure 4.1 demonstrates how chord loading affects resistance.

A comparison with the CBFEM method has been undertaken, the results of which indicate that, in cases where chord stress is absent, the results are generally similar to those of the new generation of the EN code. However, in situations where chord stress is present, a marked difference in results is observed, which may indicate that the stress function can be improved. Unlike CBFEM analyses, which demonstrate a non-linear relationship between steel grade and resistance, structural design codes assume this relationship is linear. The true nature of this relationship is not fully established. Consequently, further investigation is needed to clarify this discrepancy and inform potential improvements to the design code.

5.2 Limitations of the Study

The scope of study is limited to CHS-to-CHS connections loaded in plane. An examination of the RHS-to-RHS connections is also recommended, given their high utilization; however, the available calculated results are insufficient for conducting a behavioural study. The capacity of the study to provide detailed results based on the chord stress if applied is limited, as previously mentioned, due to the inconsistent loading resulting from the utilization of the *Stop at limit strain* functionality.

For the purpose of illustration, the distribution of actual pre-loading whereby 80% of compression load was applied is significant:

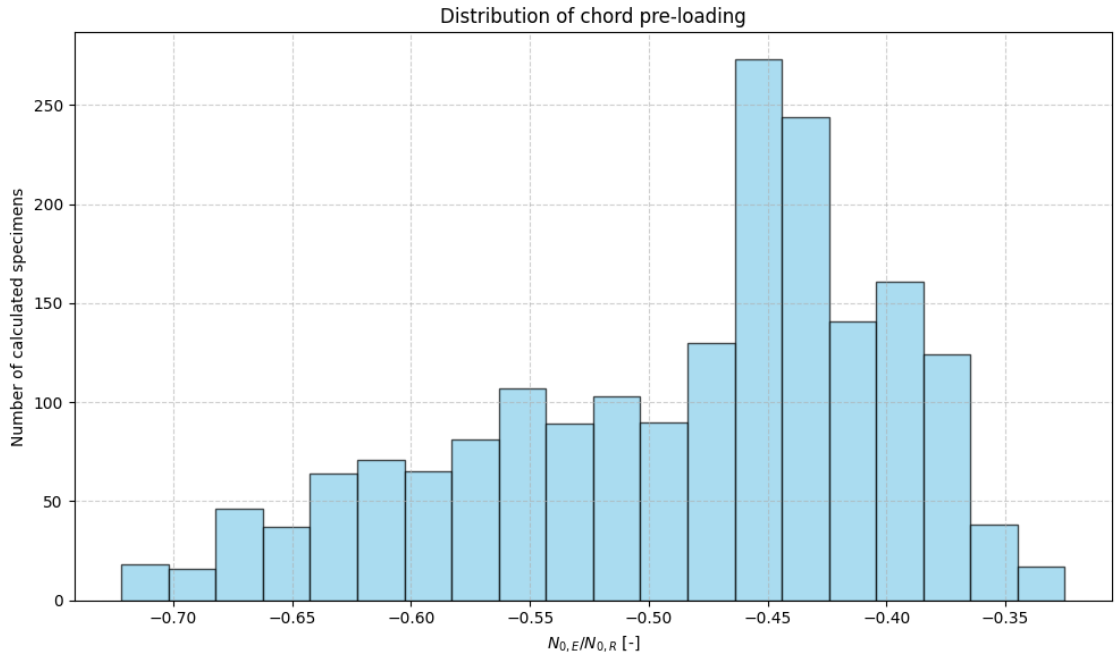

Fig. 5.1: Chord pre-loading distribution for CHS X, S420, 30°, $m_{el} = 0\%$ $n = -80\%$

5.3 Practical Implications

The results obtained can facilitate comprehension of the fundamental principles that govern the comparison of the newly developed code with the existing design codes. Given the substantial nature of the dataset, its utilization in code development is a viable proposition. It is also conceivable to utilize data for the purposes of neural network learning and the provision of equations for the design of various connection types. Nevertheless, it is imperative to undertake extensive data validation and comparison with a broader range of experiments to substantiate the statistical outcomes.

Developed scripts can be utilized for purpose identification for which geometrical and material parameters the most significant difference in prediction by design code versus CBFEM. Consequently, a more comprehensive analysis of the critical places can be executed for purpose enhancement of design code methodologies.

Although current design methodologies for hollow sections design are shared between AISC [3] and EN [2], significant differences exist in the new generation of the EN code. Therefore, adopting its newer methodology within AISC is recommended to better represent hollow structural section (HSS) behaviour.

Produced script is available to the public on the GitHub platform [11].

6 Design and Optimization of the Roof Truss

6.1 Structural Configuration

The optimization study focuses on a duo-pitch steel roof truss system spanning 40 metres, with trusses spaced at 5-metre intervals. The longitudinal structure extends 60 metres, and is situated in the Brno region's climatic conditions. The primary objective of this study is to combine weight minimization with structural compliance through the utilisation of parametric modeling and genetic algorithms.

Three load combinations are required to meet the fundamental criteria for analysis. These include the load of snow and all permanent load, wind suction and permanent load, and a characteristic combination for deflection calculation. The calculation of the roof deck was based on the fundamental assumption that the weight of the roof panels would be 20 kg/m^2, and that they would be attached to IPE 220 purlins. Snow and wind loadings were calculated acc. to Brno region typical values.

In the Kiwi!3D environment, members were modeled as beam elements, with hinges incorporated into the members at their start and end points. Roof truss were supported as simply supported beam. Cross-sections for members were added to the list, with the allocation of cross-sections to members being determined by the index of the element in the list of cross-sections. In selecting the RHS cross-sections for the top and bottom chords, the primary consideration was the feasibility of the joints. It was determined that the process of cutting the CHS-to-CHS connection would be more complex than that of the RHS-to-CHS. The remaining elements, namely the diagonals, end diagonals and struts, exhibited a CHS cross-section configuration. As previously stated, this was undertaken solely for the purpose of introducing a more realistic design.

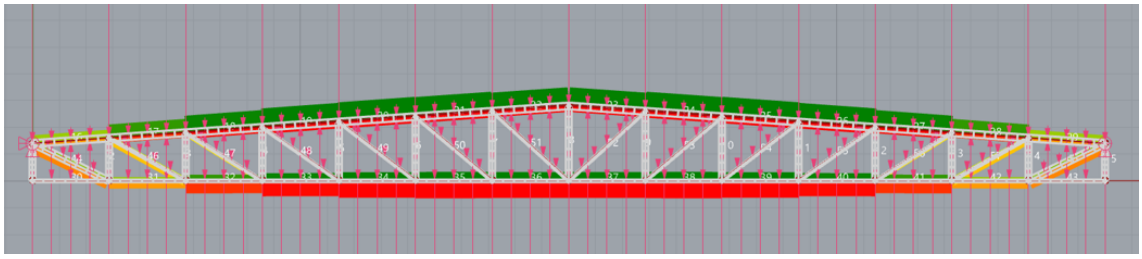

Fig. 6.1: Roof truss in Rhinoceros

Optimization Framework

The selection of this framework was motivated by the advantages offered by fast geometry parametric modelling and the consequent capacity to transfer data from Grasshopper to alternative software. This functionality is instrumental for practical engineers. Grasshopper [7] can be interpreted as a building information model (BIM) [37] hub. The computational workflow utilizes:

- **Grasshopper** [7] for parametric geometry generation
- **Rhinoceros** [15] as the base CAD platform
- **Kiwi!3D** [8] plugin for structural analysis

Optimization Parameters

The optimization parameters were configured with heights set at 0.1 m increments, a sufficient increment to effect global changes and ensure precise optimization.

Possible combinations of fitness parameters:

$$C = \underbrace{21 \times 21 \times 15}_{\substack{\text{Geometrical parameters} \\ \text{(3 variables)}}} \times \underbrace{100 \times 100 \times 100 \times 100 \times 100}_{\substack{\text{Cross-sectional parameters} \\ \text{(5 variables, 100 values each)}}} \tag{6.1}$$

Where:

$$\text{Geometrical parameters:} \quad \begin{cases} h_{\text{end}} \in [1.0, 2.0]\,\text{m} & \text{(End height, 21 values)} \\ h_{\text{mid}} \in [2.0, 3.0]\,\text{m} & \text{(Mid-span height, 21 values)} \\ n_{\text{fields}} \in \{2, \ldots, 16\} & \text{(Truss fields, 15 values)} \end{cases}$$

Cross-sectional parameters (100 values each):

- Top chord cross-sections
- Bottom chord cross-sections
- Diagonal cross-sections (excluding end diagonals)
- Strut cross-sections
- End diagonal cross-sections

Validation Criteria

Each iteration enforces:

$$\begin{cases} \text{Resistance checks:} & N_{\text{Ed}} \leq N_{\text{Rd}} \\ \text{Stability requirements:} & N_{\text{Ed}} \leq N_{\text{b,rd}} \\ \text{Deflection:} & w_{\max} \leq 160\,\text{mm} \\ \text{Constructibility:} & \text{Limits acc. to Equation 1.1} \end{cases} \tag{6.2}$$

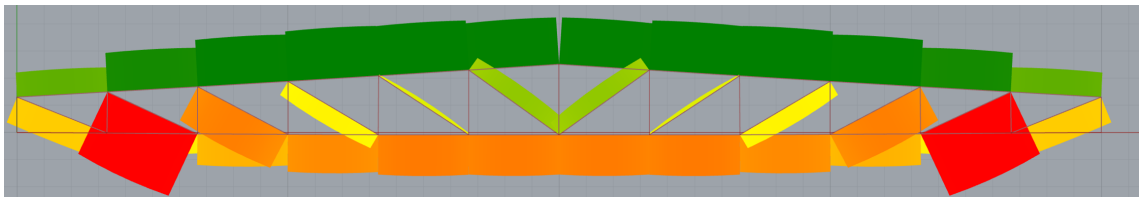

Fig. 6.2: Normal stresses for S355, maximum compression in top chord load configuration

Penalty Function Implementation

A strict penalty system ensures solution feasibility:

$$W_{\text{total}} = \begin{cases} \sum(m_{\text{members}}) & \text{if all criteria 6.2 satisfied} \\ 10^9\,\text{kg} & \text{otherwise} \end{cases} \tag{6.3}$$

Non-compliant designs receive an artificial weight penalty of 1,000,000,000 kg, effectively removing them from the solution space while maintaining genetic algorithm population diversity.

Workflow Implementation

The optimization process follows:

1. Parametric model generation in Grasshopper [7]
2. Internal force calculation via Kiwi!3D [8]
3. Automated code compliance verification
4. Fitness evaluation with penalty application
5. Genetic algorithm-driven parameter mutation

6.2 Discussion

The Galapagos plugin genetic algorithm [10], which is part of the Grasshopper [7] default tools, was utilized in this study. The optimization process for the number of parameters in this study was time-consuming; all possible combinations can be seen from Equation 6.1. It is important to note that the optimization process begins from scratch in order to find some genome of the successful results, in order to comply with all the conditions for achieving successful results, meaning the absence of the weight penalty. It is submitted that the duration of the analysis process could be reduced by enabling the optimization process to be initiated from predefined parameters. The configuration of optimization parameters that yield successful outcomes, in which

the weight penalty is not implemented, has the potential to reduce the time required for optimization.

It is important to note that utilizing genetic algorithms has the ability to yield a local minimum result, which, in principle, shouldn't be the most optimal outcome [38]. An analysis of the employment of this particular optimization technique within the domain of civil engineering reveals that, while it is unable to address every conceivable issue, its incorporation into design processes has the potential to enhance design efficiency, leading to a reduction in the weight of the structure or design structure for economic efficiency, while maintaining required safety. In the present study, optimization was pursued with the objective of structure weight optimization. However, it should be noted that the purpose of optimization can be easily modified. For instance, if the objective is to facilitate an economical design, then optimization can be conducted to reduce welding, as this process is the most expensive aspect of the structure. Optimization can be defined as the process of minimizing the perimeters of members to achieve shorter welding lengths. In terms of the practical applications of designing steel structures, optimization in the Grasshopper environment [7] is considered to be sufficient and has been demonstrated to produce effective outcomes.

Final design required change in cross-sections due to connection design, final weight is 35kg/m^2, weight obtained from the optimization process is 22kg/m^2. It is important to note that the full range of connection validity was not verified during the optimization process.

Summary

The present study examined the design codes for the calculation of circular hollow sections. A comparison was then made between these design codes and finite element analysis (FEA) software IDEA StatiCa Connection [4], which utilises the component-based finite element method (CBFEM) [28]. The primary objective of the present study is to furnish information regarding the manner in which the new generation of Eurocode differs from existing codes, and to undertake a comparative analysis with FEA.

This study computed approximately 50,000 CBFEM models using Python API calls. The results include a comparative analysis of different connection criteria.

As demonstrated in CIDECT DG 1 [14], the theoretical background of existing design methods EN 1993-1-8 [2] and AISC 360-22 [3] is shared. It is evident that the new EN code design differs from the existing design methods. The most significant differences are attributable to the explicit utilization of high-strength steel yield strength (700MPa) (100ksi) and the reduction of resistance based on tension stress in the joint.

The new generation of the EN code was found to be less conservative, with higher resistances predicted for the CHS-to-CHS K and T&Y, see Figure 4.10. The predictions for the CHS-to-CHS X resistances remained almost unchanged, see Figure 4.10.

A comparison of the results of the design code calculation and the CBFEM method reveals that the new EN code demonstrates a high degree of agreement with the absence of chord stress results, and the results scatter is also aligned.

The findings indicate that the presence of chord stress is associated with lower alignment with CBFEM calculations. As is evident from the results obtained, the CBFEM model exhibited non-linear behaviour in response to the varying steel grades. This observation necessitates further investigation to ascertain the underlying causes and implications.

References

1. CEN/TECHNICAL COMMITTEE (TC) 250. *Second Generation of the Eurocodes* [online]. 2023. Available at: https://eurocodes.jrc.ec.europa.eu/second-generation-eurocodes.
2. STANDARDIZATION (CEN), E. C. for. *Eurocode 3: Design of Steel Structures - Part 1-8: Design of Joints*. 2005. Available also from: https://eurocodes.jrc.ec.europa.eu/EN-Eurocodes/eurocode-3-design-steel-structures. EN 1993-1-8:2005.
3. AMERICAN INSTITUTE OF STEEL CONSTRUCTION (AISC). *Specification for Structural Steel Buildings (ANSI/AISC 360-22)* [https://www.aisc.org/Specification-for-Structural-Steel-Buildings-ANSIAISC-360-22-Download]. Chicago, IL : American Institute of Steel Construction, 2022. Supersedes the Specification for Structural Steel Buildings dated June 7, 2016, and all previous versions. Revised September 2023.
4. IDEA STATICA S.R.O. *IDEA StatiCa Connection – Structural design of steel connections*. 2025. Available at: https://www.ideastatica.com/support-center/general-theoretical-background; Accessed: 6 February 2025.
5. PYTHON SOFTWARE FOUNDATION. *Python Programming Language*. 2025. Available also from: https://www.python.org. Version 3.12, accessed: 6 February 2025.
6. IDEA STATICA S.R.O. *IDEA StatiCa Connection Rest API*. 2025. Available at: https://developer.ideastatica.com/docs/api/api_overview.html; Accessed: 6 February 2025.
7. DAVID RUTTEN. *Grasshopper for Rhinoceros*. 2025. Available also from: https://www.grasshopper3d.com. Version 1.0, accessed: 6 February 2025.
8. KIWI!3D DEVELOPMENT TEAM. *Kiwi!3D: A Structural Analysis Plugin for Grasshopper*. 2025. Available also from: https://www.kiwi3d.com. Version 1.0, accessed: 6 February 2025.
9. ORENSTEIN, BEN AND EVANS, CLARK AND INGERSON, BRIAN. *YAML: YAML Ain't Markup Language*. 2001–2025. Available also from: https://yaml.org. Version 1.2, accessed: 24 February 2025.
10. RUTTEN, D. *Galapagos: Evolutionary Solver for Grasshopper*. Robert McNeel & Associates, 2025. Version 1.0. Available also from: https://www.grasshopper3d.com/group/galapagos. Built-in component in Grasshopper (Rhinoceros).

11. LASTOVETSKYI, M. *Design of Hollow Section Joints: Comparison of Design Methods - Codebase*. Zenodo, 2025. Version 0.1. Available from DOI: 10.5281/zenodo.15519428. Bachelor's thesis technical appendix.

12. MORENO, M. *Photograph of the Dalí Museum in St. Petersburg, FL*. ArchDaily, 2011. Available also from: https://www.archdaily.com/103728/salvador-dali-museum-hok. Image credit: Moris Moreno.

13. WILLIBALD, S. *Bolted connections for rectangular hollow sections under tensile loading [online]*. Universität Karlsruhe (TH), 2003. Available from DOI: 10.5445/IR/1672003. PhD thesis. Universität Karlsruhe (TH). Fak. f. Bauingenieur-, Geo- und Umweltwissenschaften, Diss. v. 23.5.2003.

14. WARDENIER, J.; KUROBANE, Y.; PACKER, J.; VEGTE, G. van der; ZHAO, X.-L. *Design Guide 1 for Circular Hollow Section (CHS) Joints Under Predominantly Static Loading*. 2008. ISBN 978-3-938817-03-2. Second Edition, CIDECT: Comité International pour le Développement et l'Étude de la Construction Tubulaire.

15. ROBERT MCNEEL & ASSOCIATES. *Rhinoceros 3D*. 2025. Available also from: https://www.rhino3d.com. Version 8.0, accessed: 6 February 2025.

16. STANDARDIZATION (CEN), E. C. for. *Eurocode: Basis of structural design*. 2005. Available also from: https://eurocodes.jrc.ec.europa.eu/EN-Eurocodes/eurocode-basis-structural-design. EN 1990:2002/A1:2005.

17. ASGARIAN, B.; MOKARRAM, V.; ALANJARI, P. Local joint flexibility equations for Y-T and K-type tubular joints. *International Journal of Ocean Systems Engineering*. 2014, vol. 4, pp. 151–167. Available from DOI: 10.12989/ose.2014.4.2.151.

18. KUROBANE, Y.; MAKINO, Y.; MITSUI, Y. *Ultimate strength formulae for simple tubular joints*. Kumamoto, Japan, 1976. Tech. rep., IIW Doc. XV-385-76. Kumamoto University.

19. WARDENIER, J. *Hollow Section Joints*. Delft, The Netherlands : Delft University Press, 1982.

20. TOGO, T. *Experimental study on mechanical behaviour of tubular joints*. Osaka, Japan, 1967. PhD thesis. Osaka University. D.Eng. thesis. In Japanese.

21. WASHIO, K.; TOGO, T.; MITSUI, Y. *Cross Joints of Tubular Members*. Japan, 1966. Tech. rep. Kinki Branch of the Architectural Institute of Japan (AIJ). In Japanese.

22. LU, L.; WINKEL, G. de; YU, Y.; WARDENIER, J. Deformation limit for the ultimate strength of hollow section joints. In: *Proceedings of the 6th International Symposium on Tubular Structures*. Melbourne, Australia : A.A. Balkema, 1994, pp. 341–347.

23. KOSTESKI, N.; PACKER, J.; PUTHLI, R. A finite element method based yield load determination procedure for hollow structural section connections. *Journal of Constructional Steel Research*. 2003, vol. 59, no. 4, pp. 453–471. ISSN 0143-974X. Available from DOI: https://doi.org/10.1016/S0143-974X(02)00066-4.

24. CIDECT. *International Committee for the Development and Study of Tubular Structures*. n.d. Available also from: https://www.cidect.org. Organization contributing to research and standardization of tubular structures.

25. TUAN, Y.; RONDAL, J.; THONARD, F. *Flat Cutting of Tube Ends for Joining Circular Hollow Sections*. Belgium, 1985-09. Final Report, 5AH-85/1E. Université de Liège and Utema-Travhydro. CIDECT Research Project 5AH.

26. VEGTE, G. J. van der. *The static strength of uniplanar and multiplanar tubular T- and X-joints*. Delft, The Netherlands, 1995. PhD thesis. Delft University of Technology.

27. KUROBANE, Y.; MAKINO, Y.; OCHI, K. Ultimate resistance of unstiffened tubular joints. *Journal of Structural Engineering, American Society of Civil Engineers (ASCE)*. 1984, vol. 110, no. 2, pp. 385–400.

28. IDEA STATICA. *CBFEM: Component-Based Finite Element Method* [https://www.cbfem.com/]. 2025. Accessed: 2025-05-28.

29. IDEA STATICA. *Condensed superelements - invisible but essential* [https://www.ideastatica.com/blog/condensed-superelements-invisible-but-essential]. 2021. Available also from: https://www.ideastatica.com/blog/condensed-superelements-invisible-but-essential. Accessed: 2025-02-08.

30. COMPUTING OBJECTS SARL. *CM2 MeshTools SDK* [https://www.computing-objects.com]. 2025. N.d. Available also from: https://www.computing-objects.com/cm2-meshtools-sdk/. Accessed: 2025-02-7.

31. KOŽICH, M. *Plate to Circular Hollow Section Connections Made from High Strength Steel*. 2024. Available also from: http://hdl.handle.net/10467/118102. PhD Thesis. Czech Technical University in Prague. KOS Identifier: 824450495105.

32. IDEASTATICA. *General Theoretical Background for Idea StatiCa Connection* [Online]. 2014. Available also from: https://www.ideastatica.com/support-center/general-theoretical-background. Accessed: 01-2025.

33. FIELDING, R. T. *Architectural Styles and the Design of Network-based Software Architectures*. 2000. Tech. rep. University of California, Irvine. Available also from: https://www.ics.uci.edu/~fielding/pubs/dissertation/top.htm.

34. ORACLE CORPORATION. *MySQL Database Management System* [https://www.mysql.com/]. 2025. Version 8.0. Available also from: https://www.mysql.com/. Relational database management system.

35. WALD, F.; SABATKA, L.; BAJER, M.; BARNAT, J.; GODRICH, L.; HOLOMEK, J.; JEHLICKA, P.; KABELAC, J.; KOCKA, M.; KOLAJA, D.; KRAL, P.; KURIKOVA, M.; VILD, M. *Benchmark cases for advanced design of structural steel connections*. 2nd extended ed. Prague : Czech Technical University in Prague, 2017.

36. UMMENHOFER, T.; LIPP, A. *5CC-6/13, New Chord Load Function*. Karlsruhe, Germany, 2013-11. Tech. rep. University of Karlsruhe. Available also from: https://www.cidect.org/research-publications/. Language: English.

37. *ISO 19650-1:2018 - Organization and digitization of information about buildings and civil engineering works, including building information modelling (BIM)*. International Organization for Standardization, 2018. Available also from: https://www.iso.org/standard/68078.html.

38. RUTTEN, D. *Evolutionary Principles applied to Problem Solving* [Blog post series on *I Eat Bugs For Breakfast*]. 2011. Available also from: https://ieatbugsforbreakfast.com/2011/03/04/epatps01/. Adapted from lecture delivered at AAG10 conference, Vienna, 2010-09-21. Part of a technical series explaining Galapagos' implementation in Grasshopper 3D.

List of appendices

A CBFEM to code results

Note: The AISC 360-22 [3] design code results are limited to steel grades $\leq$ 360MPa *(*52ksi*), as this represents the maximum grade permitted by the standard.*

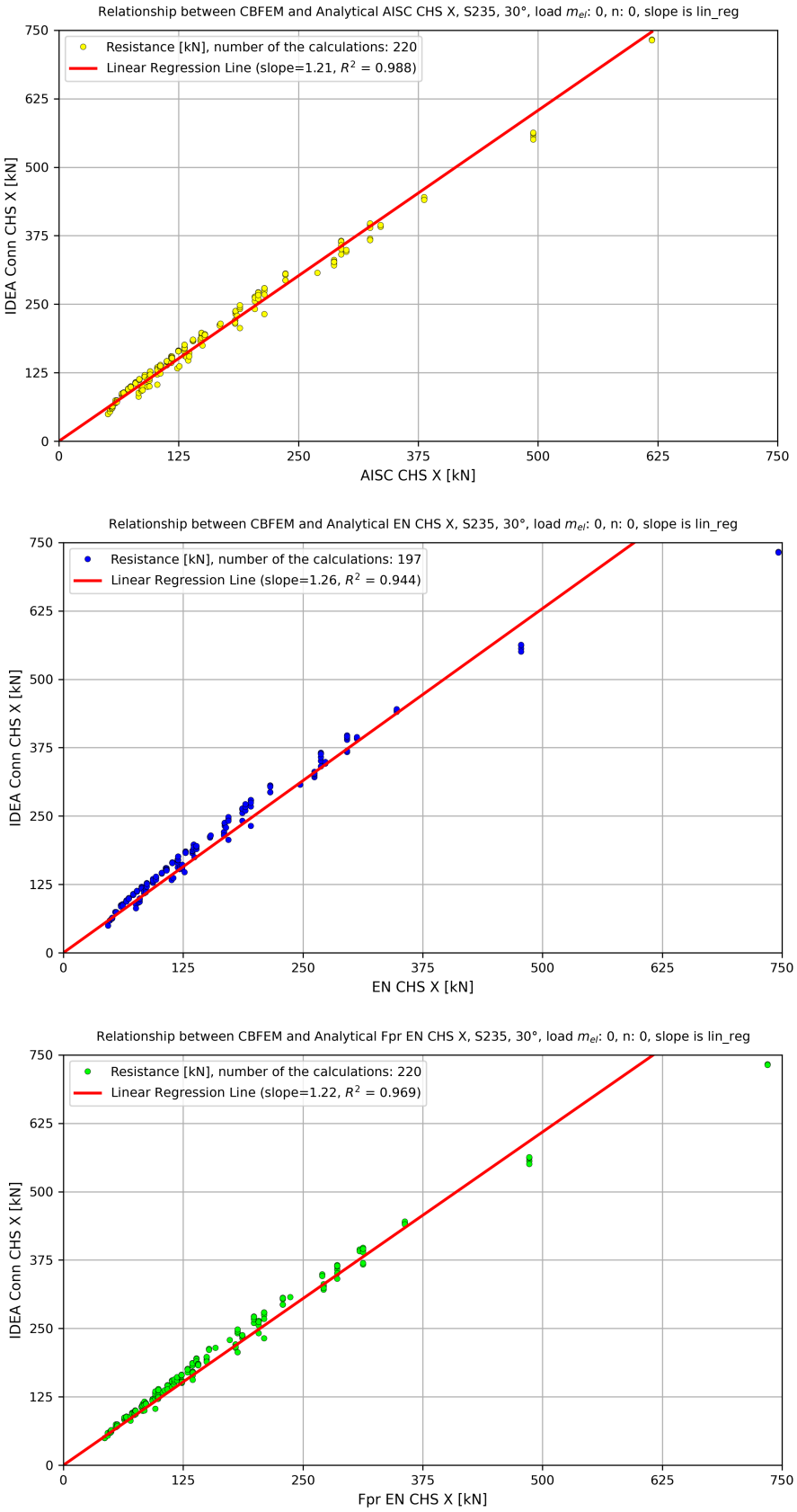

Fig. A.1: Analytical calculation and CBFEM comparison

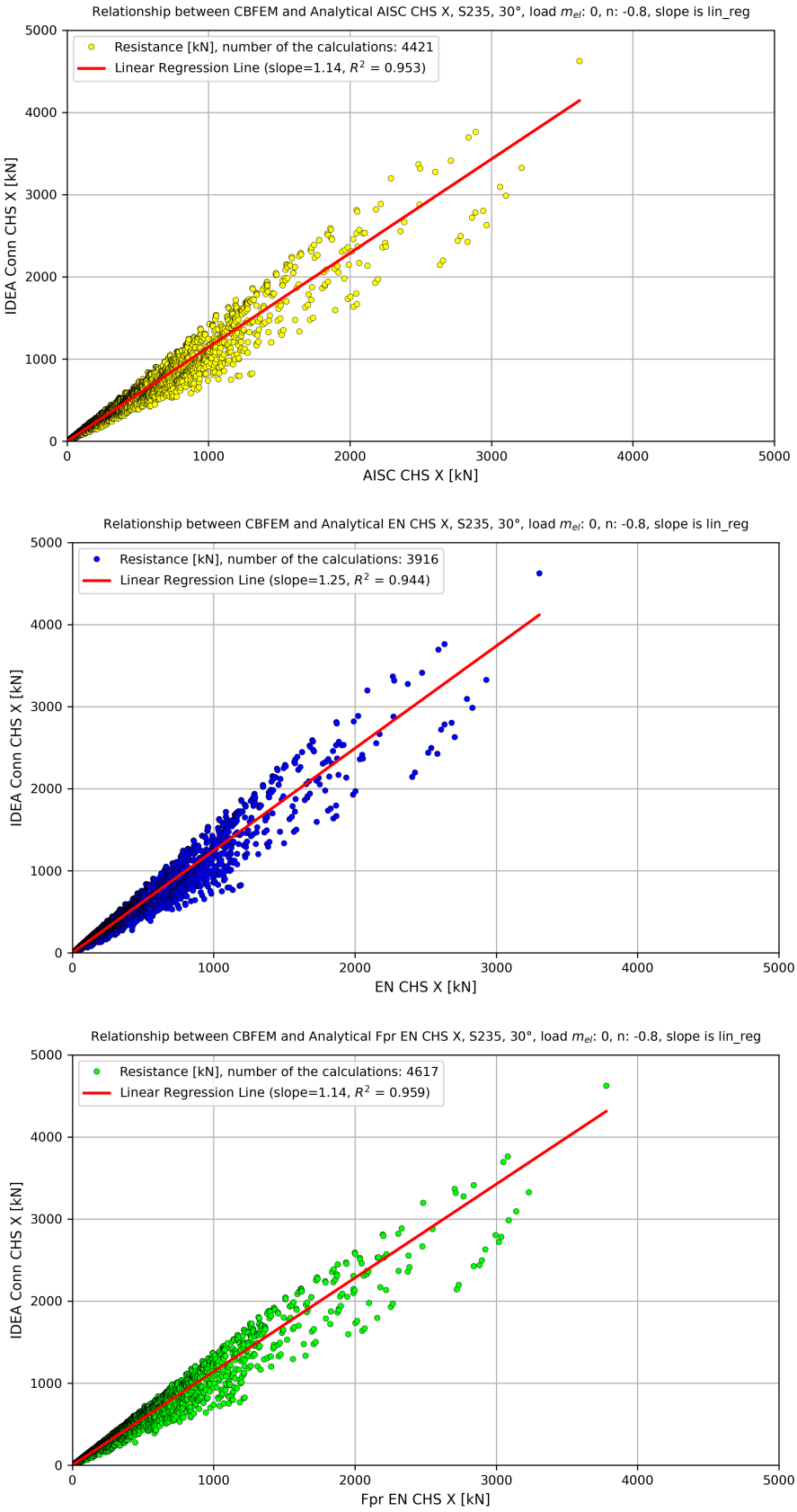

Fig. A.2: Analytical calculation and CBFEM comparison

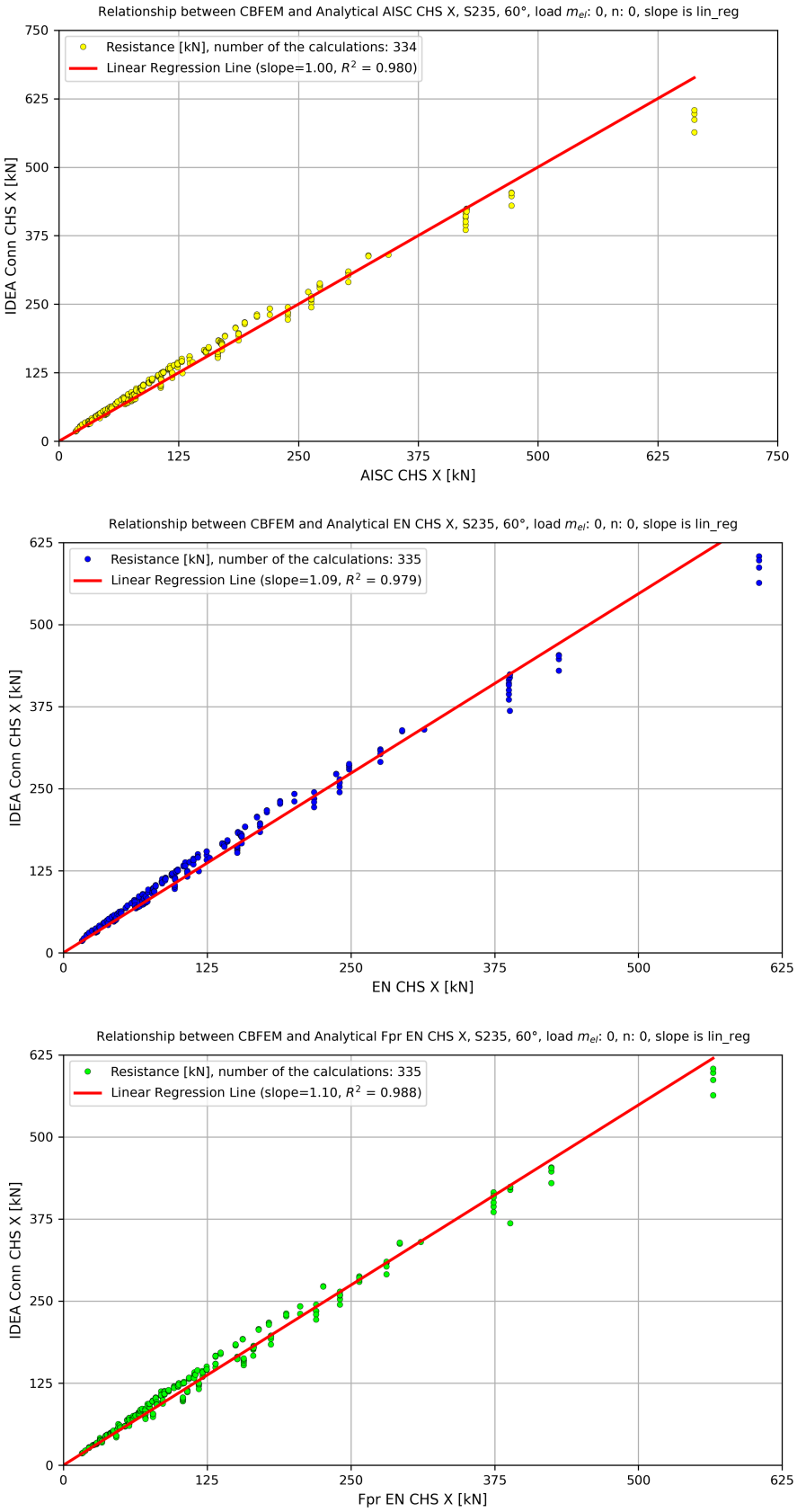

Fig. A.3: Analytical calculation and CBFEM comparison

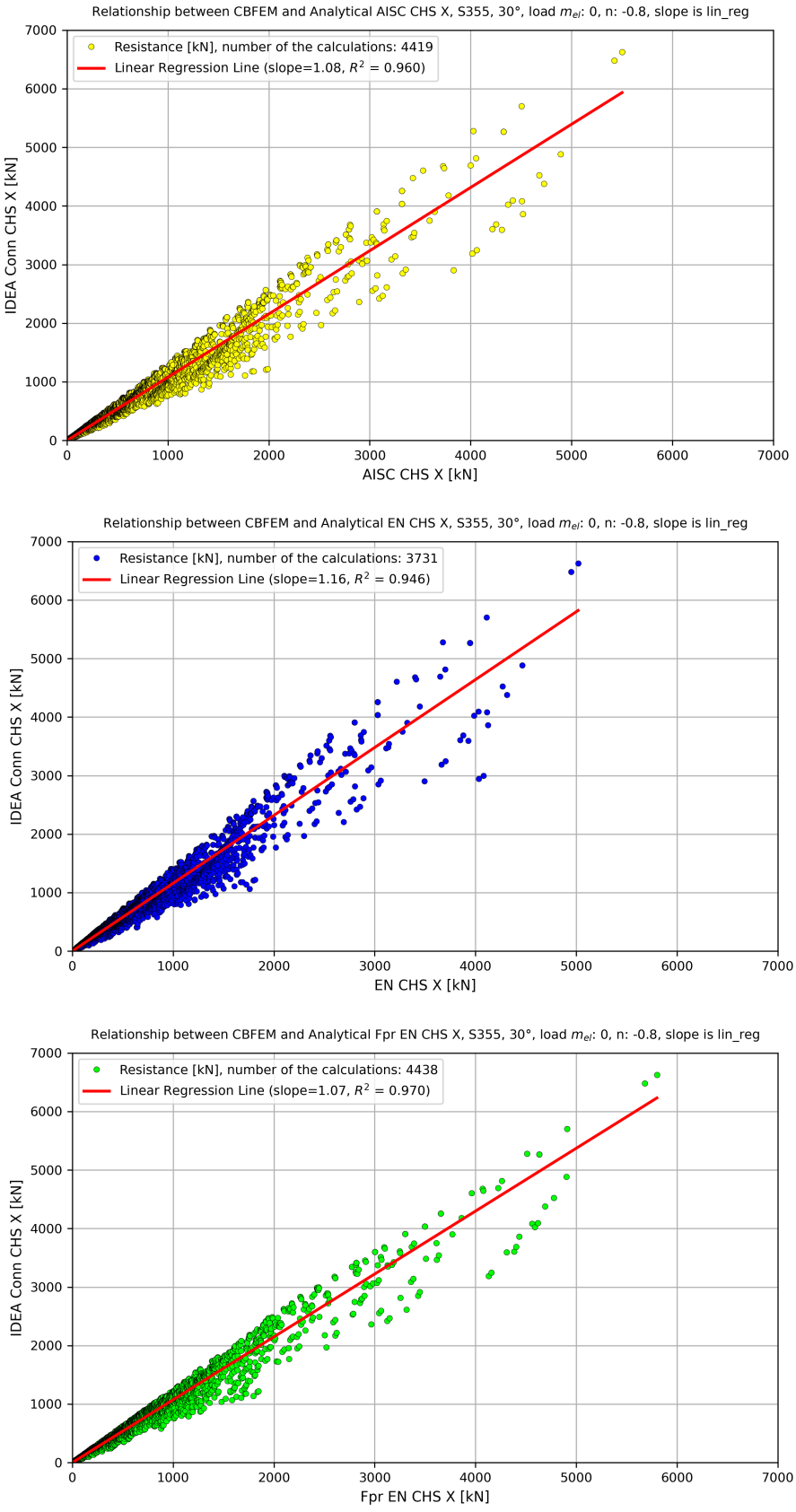

Fig. A.4: Analytical calculation and CBFEM comparison

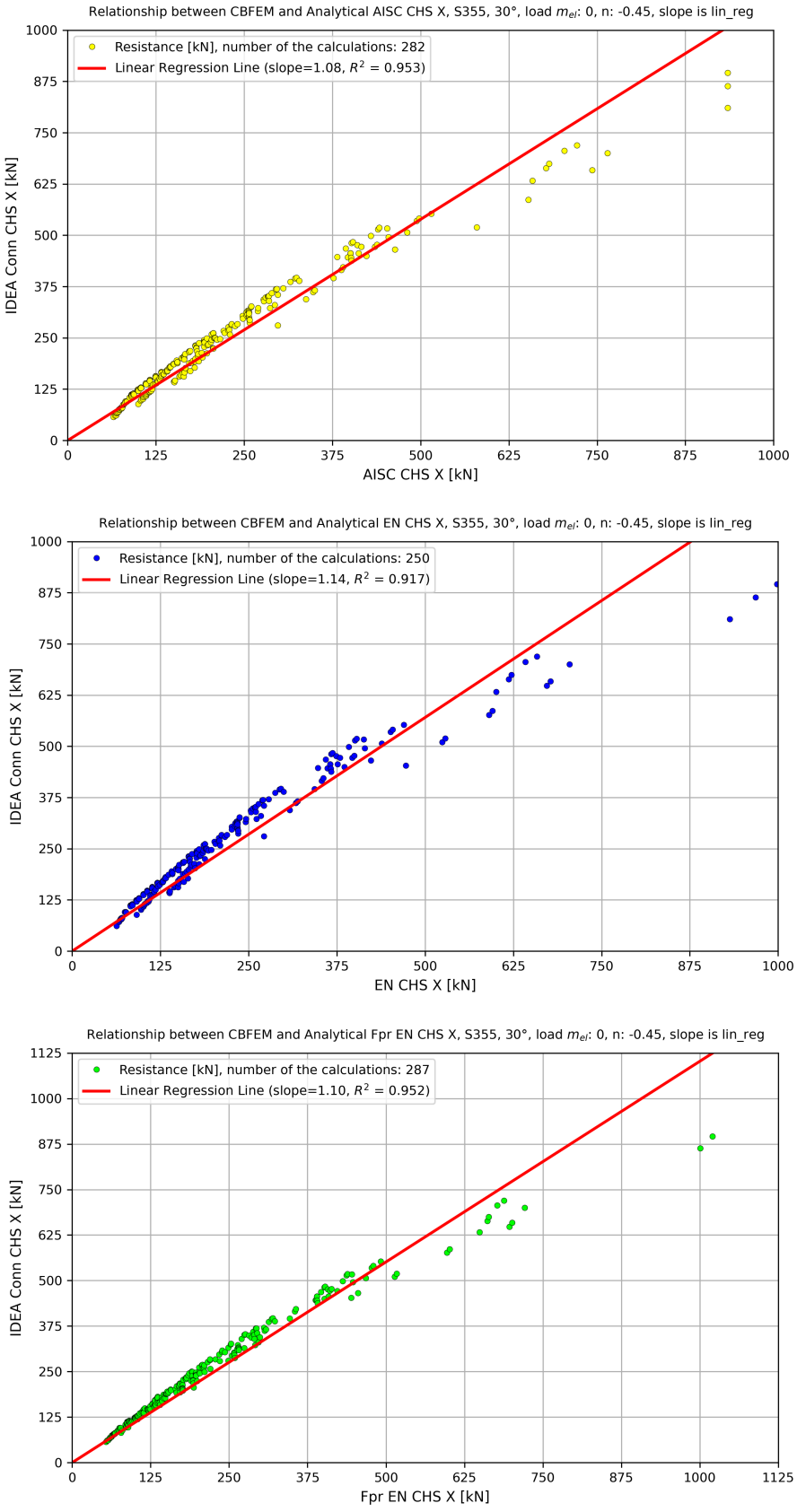

Fig. A.5: Analytical calculation and CBFEM comparison

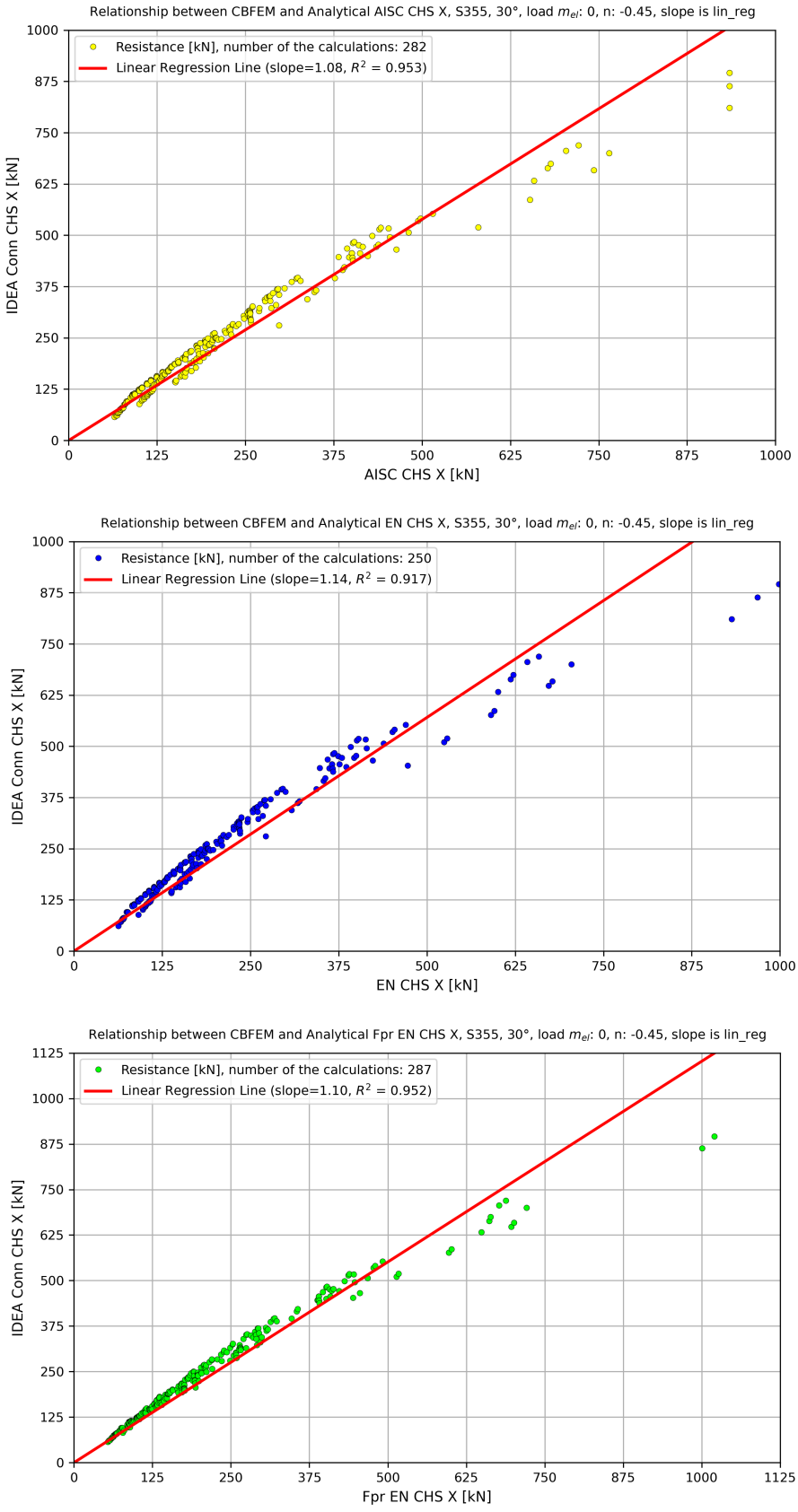

Fig. A.6: Analytical calculation and CBFEM comparison

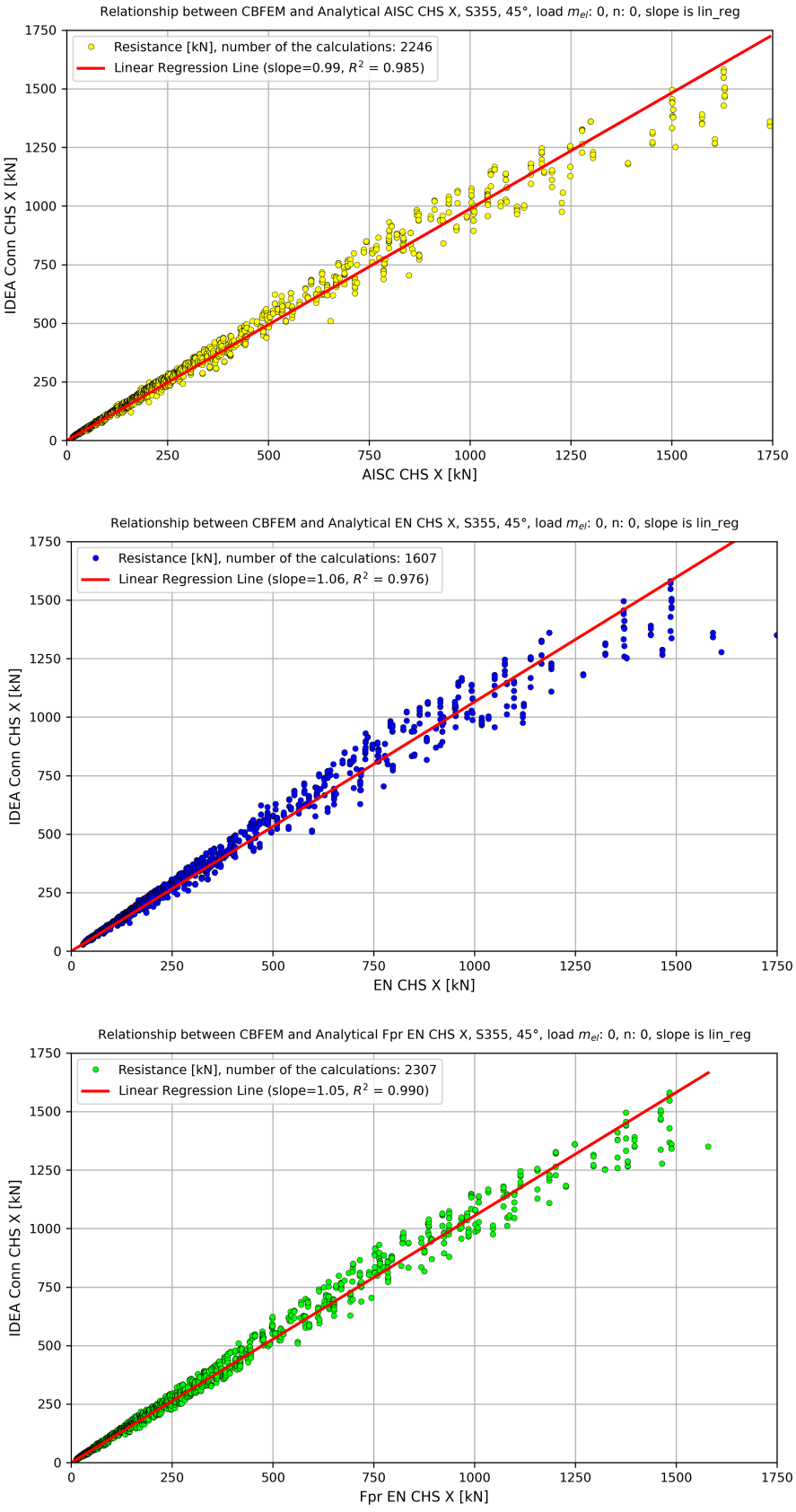

Fig. A.7: Analytical calculation and CBFEM comparison

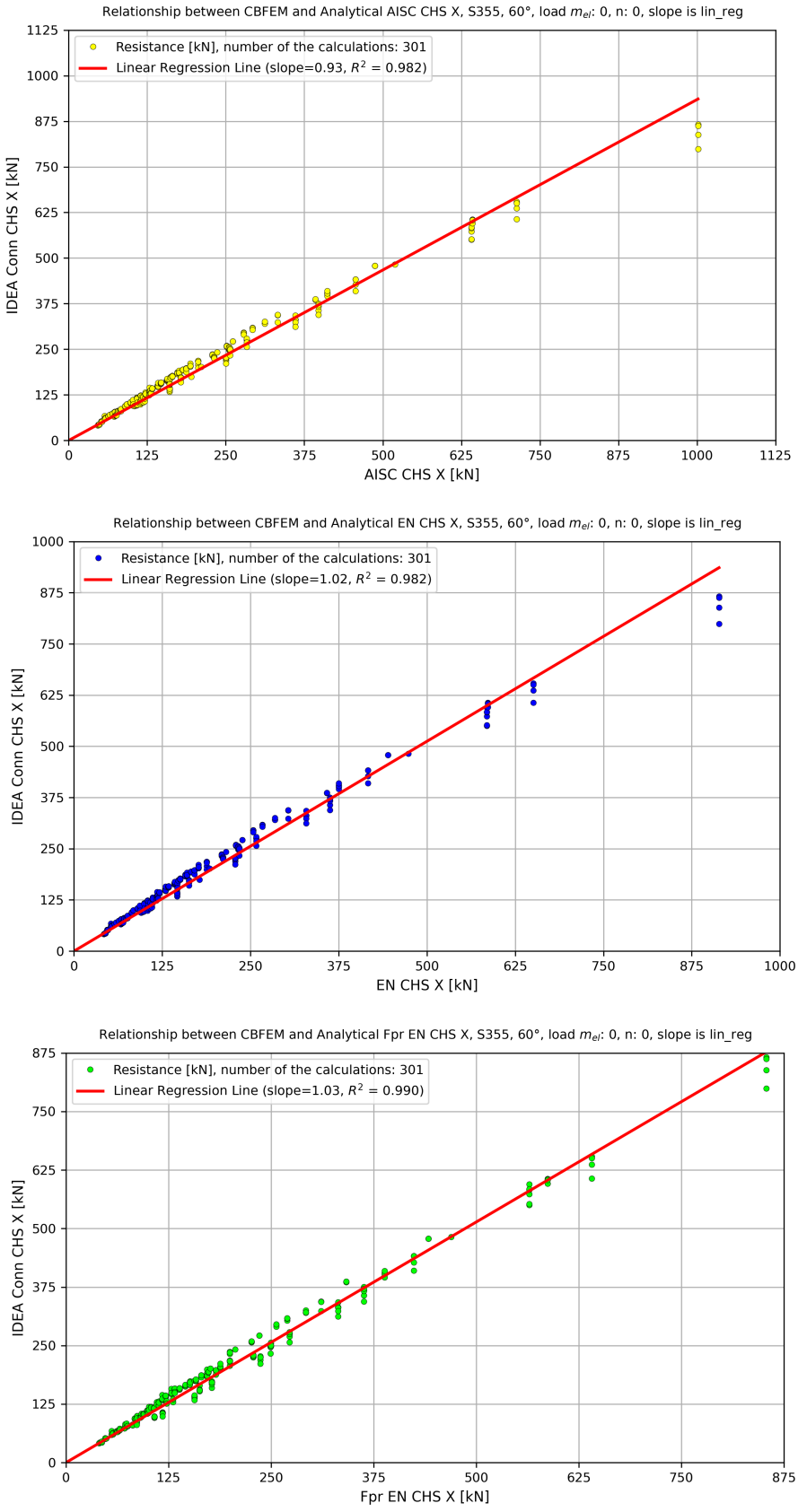

Fig. A.8: Analytical calculation and CBFEM comparison

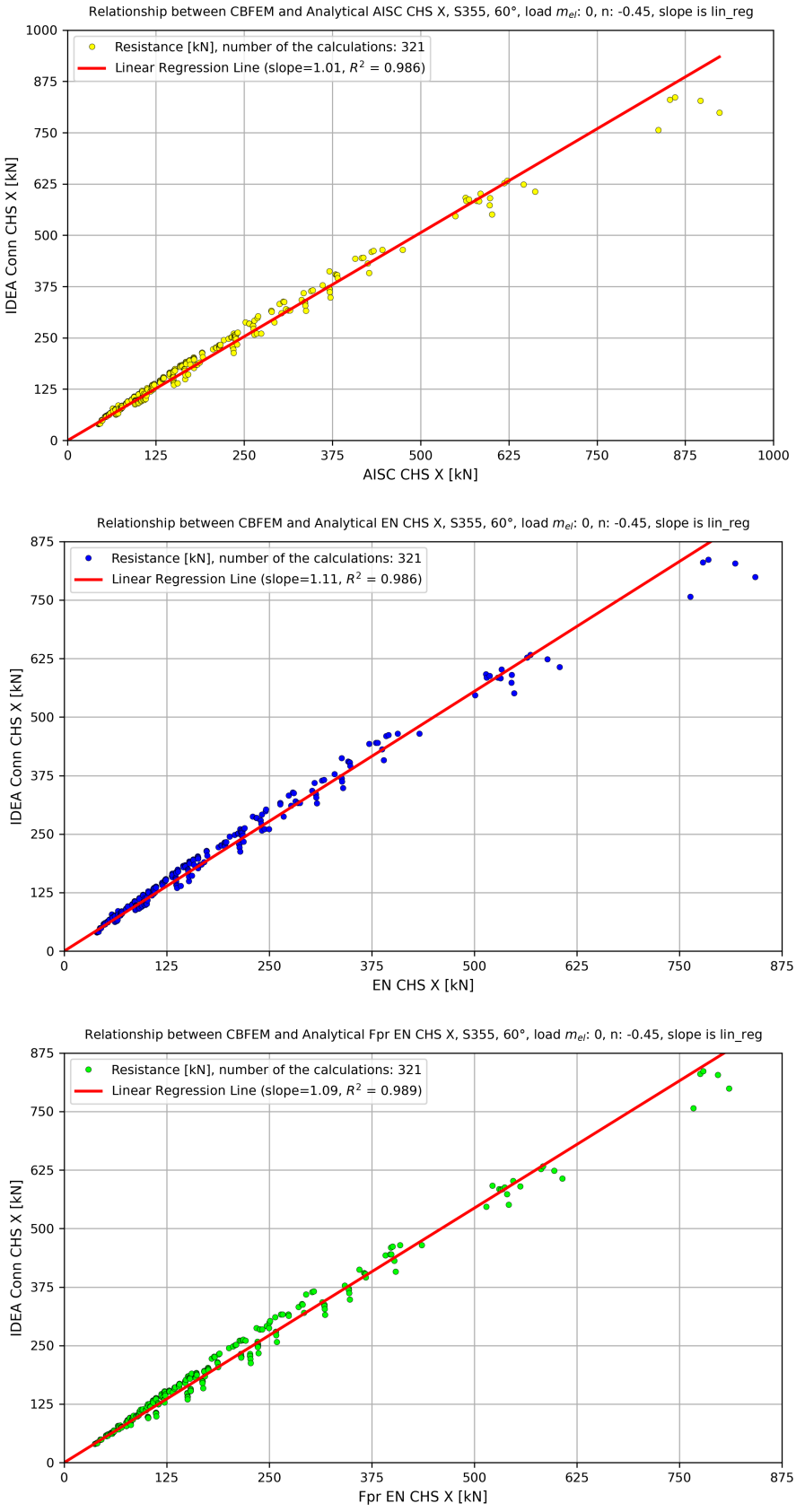

Fig. A.9: Analytical calculation and CBFEM comparison

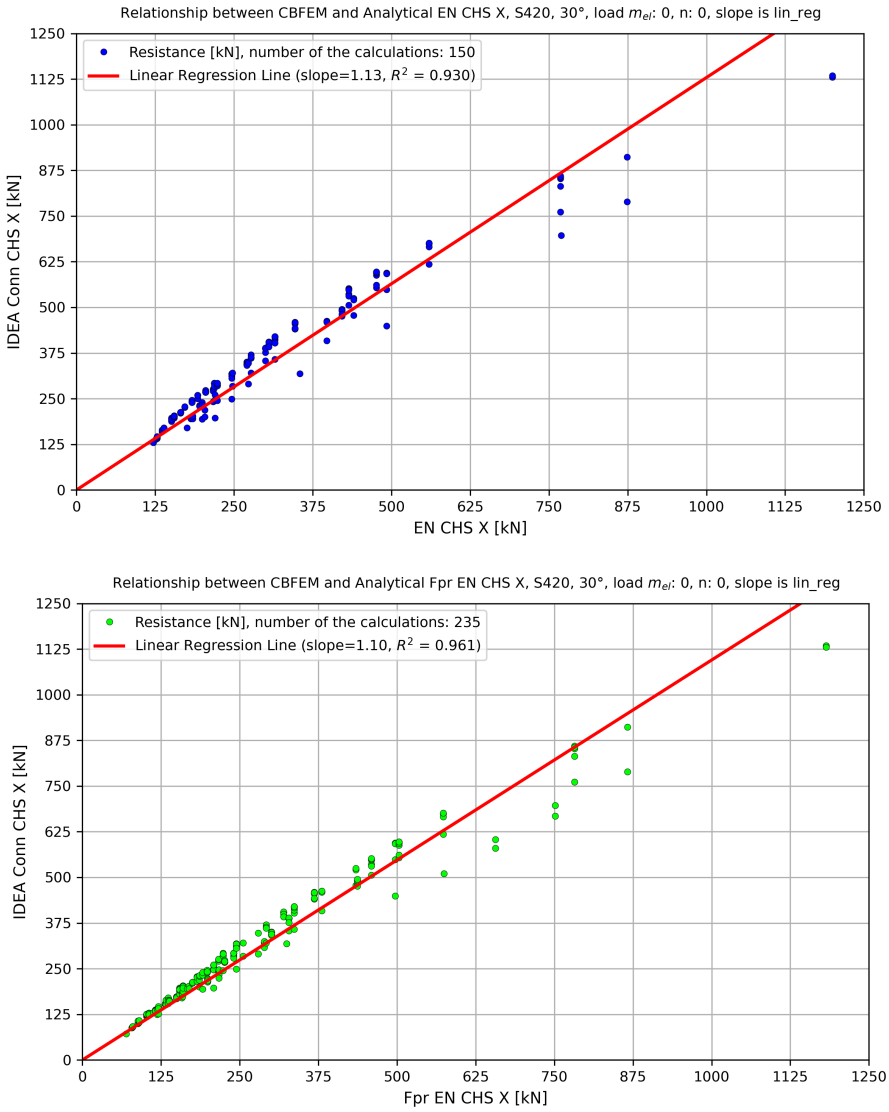

Fig. A.10: Analytical calculation and CBFEM comparison

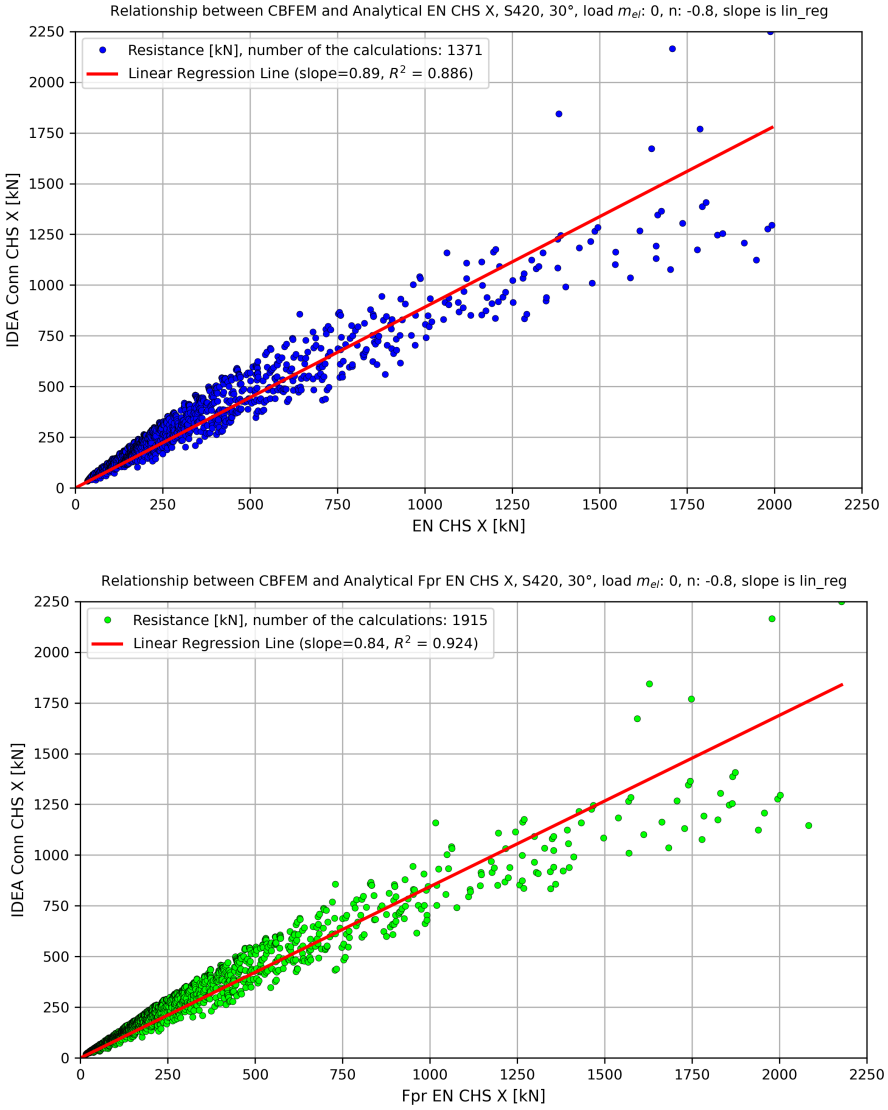

Fig. A.11: Analytical calculation and CBFEM comparison

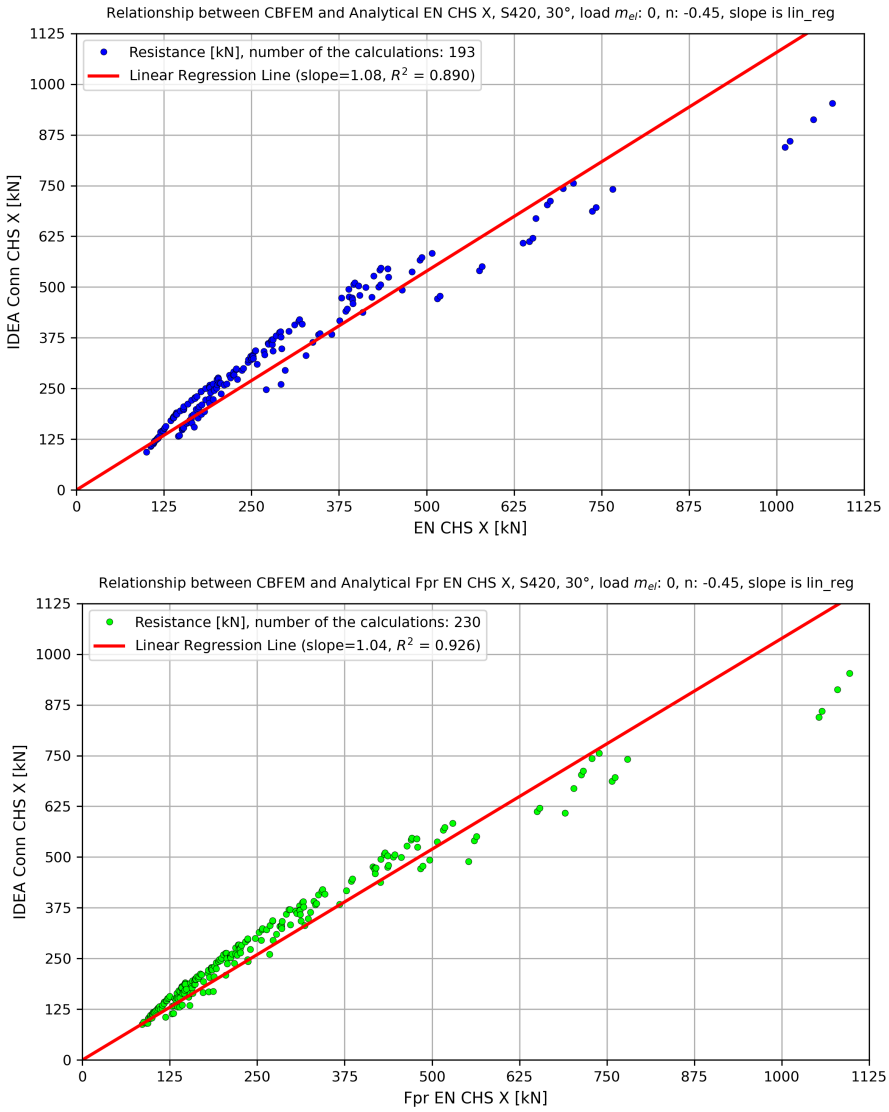

Fig. A.12: Analytical calculation and CBFEM comparison

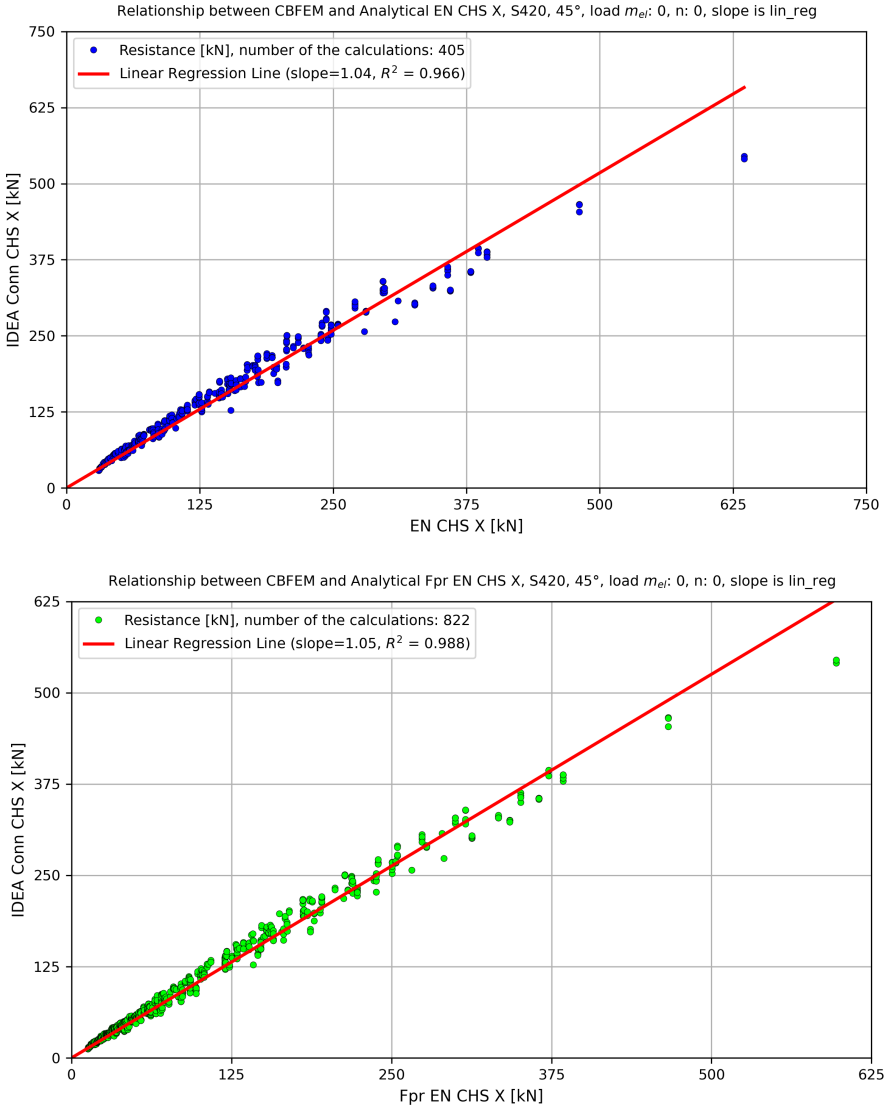

Fig. A.13: Analytical calculation and CBFEM comparison

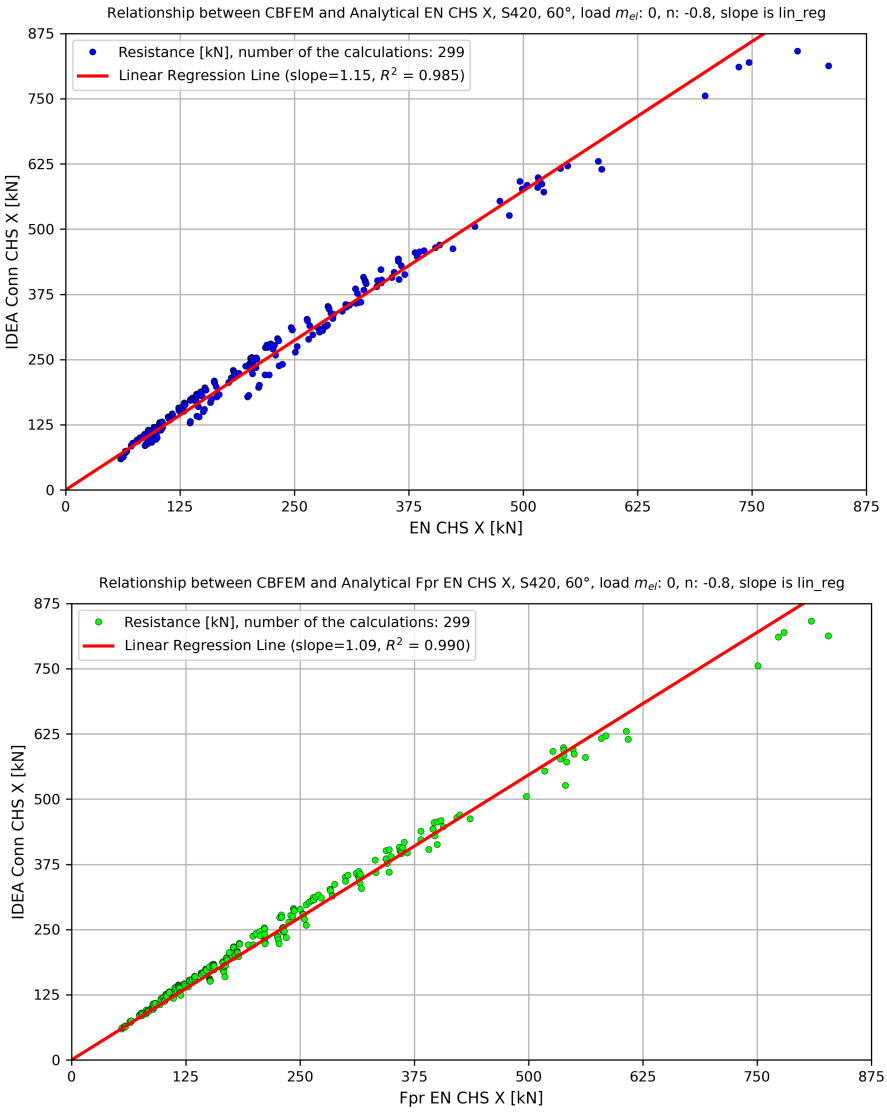

Fig. A.14: Analytical calculation and CBFEM comparison

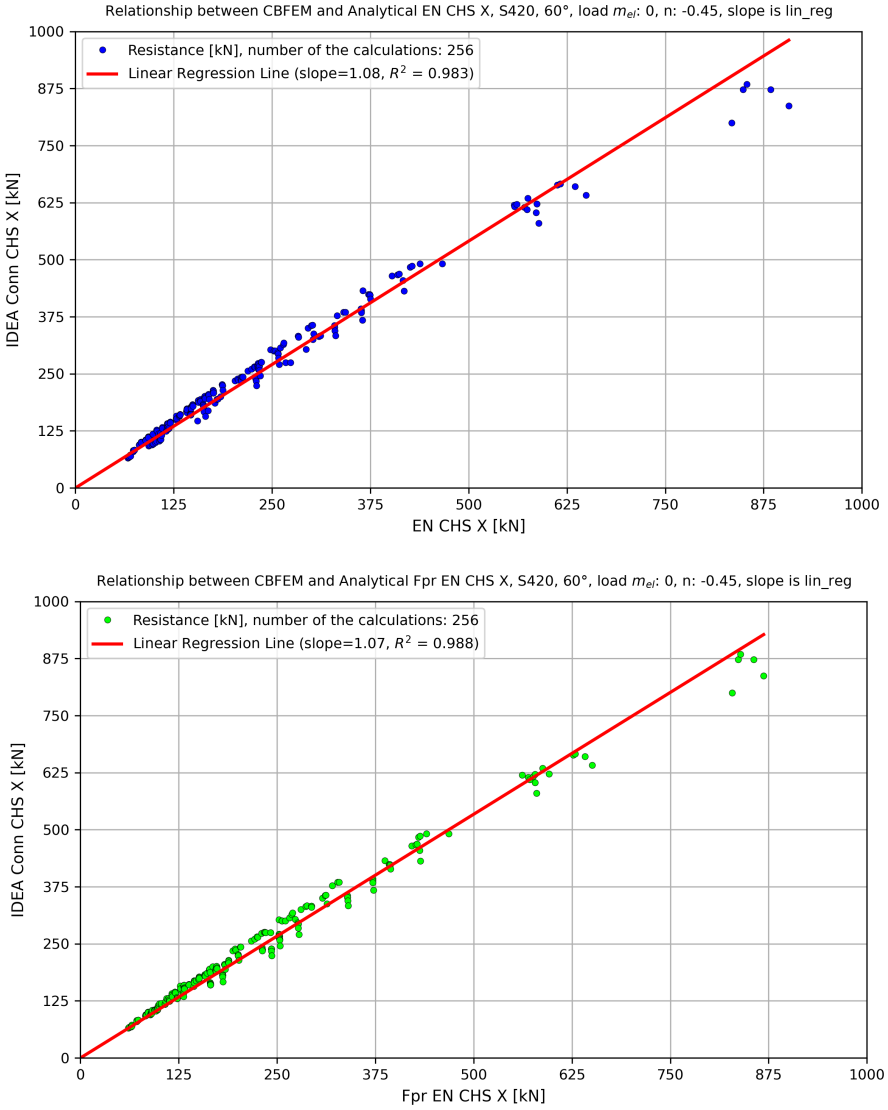

Fig. A.15: Analytical calculation and CBFEM comparison

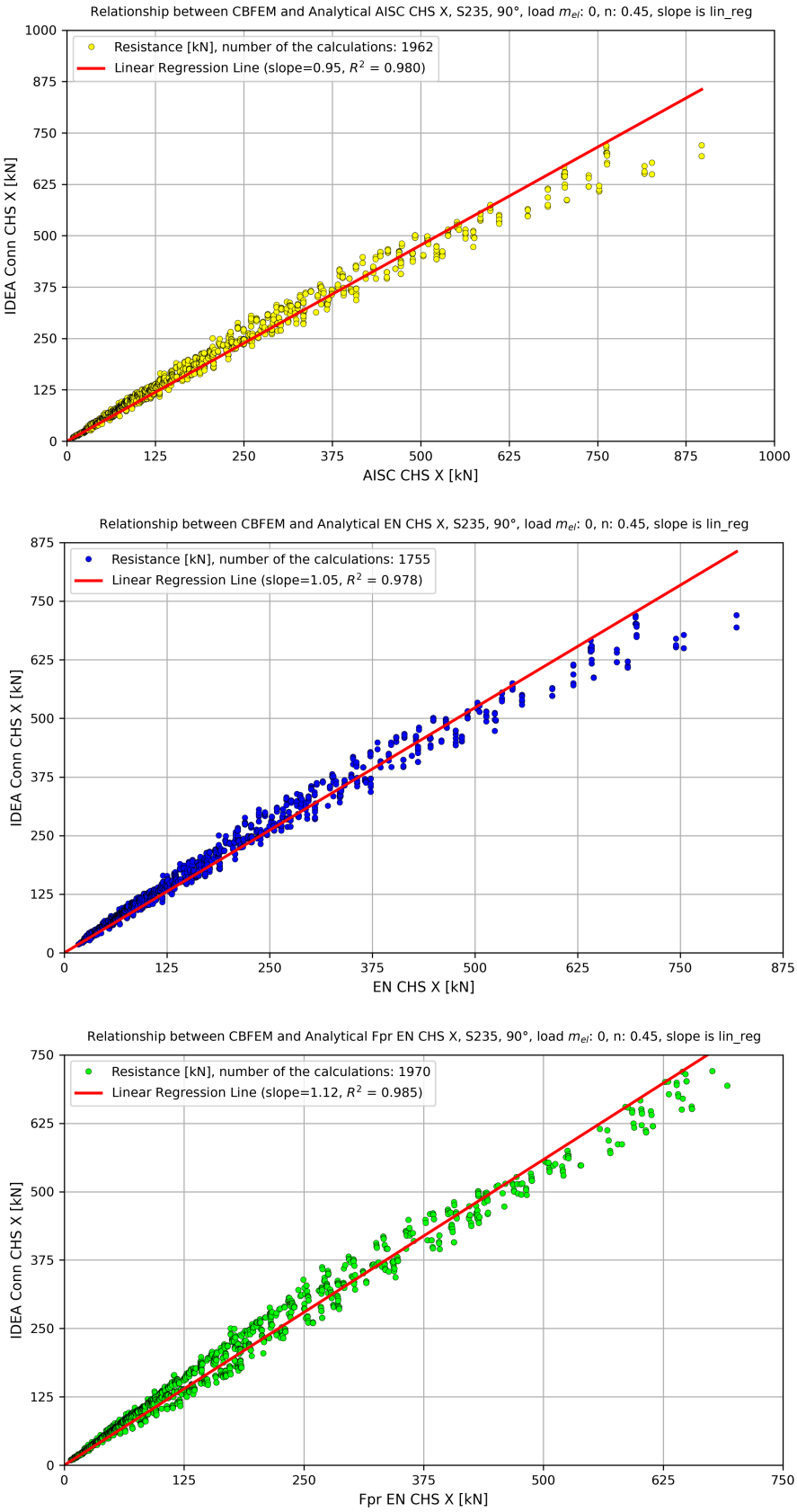

Fig. A.16: Analytical calculation and CBFEM comparison

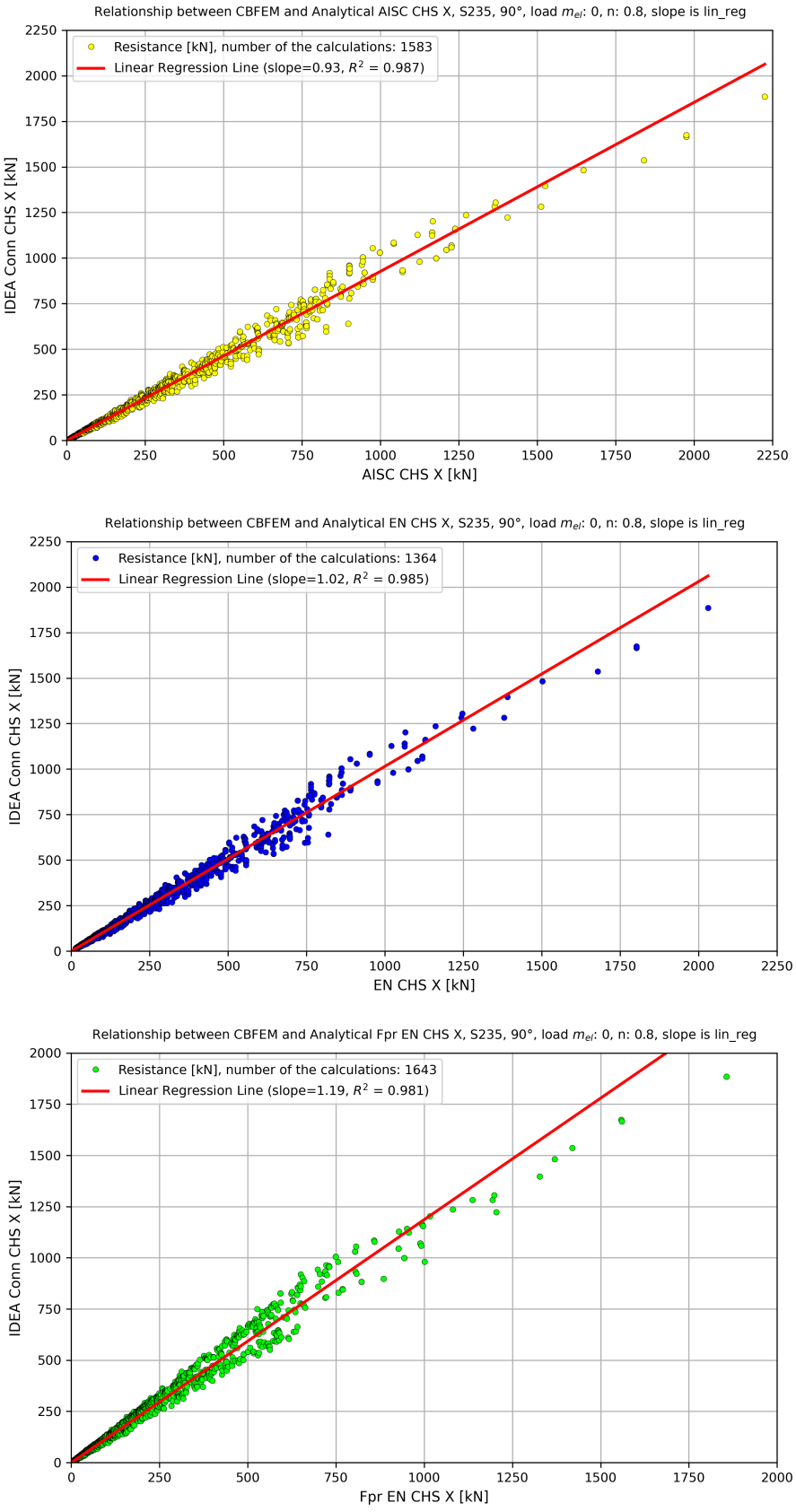

Fig. A.17: Analytical calculation and CBFEM comparison

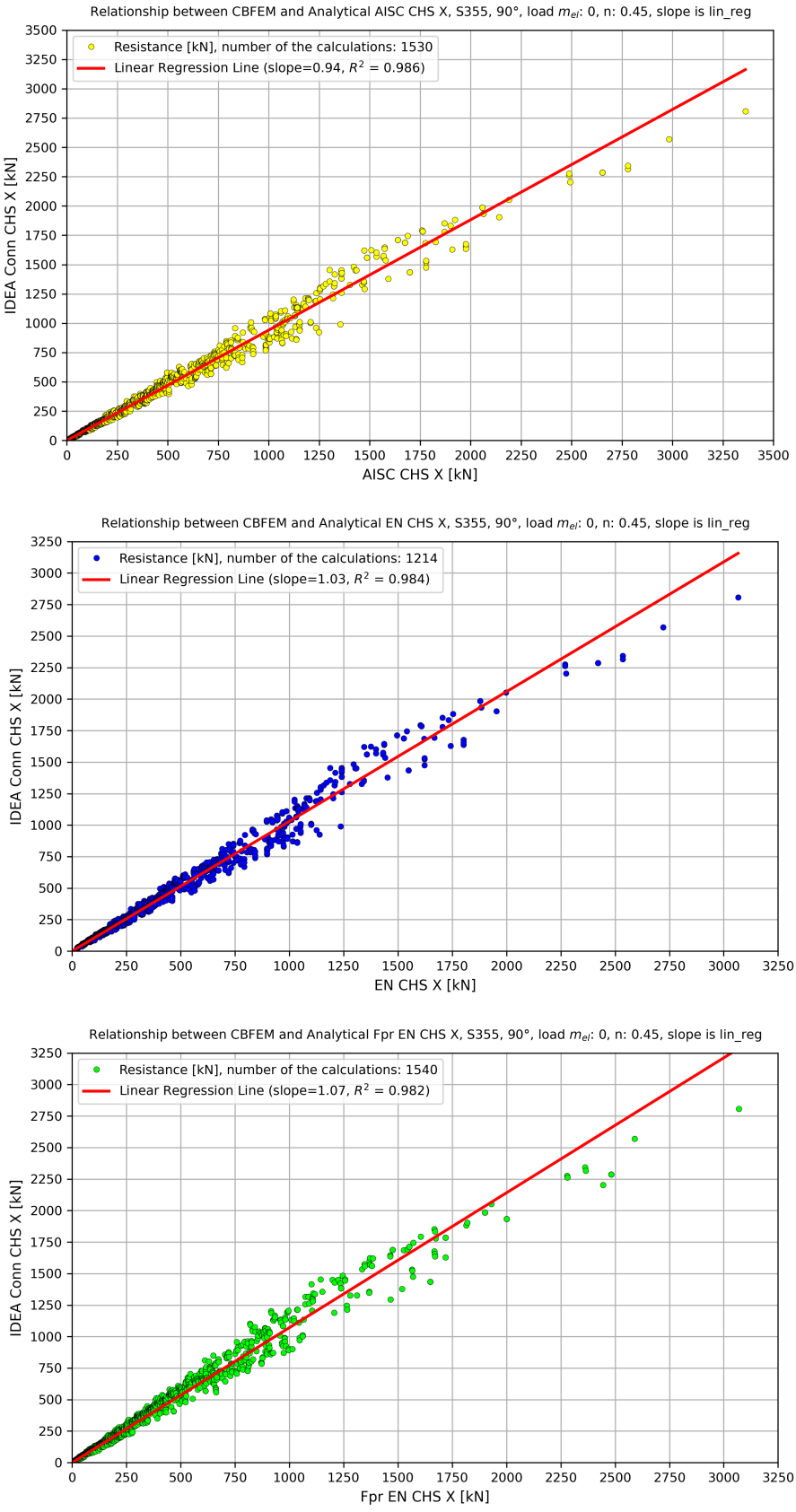

Fig. A.18: Analytical calculation and CBFEM comparison

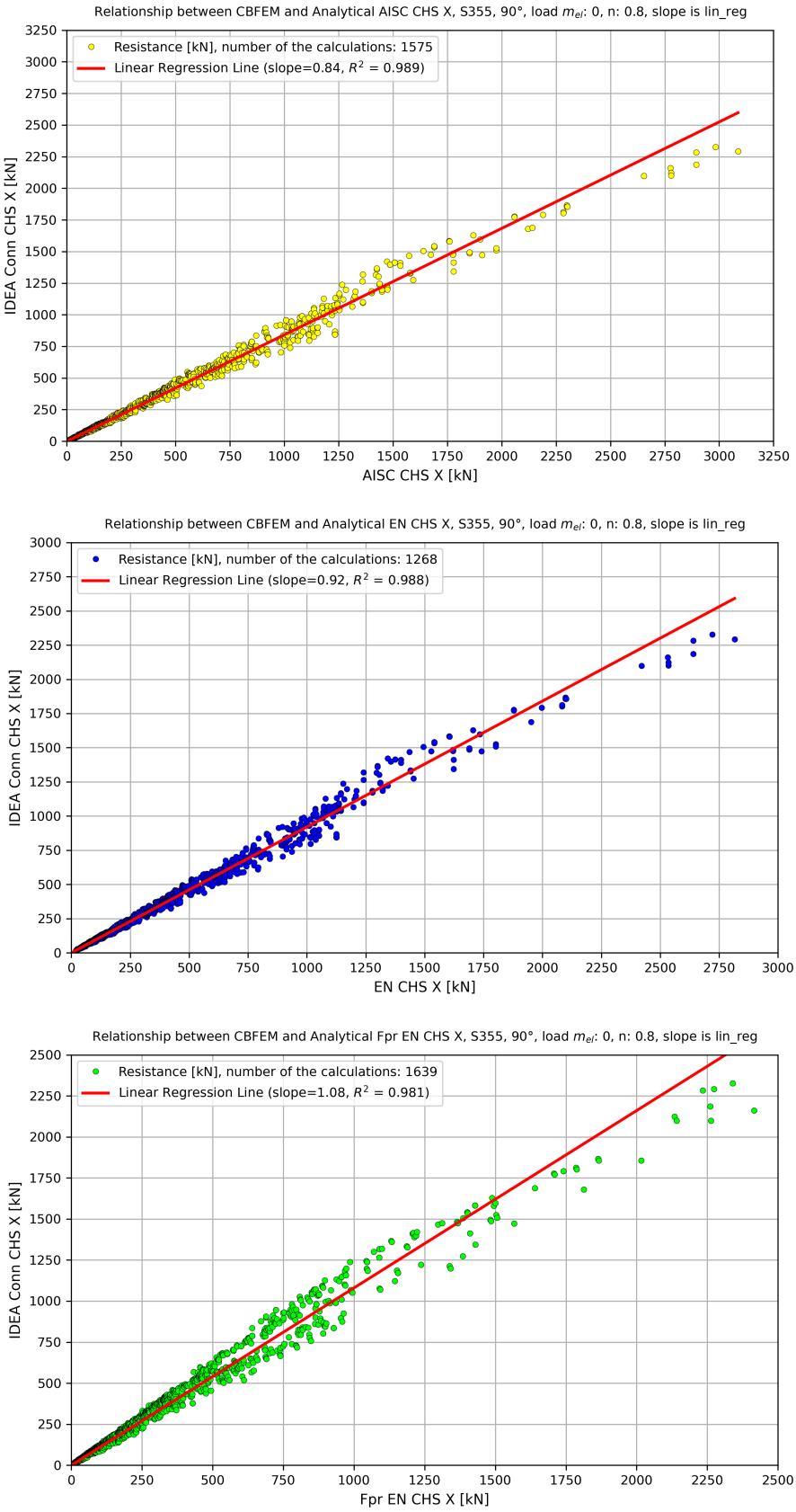

Fig. A.19: Analytical calculation and CBFEM comparison

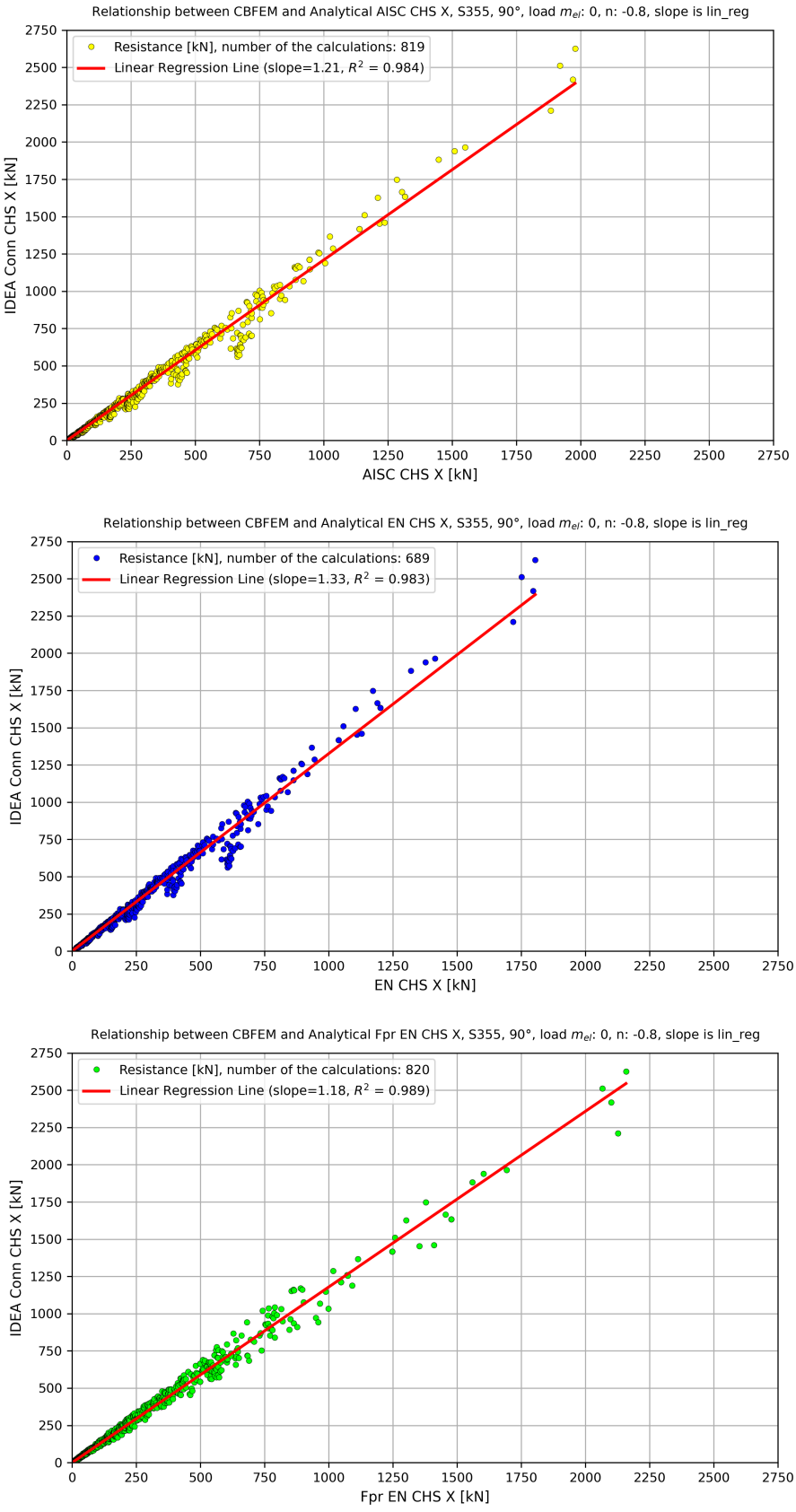

Fig. A.20: Analytical calculation and CBFEM comparison

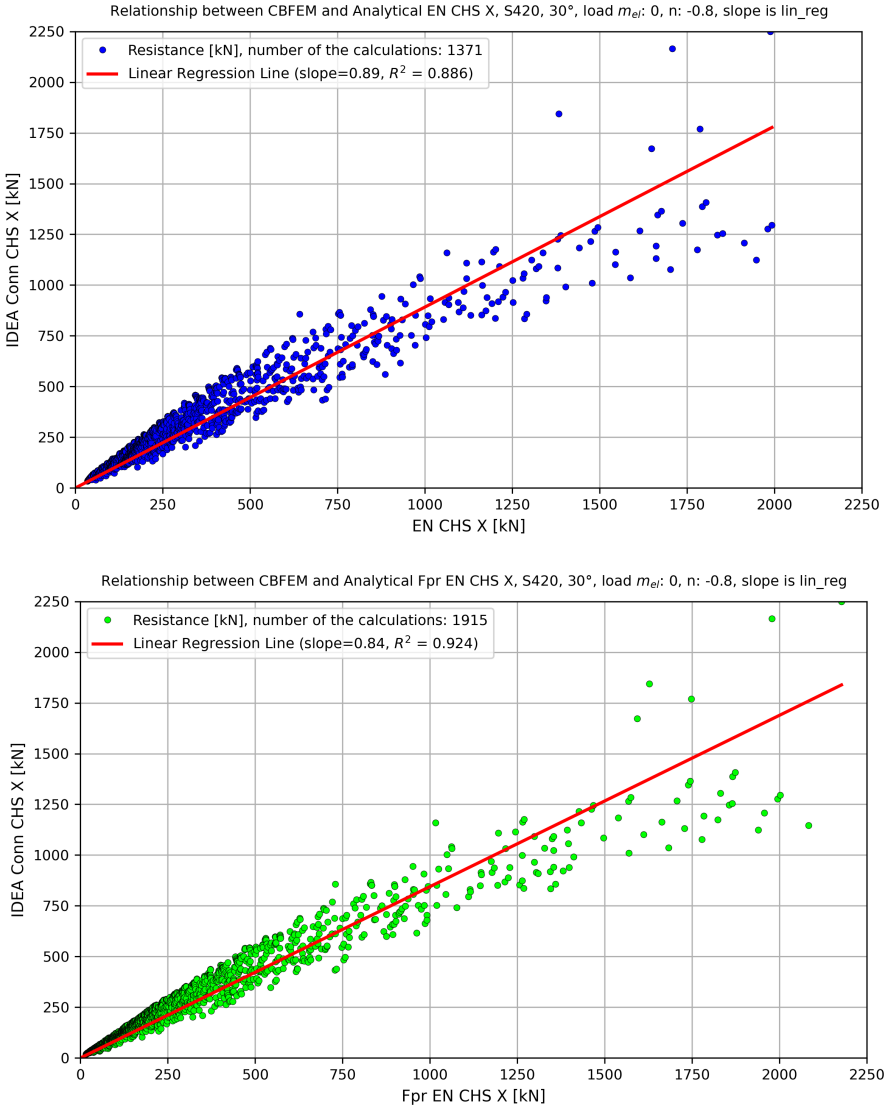

Fig. A.21: Analytical calculation and CBFEM comparison

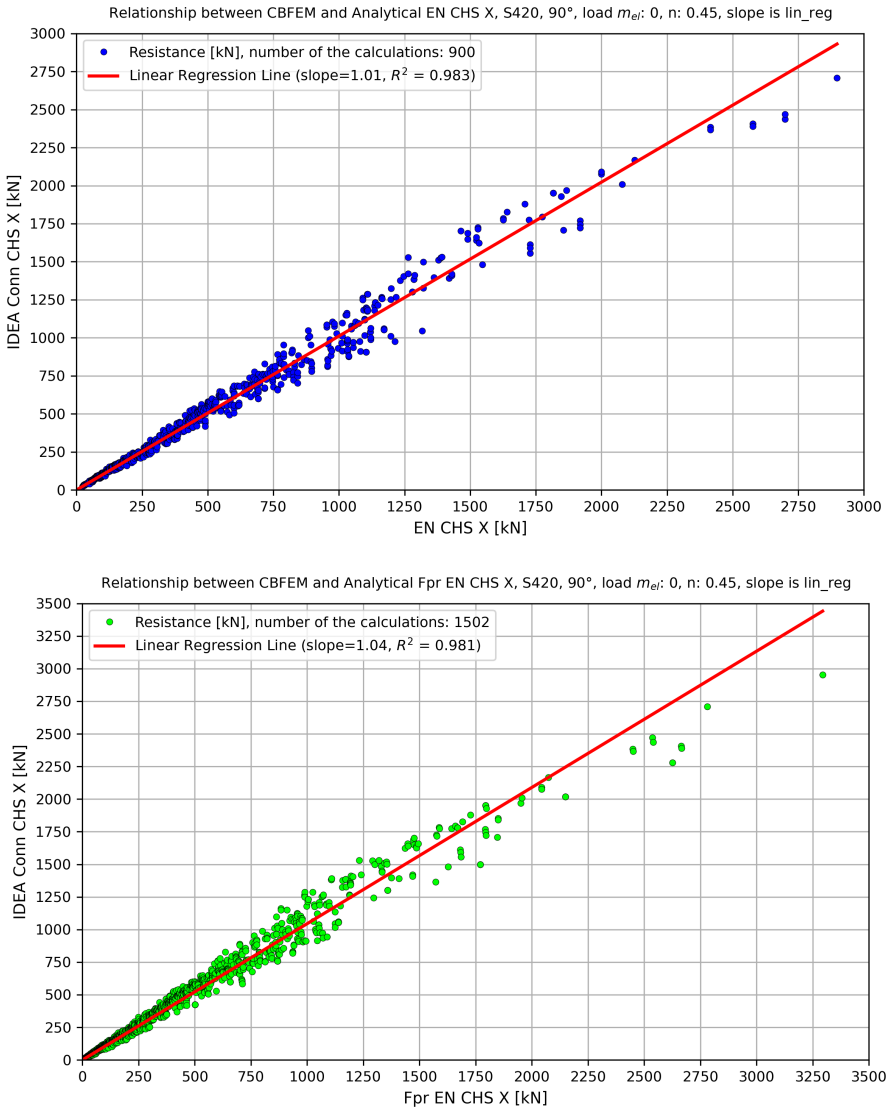

Fig. A.22: Analytical calculation and CBFEM comparison

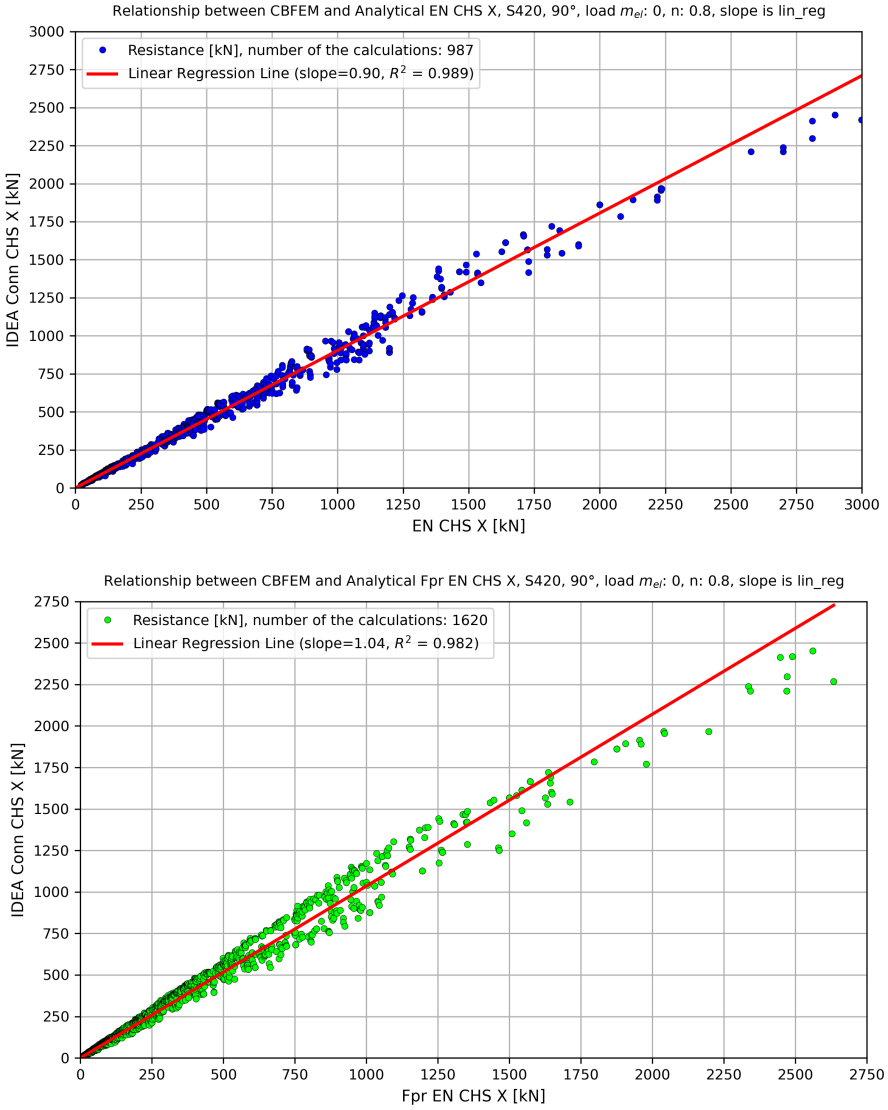

Fig. A.23: Analytical calculation and CBFEM comparison

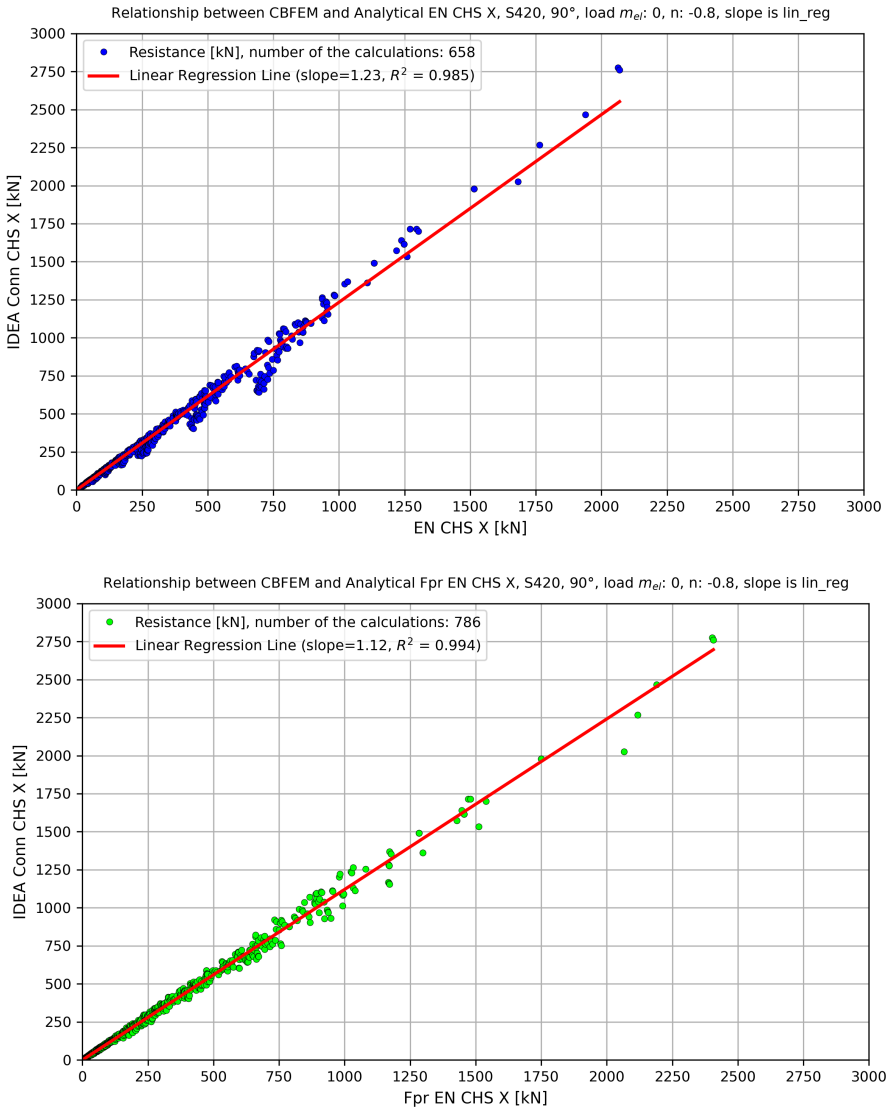

Fig. A.24: Analytical calculation and CBFEM comparison

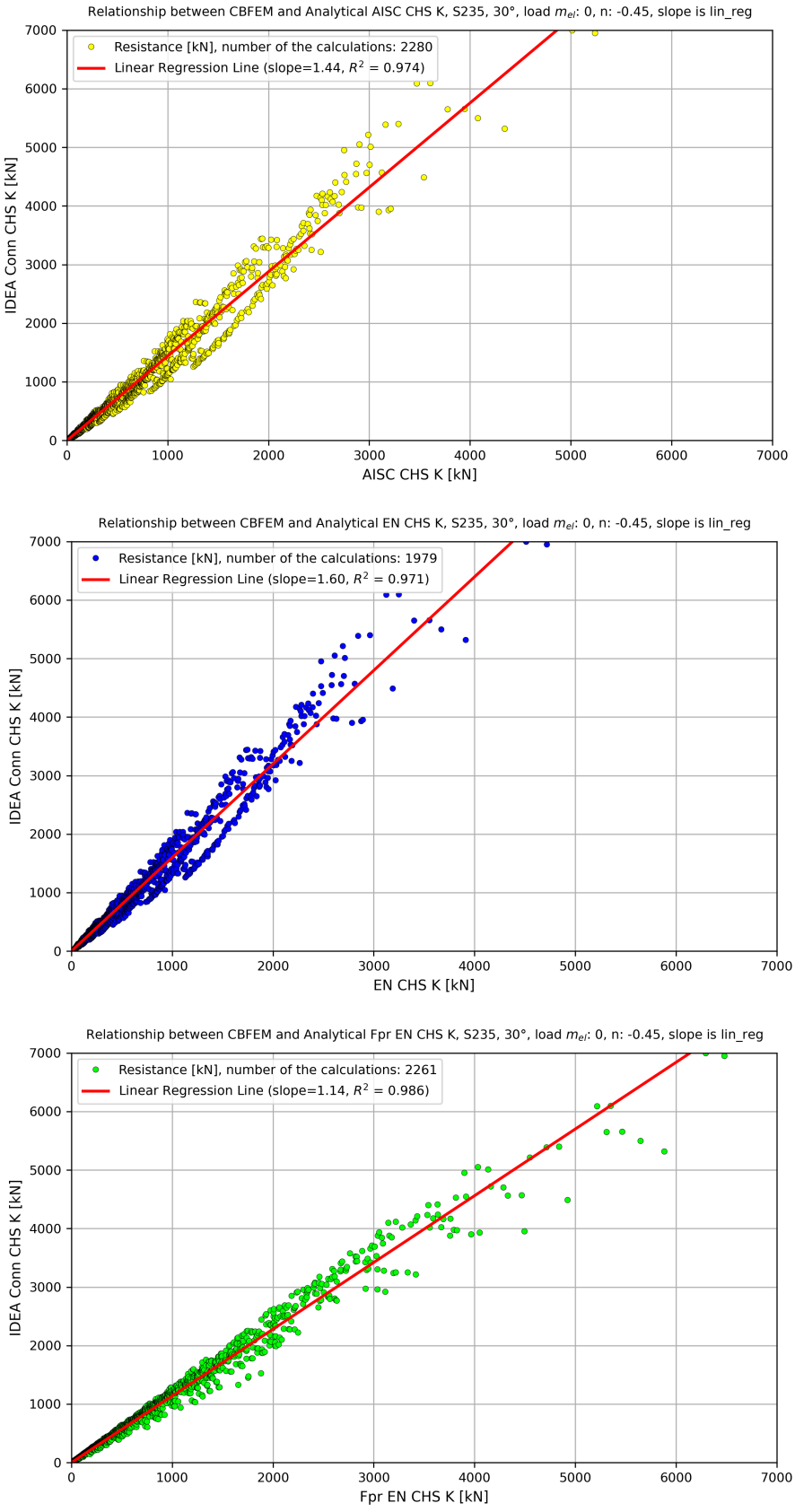

Fig. A.25: Analytical calculation and CBFEM comparison

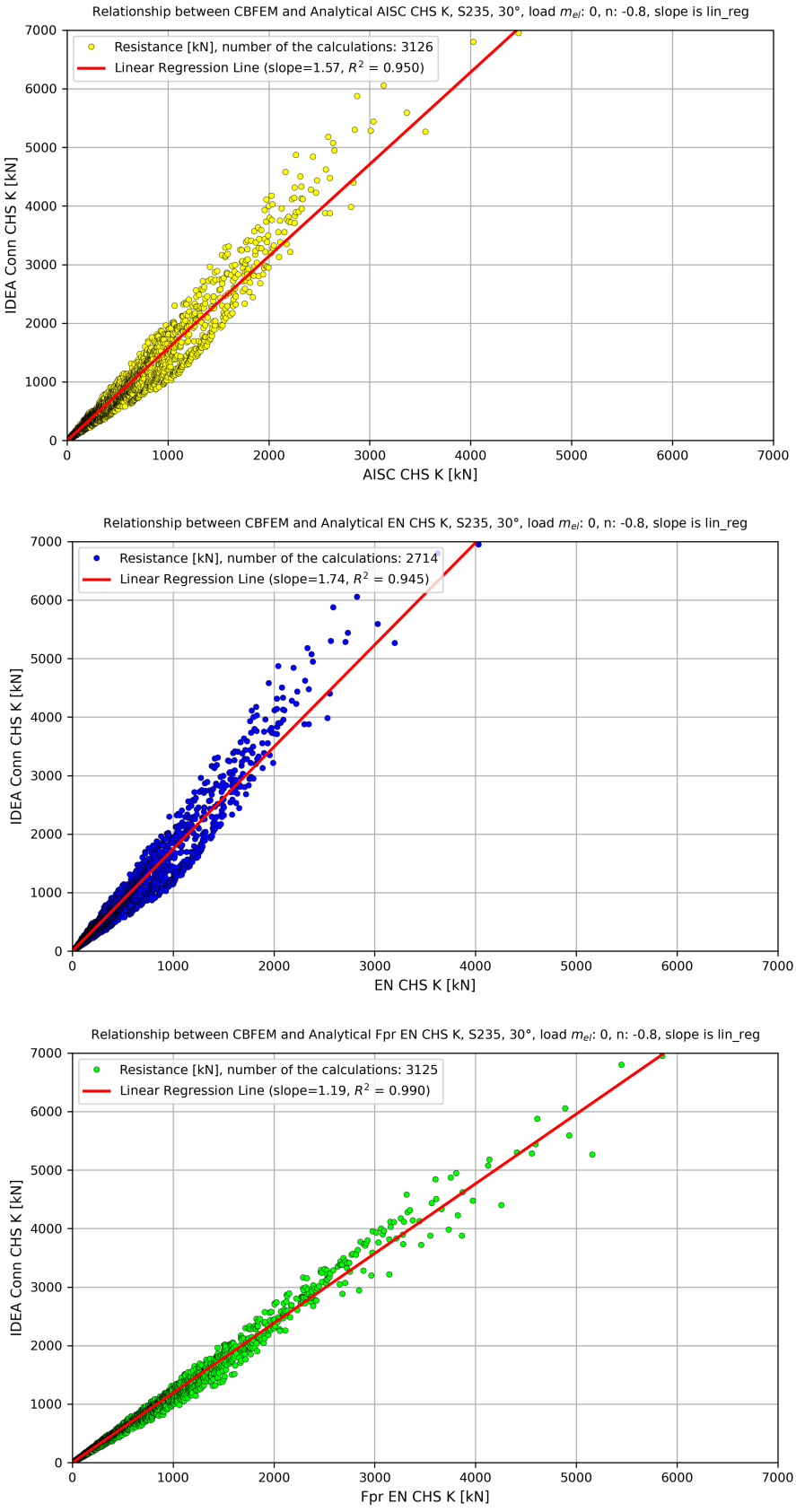

Fig. A.26: Analytical calculation and CBFEM comparison

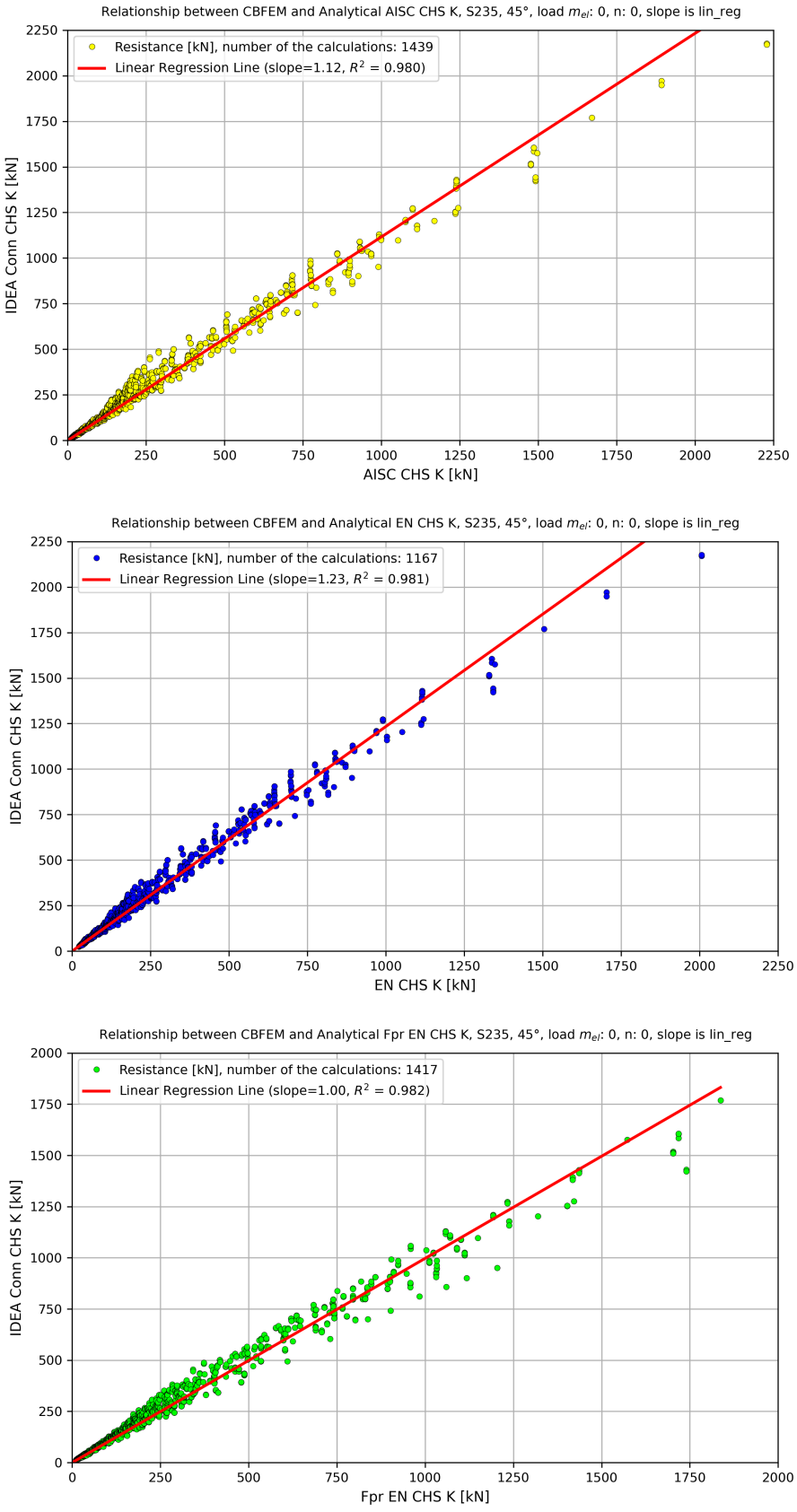

Fig. A.27: Analytical calculation and CBFEM comparison

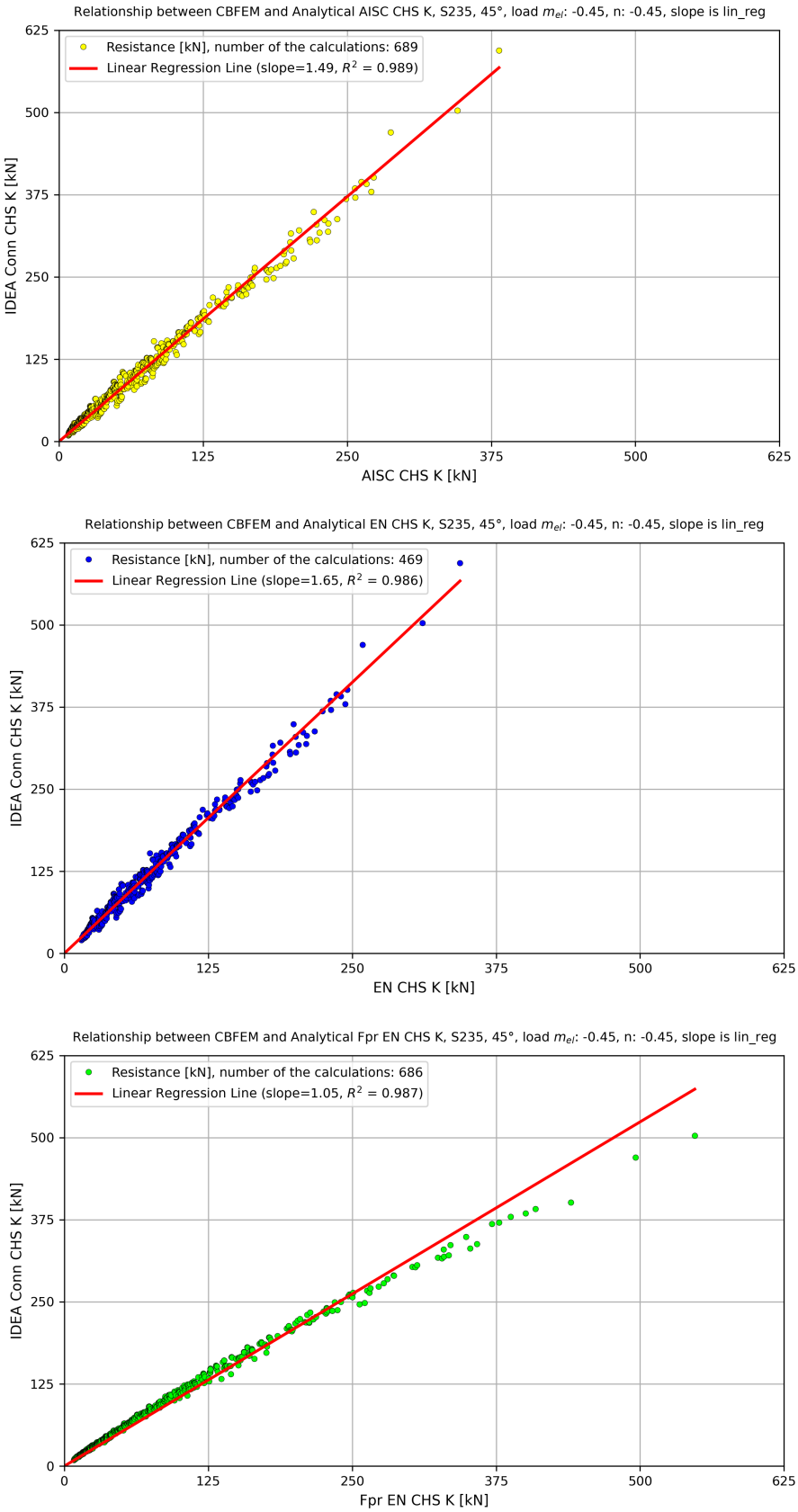

Fig. A.28: Analytical calculation and CBFEM comparison

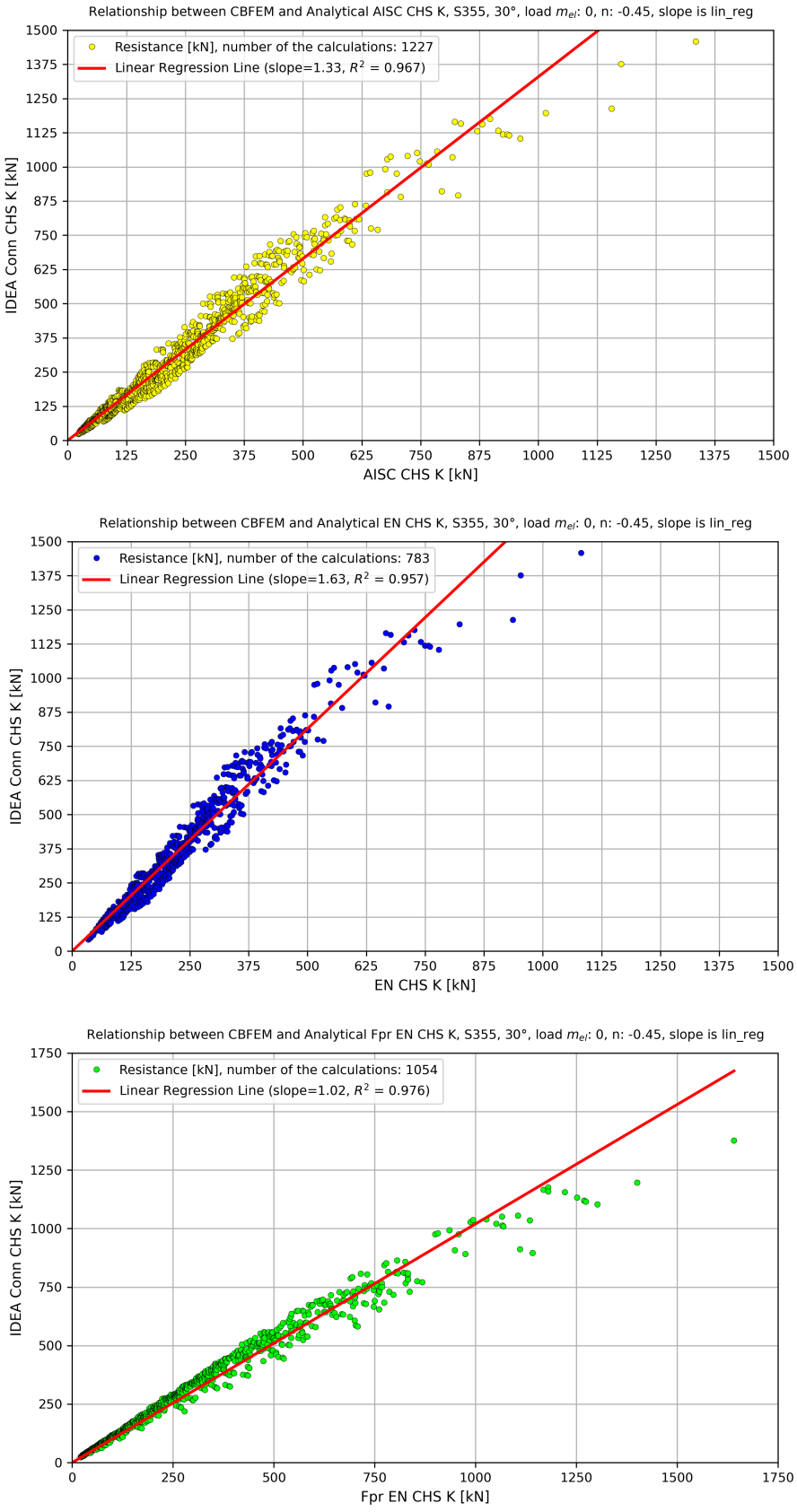

Fig. A.29: Analytical calculation and CBFEM comparison

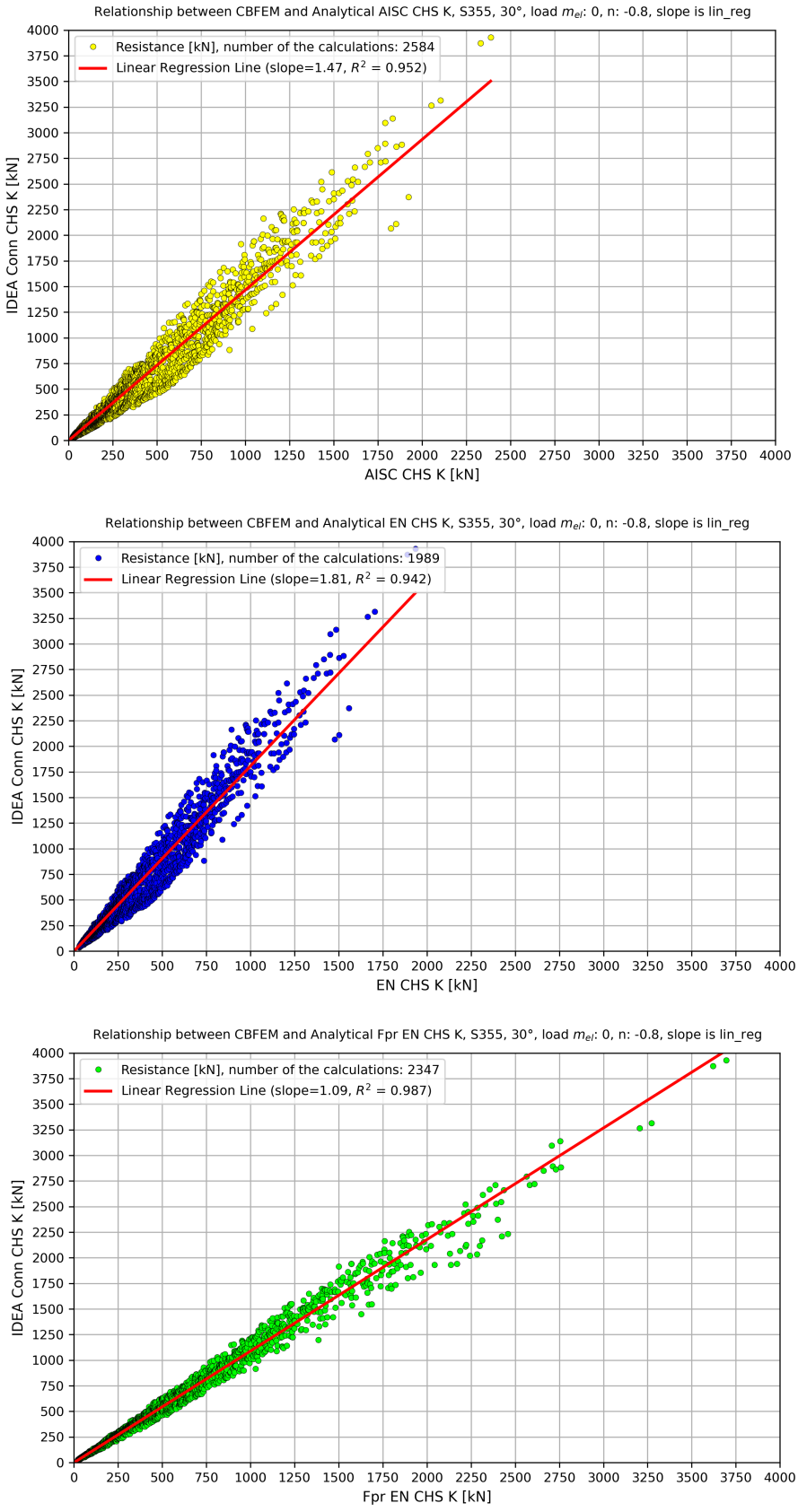

Fig. A.30: Analytical calculation and CBFEM comparison

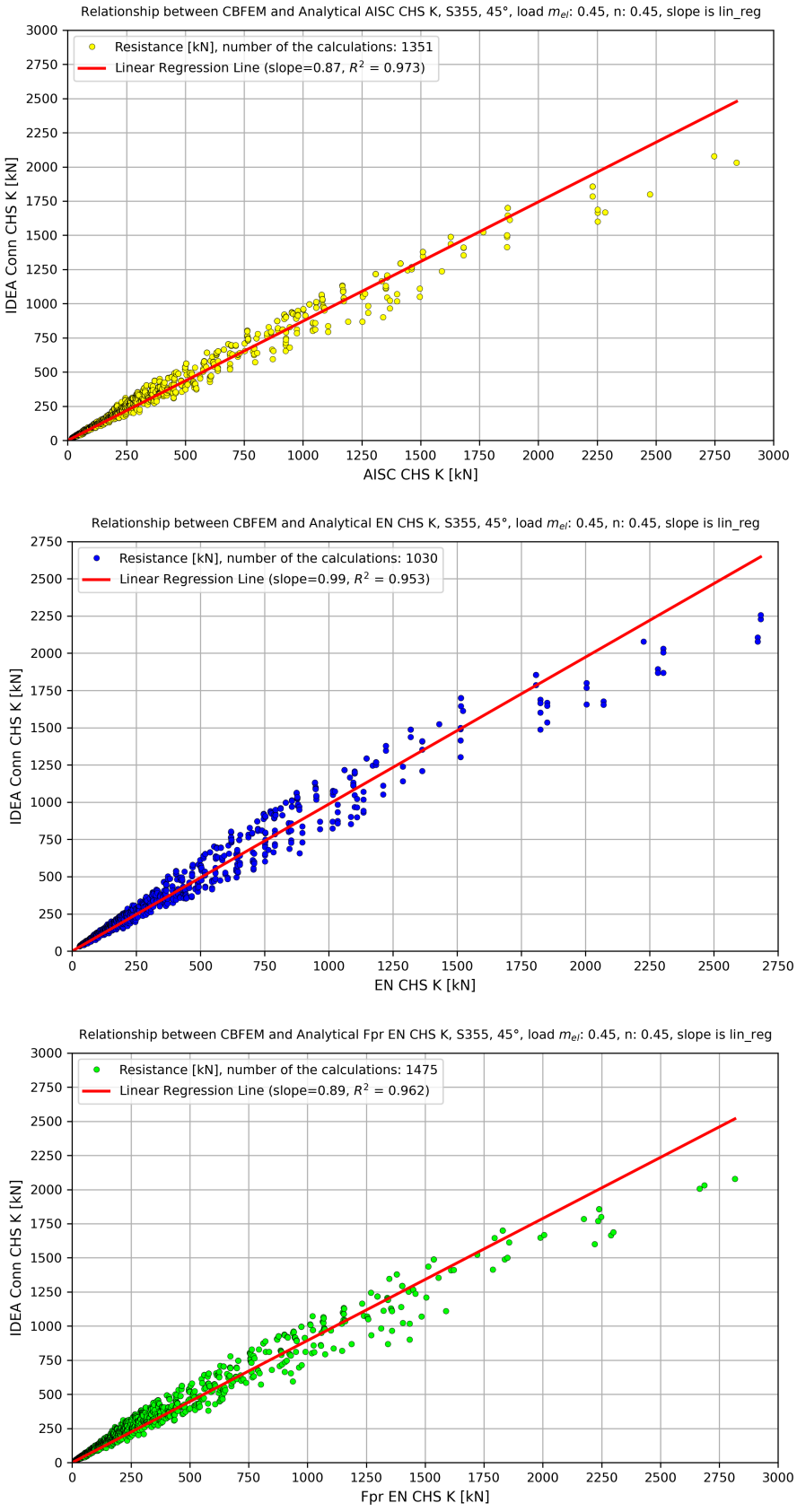

Fig. A.31: Analytical calculation and CBFEM comparison

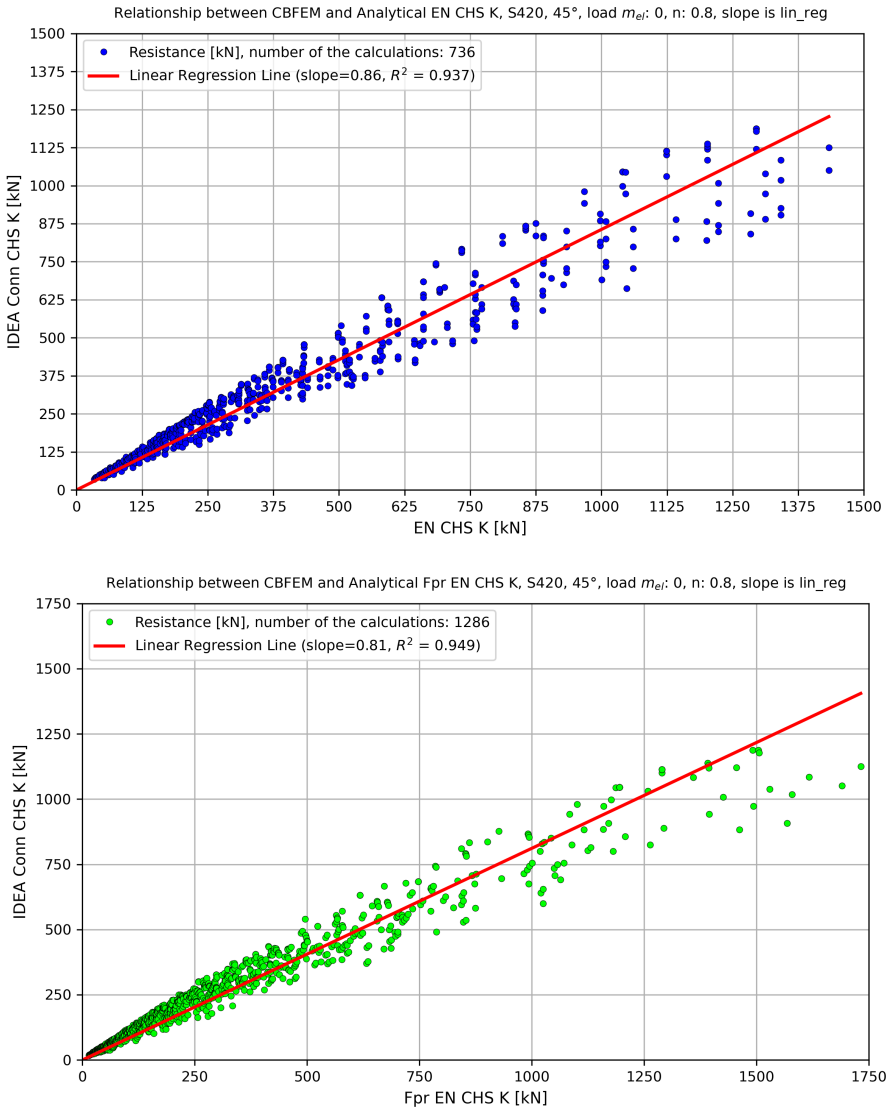

Fig. A.32: Analytical calculation and CBFEM comparison

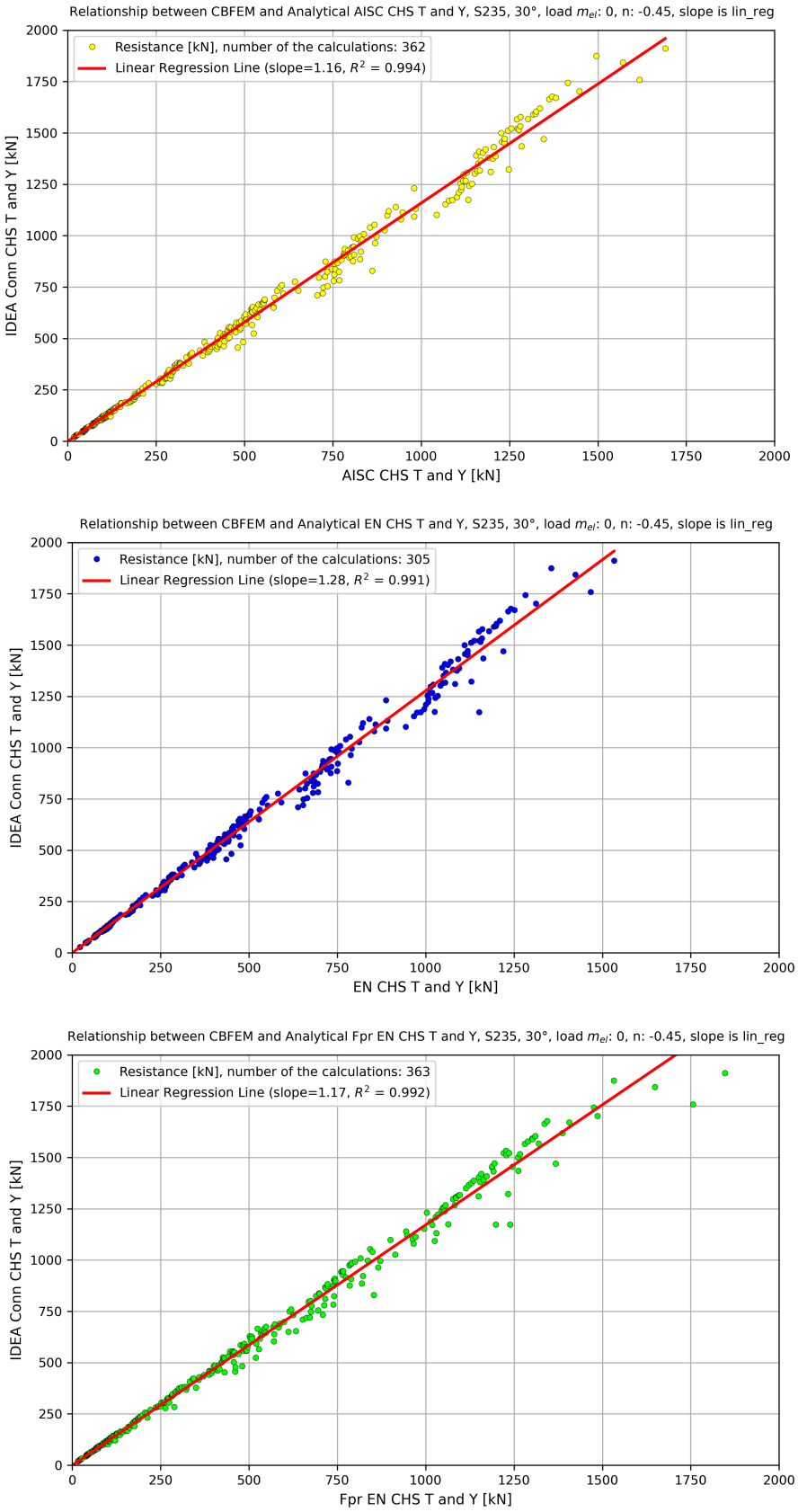

Fig. A.33: Analytical calculation and CBFEM comparison

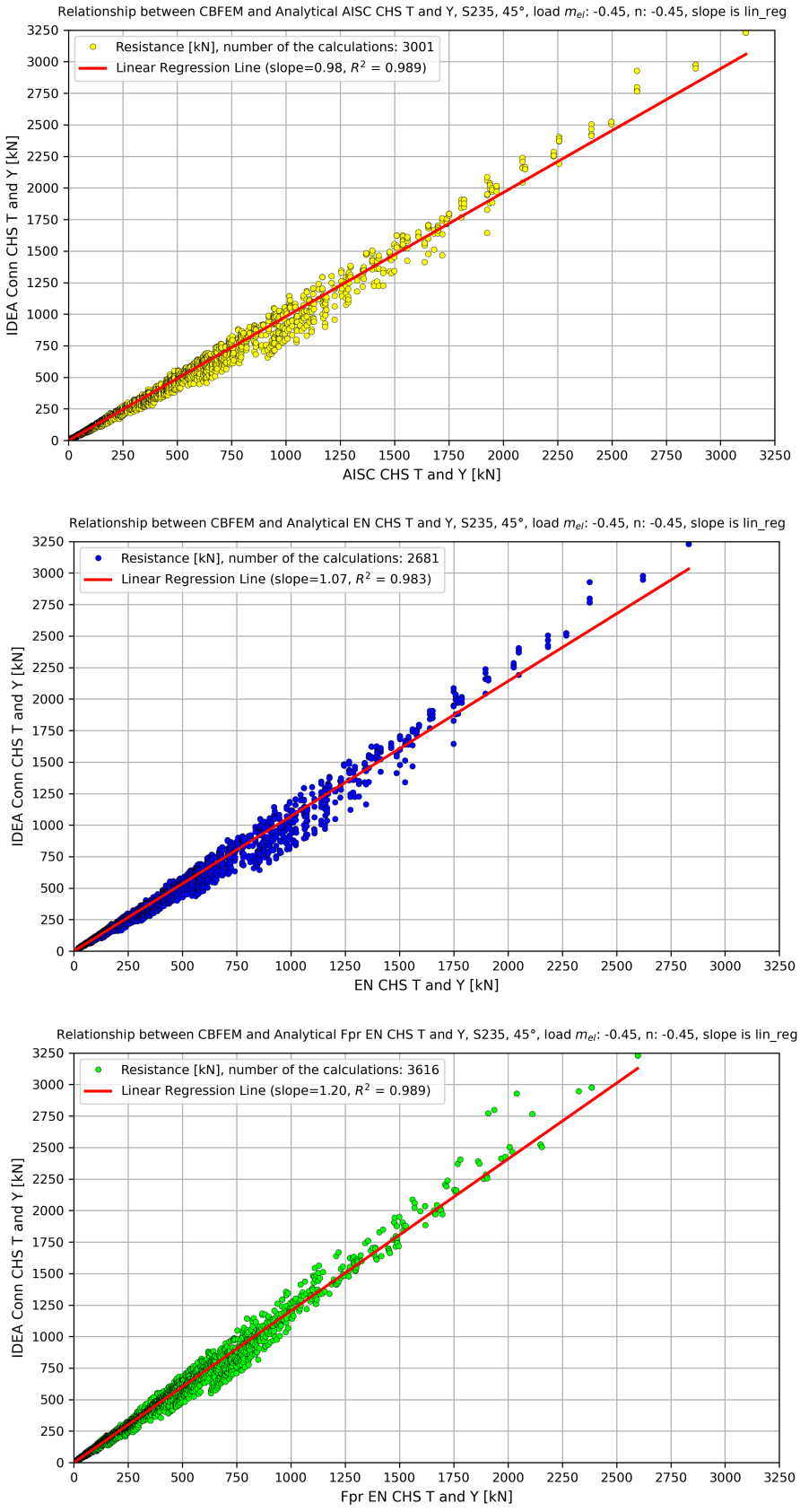

Fig. A.34: Analytical calculation and CBFEM comparison

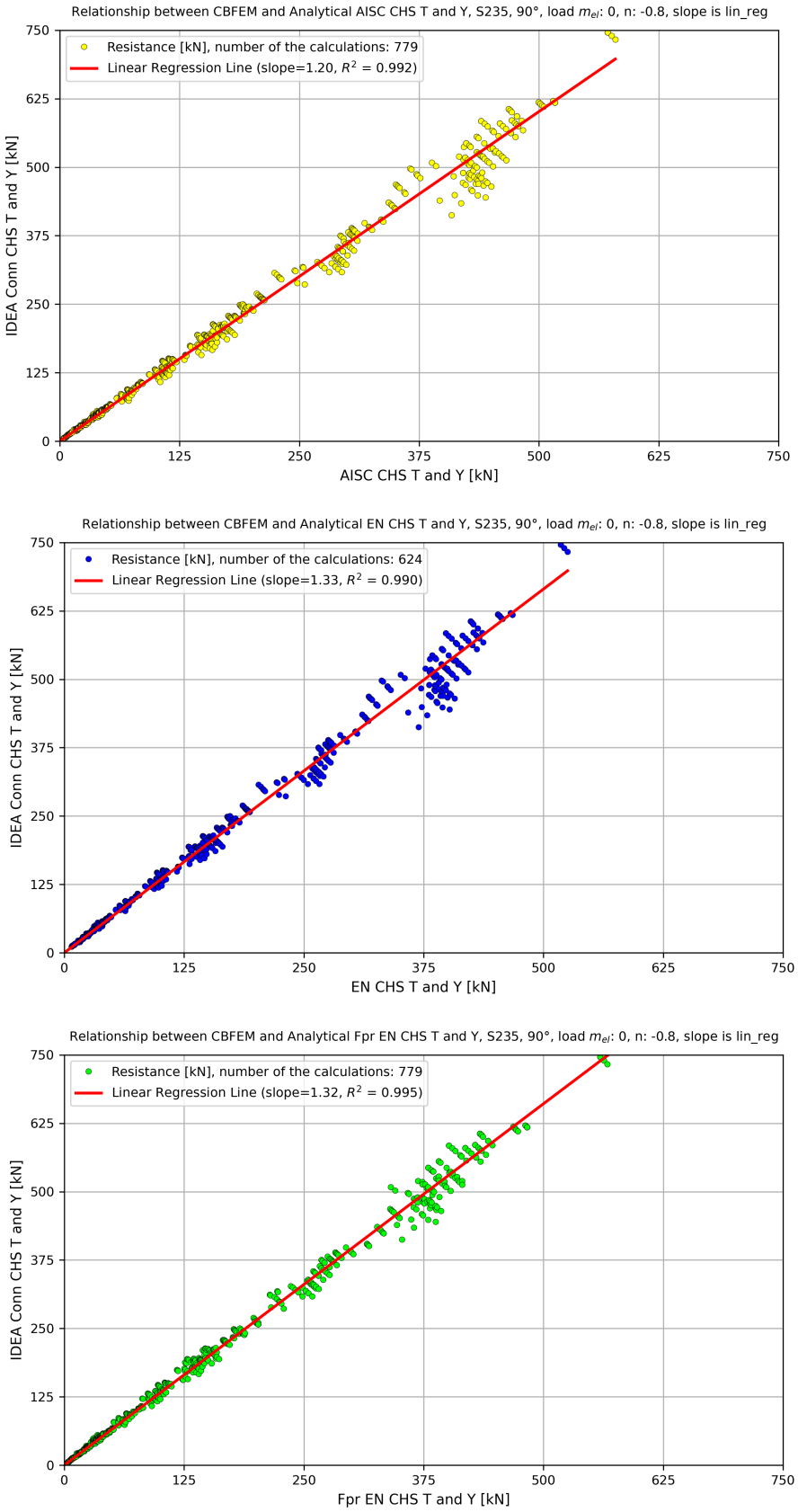

Fig. A.35: Analytical calculation and CBFEM comparison

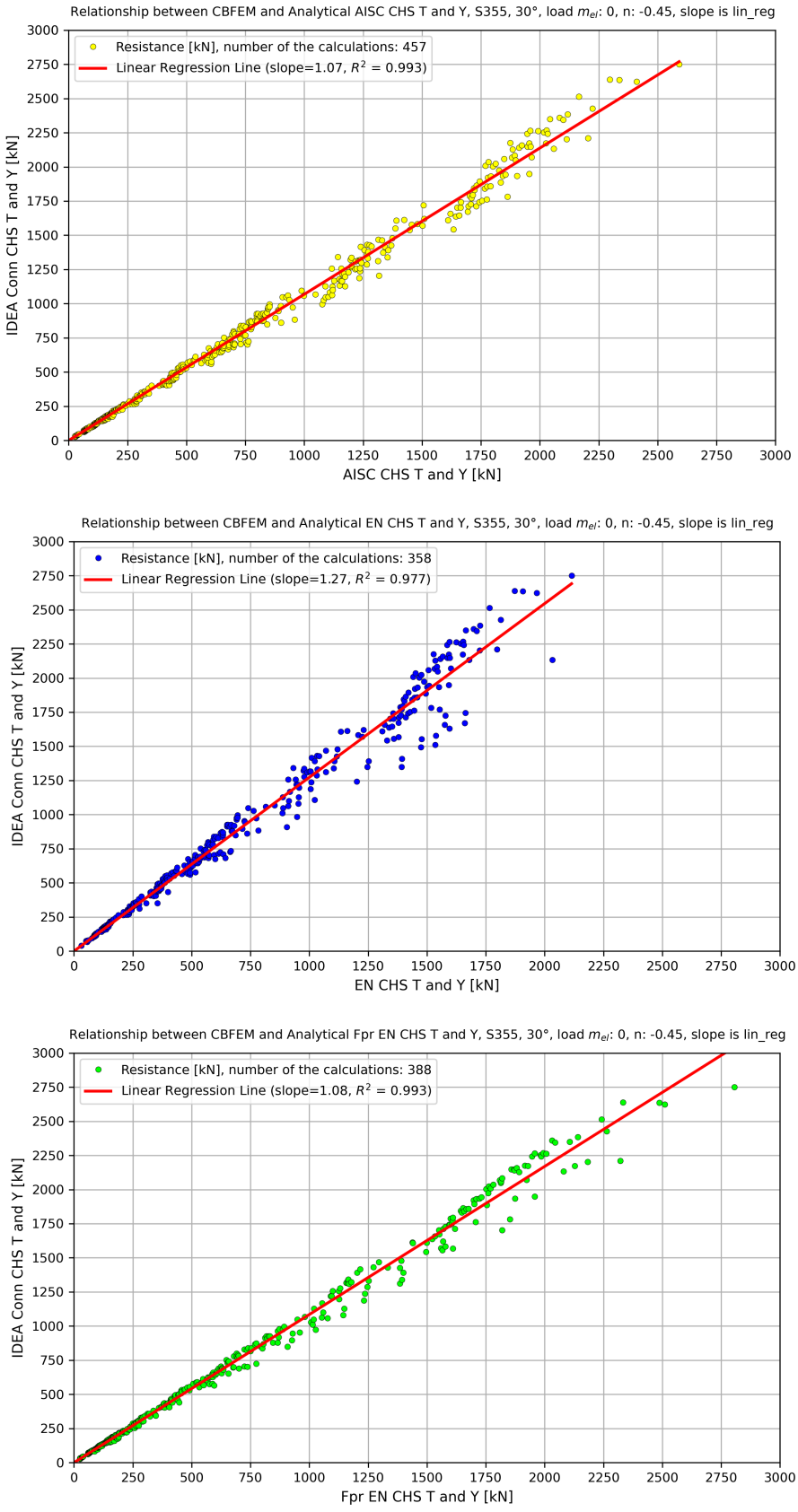

Fig. A.36: Analytical calculation and CBFEM comparison

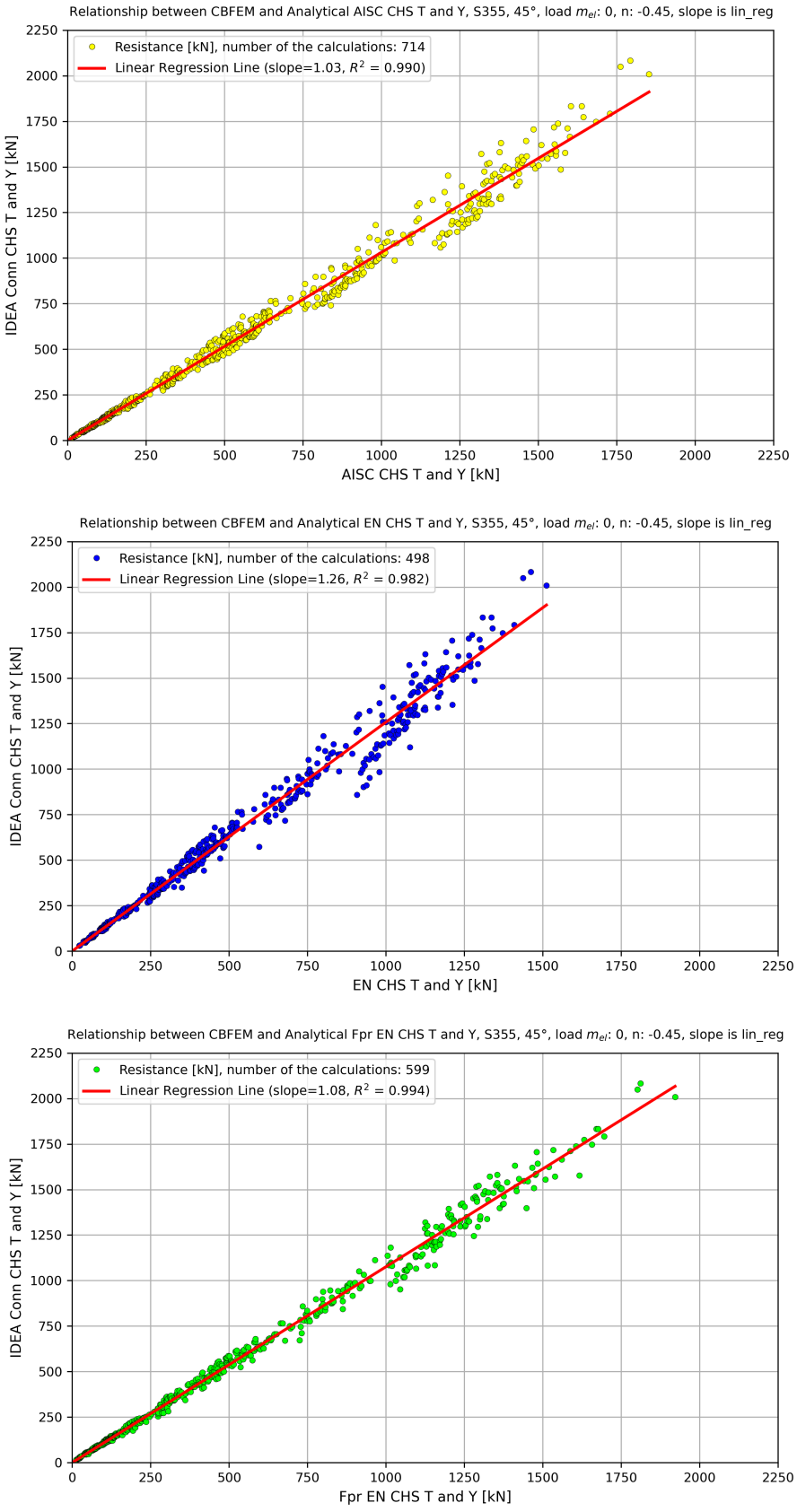

Fig. A.37: Analytical calculation and CBFEM comparison

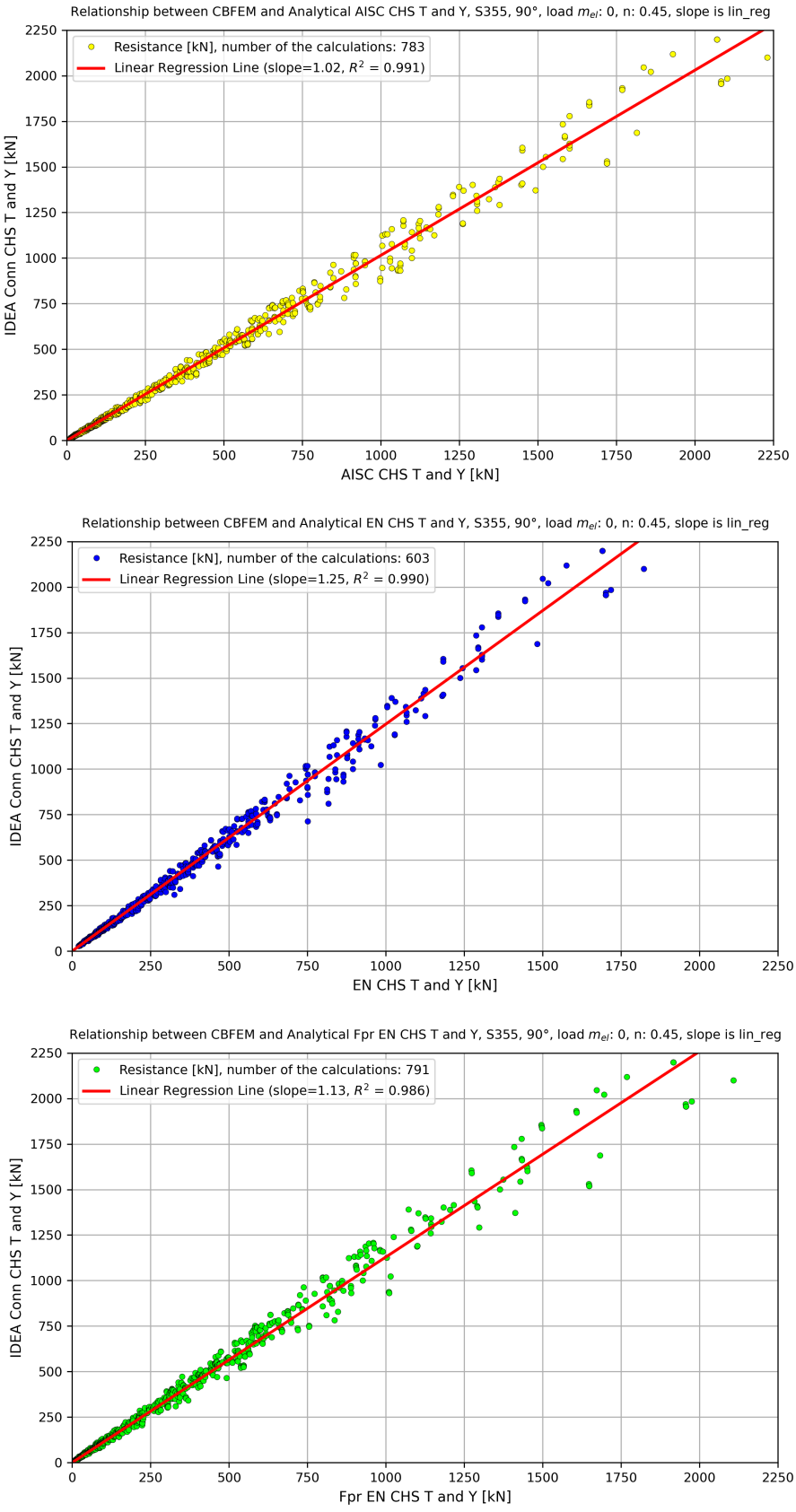

Fig. A.38: Analytical calculation and CBFEM comparison

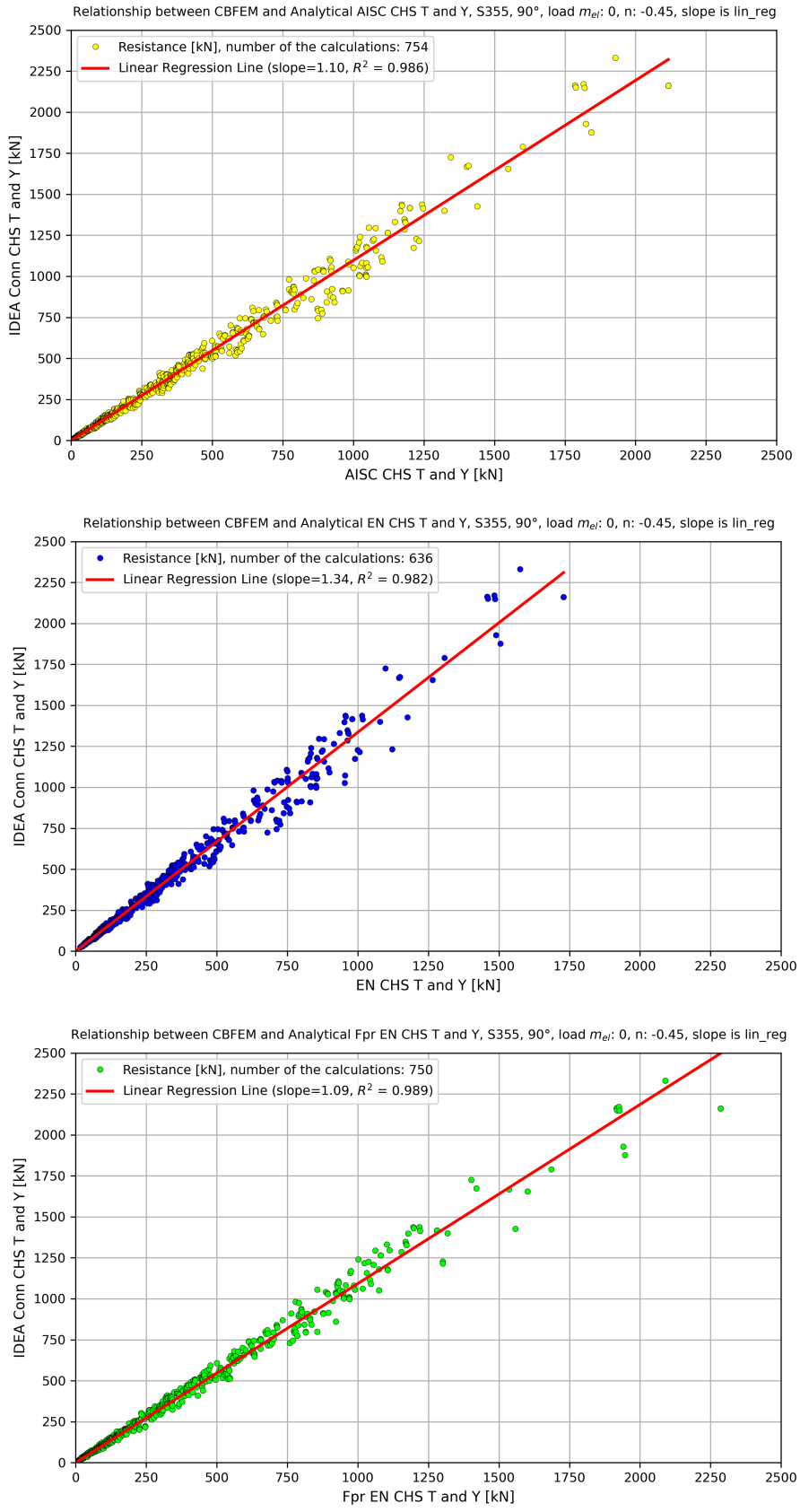

Fig. A.39: Analytical calculation and CBFEM comparison

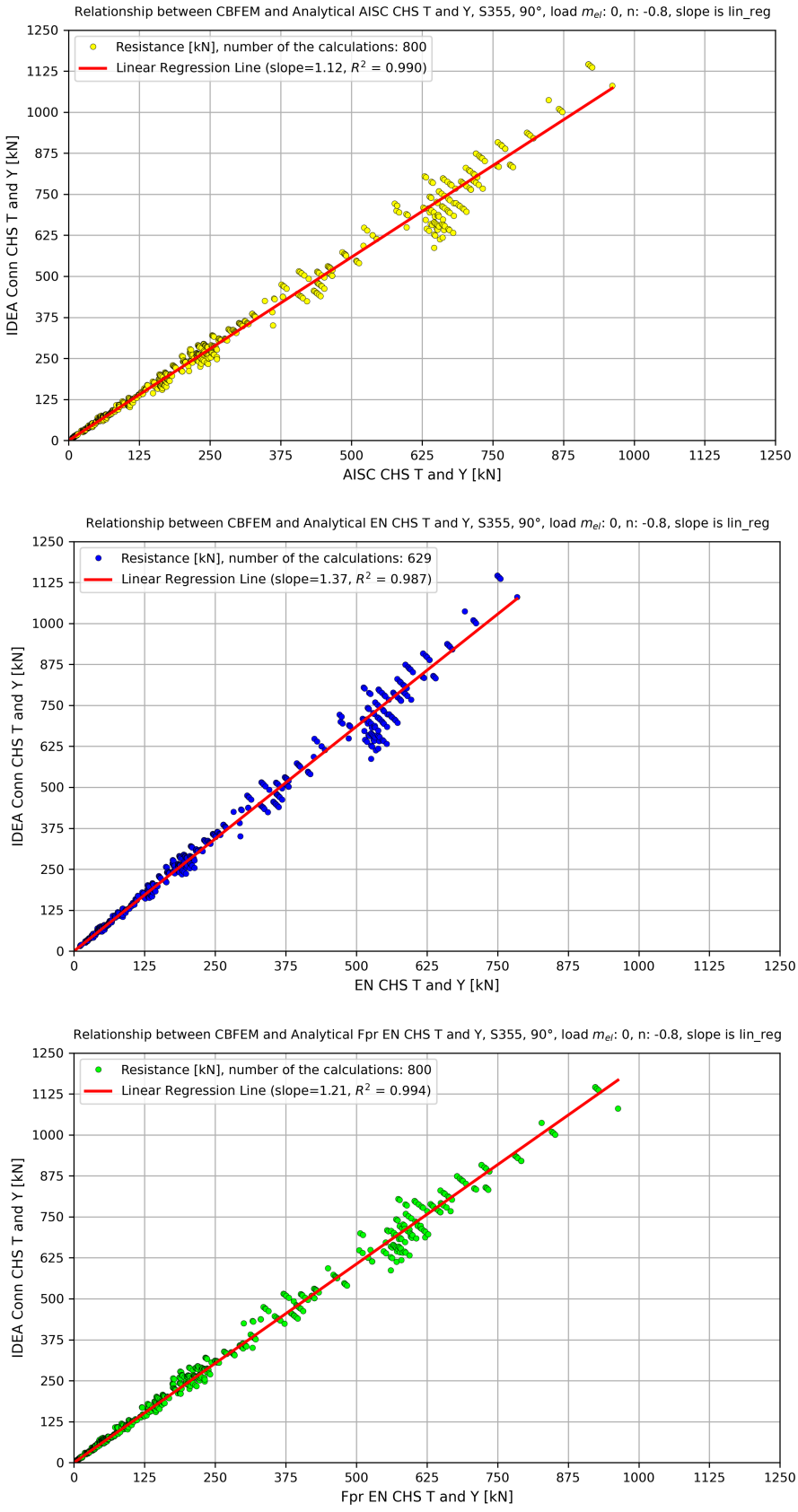

Fig. A.40: Analytical calculation and CBFEM comparison

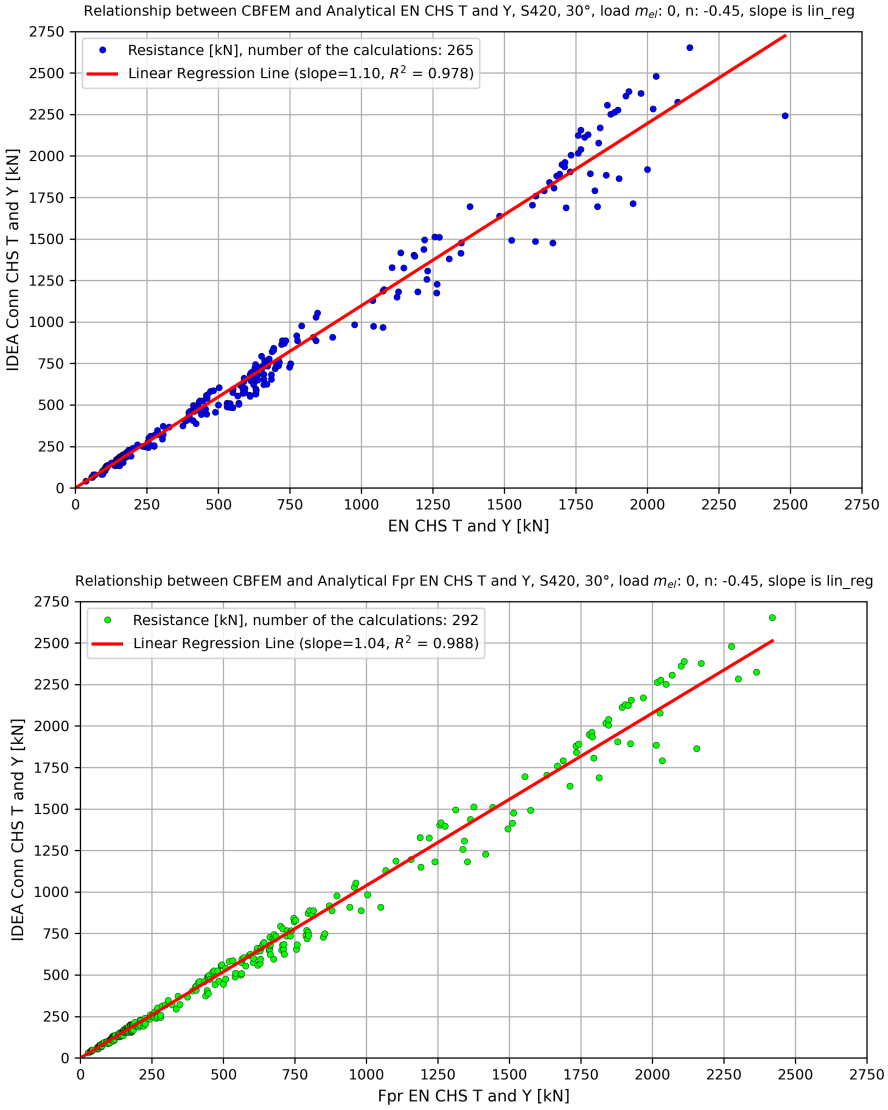

Fig. A.41: Analytical calculation and CBFEM comparison

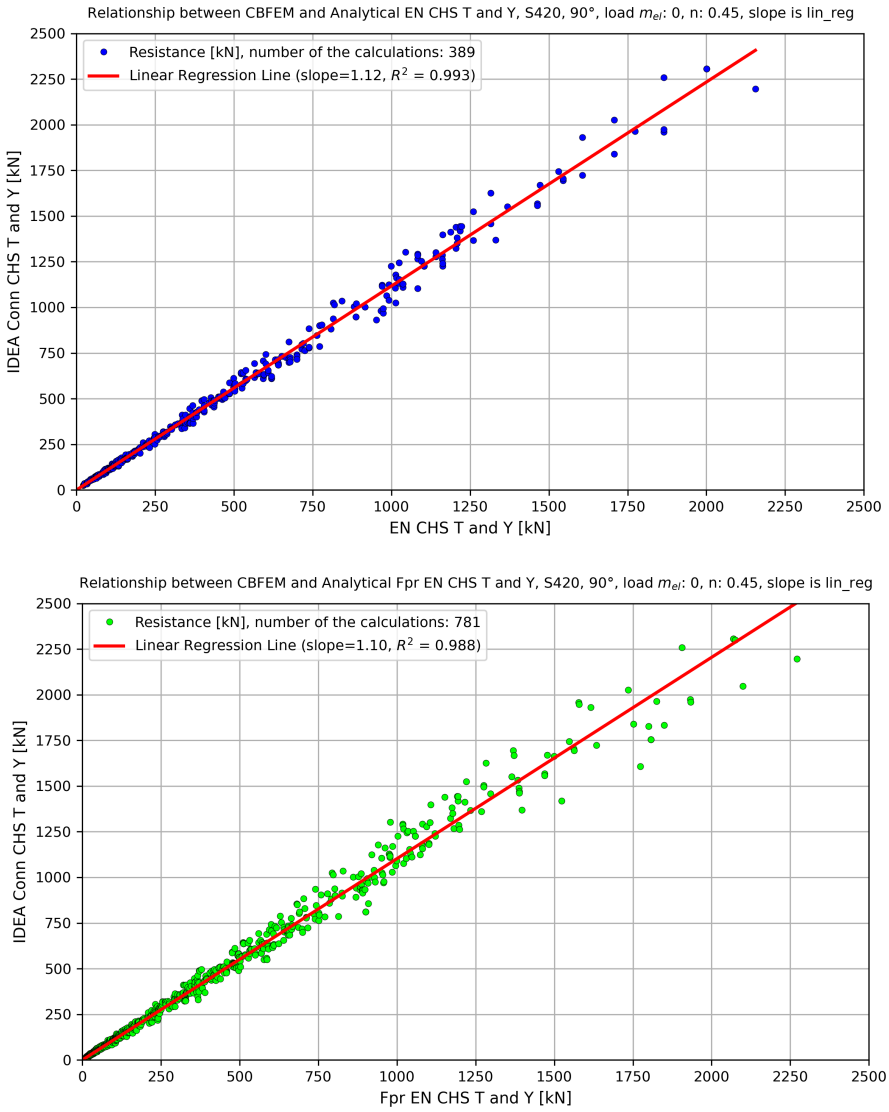

Fig. A.42: Analytical calculation and CBFEM comparison

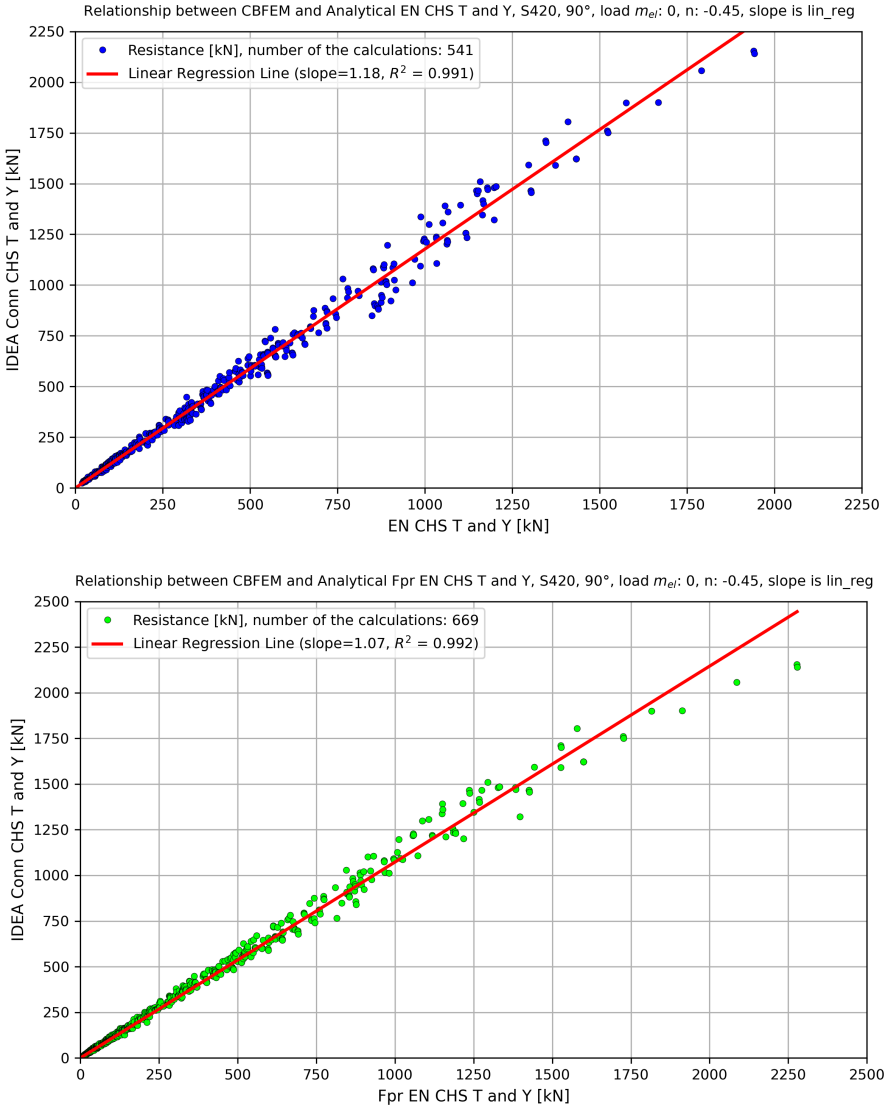

Fig. A.43: Analytical calculation and CBFEM comparison

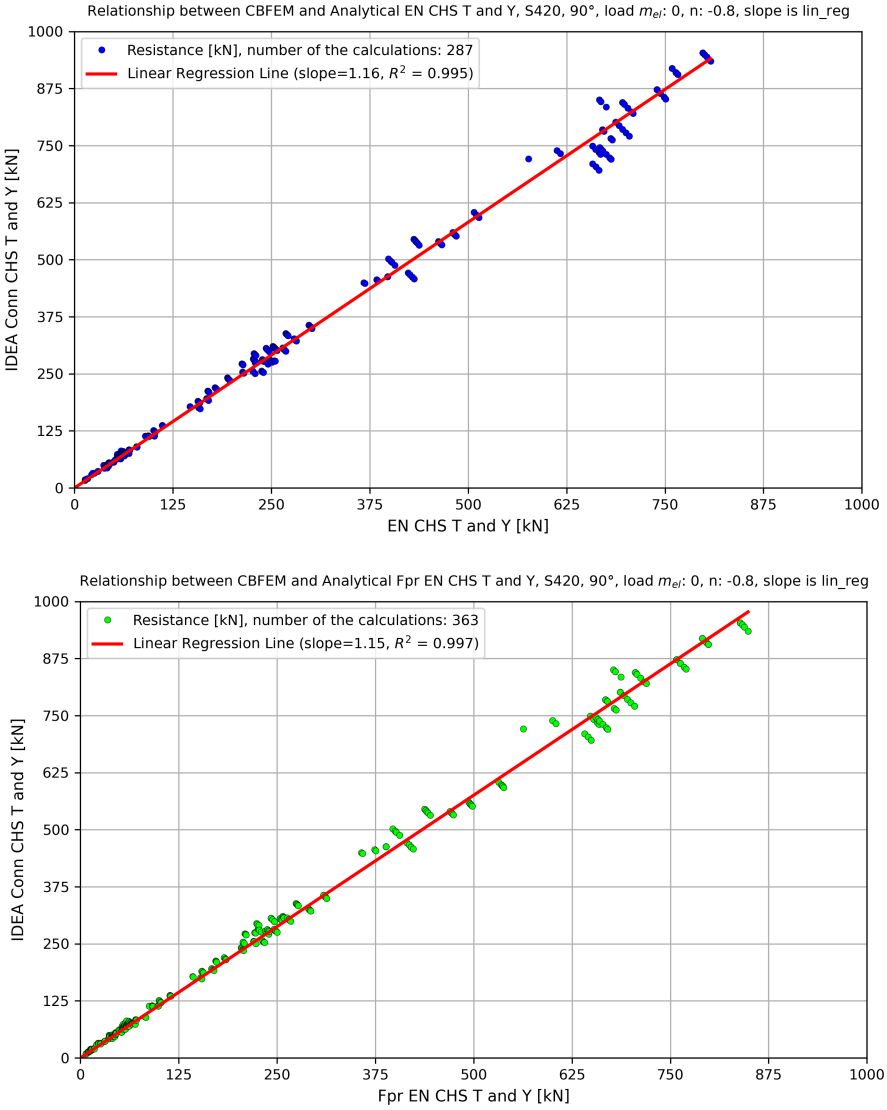

Fig. A.44: Analytical calculation and CBFEM comparison

B Code base structure

```
bachelor_thesis_doi/ ..... root directory of the thesis archive
└── bachelor_thesis_doi/ ..... project root
    ├── Code_Config_yaml/ ..... configuration files for design standards
    │   ├── AISC/ ..... American Institute of Steel Construction configurations
    │   │   ├── CHS_K.yaml
    │   │   ├── CHS_T_and_Y.yaml
    │   │   └── CHS_X.yaml
    │   ├── EN/ ..... Eurocode configurations
    │   │   ├── CHS_K.yaml
    │   │   ├── CHS_T_and_Y.yaml
    │   │   └── CHS_X.yaml
    │   └── Fpr_EN/ ..... draft Eurocode configurations
    │       ├── CHS_K.yaml
    │       ├── CHS_T_and_Y.yaml
    │       └── CHS_X.yaml
    ├── csv_cross_section/ ..... cross-section data files
    │   ├── Circular_hollow_CHS(cf).csv
    │   ├── Circular_hollow_CHS.csv
    │   ├── Rectangular_hollow_RHS.csv
    │   └── Rectangular_hollow_SHS.csv
    ├── idea_model/ ..... IDEA StatiCa connection models
    │   ├── chs_k.ideaCon
    │   ├── chs_x.ideaCon
    │   └── chs_y.ideaCon
    ├── src/ ..... source code directory
    │   ├── calc/ ..... calculation modules
    │   │   ├── gen_sample_helper/ ..... sample generation utilities
    │   │   │   └── [...]
    │   │   ├── base_classes.py
    │   │   ├── generate_samples.py
    │   │   ├── idea_calculator.py
    │   │   └── idea_load_generator.py
    │   ├── e/ ..... evaluation scripts
    │   │   ├── eval_code_to_code.py
    │   │   ├── eval_linear_regression.py
    │   │   ├── eval_multiple_plots.py
    │   │   ├── eval_res_code_runner.py
    │   │   └── eval_res_to_diff_code.py
    │   └── u/ ..... utility modules
    │       └── [...]
    ├── .gitignore
    ├── LICENSE
    ├── db_schema.sql
    └── requirements.txt
```

C Duo pitch roof truss

Duo pitch roof truss code check calculation and technical drawings will be provided in separate appendix.